UNIVERISTY OF CALIFORNIA
RIVERSIDE

Microbial and Colloidal Deposition to Solid Surfaces: Effect of Heterogeneity

A Dissertation submitted in partial satisfication
of the requirement for the degree of

Doctor of Philosophy

in

Chemical and Environmental Engineering

by

Gexin Chen

December 2009

Dissertation Committee:
Dr. Sharon L. Walker, Chairperson
Dr. Mark Matsumoto
Dr. Yushan Yan

The Dissertation of Gexin Chen is approved:

_____

_____

_____

Committee Chairperson

University of California, Riverside

ACKNOWLEDGEMENTS

I wish to express my sincere gratitude and appreciation to my advisor, Dr. Sharon L. Walker, for her invaluable guidance, patience, encouragement and input throughout the course of my graduate studies, without her support and help this dissertation would not have been possible. I also owe a deep gratitude to Professor Yushan Yan, for his valuable guidance and input on my research work. I would also like to thank my committee member Professor Mark Matsumoto for his support and valuable input during the review of my work.

So many people have impacted and enhanced my life during my study at UCR. Special thanks must be extended to my colleagues and friends in Dr. Walker's group for their help and tolerating me through the highs and lows of my research. I also want to thank my good friends, Shanpeng Song, Xin Cai, Jinlong Gong, Xinhua Liang, Tao Jiang, Yao Ma, Jianxin Feng. Being thousands of miles away from home, it's nice to have you all around.

Finally, I sincerely appreciated all the assistance from the staff of the Chemical and Environmental Engineering Department at UCR.

I would like to dedicate this dissertation to my loving family.

ABSTRACT OF THE DISSERTATION

Microbial and Colloidal Deposition to Solid Surfaces: Effect of Heterogeneity

by

Gexin Chen

Doctorate Philosophy, Graduate Program in Chemical and Environmental Engineering
University of California, Riverside, December 2009
Dr. Sharon L. Walker, Chairperson

Microbial and colloidal particle transport and deposition onto solid surfaces are of great significance to many environmental and technological processes. Initial attachment of particles is governed by the interactions between particles and surfaces. Classic Derjaguin-Landau-Verwey-Overbeek (DLVO) theory is utilized to predict interactions between particles and surfaces. However, discrepancies between experimental observations and theoretical predictions exist and the failure of the predictive model is often attributed to particle and solid collector physical and chemical heterogeneities.

This work sought to elucidate the contribution of heterogeneity to the initial particle deposition behavior in a radial stagnation point flow system or a parallel plate flow chamber system by systematically adjusting particle type and size, as well as collector surface chemical and/or physical properties. In Chapter 2 and 3, the role of particle heterogeneity (type and size) was examined. Comparable deposition trends were observed between particles, in this case groundwater and marine bacteria, *Burkholderia cepacia* G4g and *Halomonas pacifica* g, respectively. However, the

deposition kinetics of *H. pacifica* g appeared to be more sensitive to solution chemistry than that of *B. cepacia* G4g. Experimental results also demonstrated that particle size (colloidal and bacterial) had a considerable impact on the transport and interaction with surfaces. In Chapter 4, a method to influence collector surface charge and subsequent colloid deposition was described. Experimental results suggest colloids respond to local variations in surface potential through electrostatic interactions, altering particle streamlines flowing along the surface, and ultimately the extent of deposition. In Chapter 5, cell deposition onto bare and zeolite coated aluminum alloy and stainless steel surfaces was investigated using bacterium *H. pacifica* g. Collector surface properties found to have the most notable effect on cell attachment were the electrokinetic and hydrophobic nature of the bare metal and zeolite coated surfaces. In Chapter 6, the relative impact of physical roughness on antifouling nature of zeolite surfaces, as compared to these other chemical mechanisms was investigated.

This comprehensive dissertation project established both particle and collector surface heterogeneity has a significant effect on particle deposition, which was clearly identified by altering various physical and chemical interaction parameters between particles and surfaces.

TABLE OF CONTENTS

LIST OF FIGURES

LIST OF TABLES

CHAPTER 1

INTRODUCTION

1.1 MOTIVATION AND BACKGROUND

Microbial and colloidal particle transport and deposition in flowing suspensions onto solid surfaces are of great significance to many natural and man-made processes such as pathogen transport[1, 2], biofilm control[3, 4], drinking water filtration[5, 6], bioremediation[7-9], and microbe-facilitated contaminant transport[10]. For instance, once microbes are attached to a substratum surface, a multi-step process starts leading to the formation of a complex, adhering microbial community that is termed a "biofilm"[11, 12]. Biofilm formation is initiated and governed by the deposition of individual microbial cells on solid surfaces. Preventing initial attachment can inhibit the biofilm formation process, which would be greatly beneficial in such fields as ship industry and marine structures[13, 14], food processing[15], water distribution[16] and medical devices[17].

Deposition of microbial and colloidal particle is considered the outcome of two consecutive steps: (i) particle transport from the bulk of a flowing suspension to the collector surface and (ii) attachment. The three transport mechanisms leading to collision between the particle and collector surfaces are widely defined to be Brownian diffusion, interception, and sedimentation[18]. The initial attachment of particles is governed by the interaction forces between the particles and surfaces occurring upon close approach. Classic Derjaguin-Landau-Verwey-Overbeek (DLVO) theory which defines the interactions between a particle and a collector surface as the sum of attractive van der Waals[19] forces and electrostatic double layer

interactions[20] has been applied to predict the interaction forces between particles and surfaces, and ultimately particle deposition behavior. When particles and collector surfaces are similarly charged, particle deposition is considerably impeded due to the existence of the repulsive electrostatic interactions and is termed unfavorable under these conditions. On the other hand, attractive electrostatic forces appear when particles and collector surfaces are oppositely charged and conditions are chemically favorable for deposition[21]. This approach has proven merits for predicting particle adhesion under well-controlled environments for certain colloids and bacterial species and strains; however, it fails to yield a universally applicable description[22].

Despite extensive efforts in modeling and experimentation, discrepancies between experimental observations and theoretical predictions exist[23-26], especially under unfavorable conditions. Understanding and predicting the transport and deposition of particles in natural subsurface environments as well as engineered systems is a challenging problem[27] because it involves a combination of physical and chemical factors (as well as biological for microbes) including solution chemistry[7, 28], collector surface heterogeneity[29], hydrodynamic condition[30, 31], particle properties[32], etc. acting at the solid/water interface which may affect the interaction forces governing the approach and attachment of a particle to the surface, such as gravitational, electrostatic, van der Waals, hydrophobic, hydration, and other specific forces[33]. The failure of the predictive models is commonly attributed to particle and solid collector physical and chemical heterogeneities.

Cell surface characteristics (i.e. cell type[34], growth phase[35], hydrophobic interactions[36, 37], surface charge characteristics[38] and presence and composition of surface macromolecules[39]) and collector surface properties (morphology[40], surface chemistry[41, 42], and roughness[43-45]) can influence bacteria adhesion to surfaces. Experimental studies have demonstrated the importance of these properties. These factors effect one or more of the many forces that govern the approach and adhesion of a particle to the surface, including electrostatic interactions, van der Waals forces, as well as hydrophobic, hydration, and specific chemicals forces. However, contradicting results have been widely noticed[46-55]. Additionally, the extent to which heterogeneity of these physical and chemical characteristics impacts the overall particle deposition has not been fully explained. Based on the available theoretical and experimental studies to date, the presence of surface charge heterogeneity can decrease electrostatic repulsion at the local scale and increase the rate of irreversible particle attachment [56-61]. The inter-related role of physical heterogeneity along with chemical heterogeneity, as well as the impact of scale of these features, remains to be established.

Clearly, a systematic investigation of microbial and colloidal deposition behavior in well-defined experimental systems may reveal considerable insight with respect to the cause of discrepancies between experimental observations and theoretical predictions. This doctoral work sought to elucidate physical and/or chemical heterogeneity contributions to the initial microbial and colloidal particles deposition

behavior in a radial stagnation point flow system and a parallel plate flow chamber system by systematically adjusting particle type and size, collector surface chemical and/or physical heterogeneities.

1.2 OBJECTIVES

The overall objective of this work is to determine the extent to which multi-scale physical and chemical heterogeneity contributes to the initial stages of microbial and colloidal deposition. Specifically, this research focused on the interactions occurring between a model particle (a known bacterium or a surrogate polystyrene colloid) and collector surfaces in simulated groundwater or seawater. Both the physical and chemical nature of the particle and collector surfaces was systematically modified and utilized in well-controlled deposition experiments within a radial stagnation point flow system or a parallel plate flow chamber system. The physical heterogeneity involved the surface roughness on the collector and the type and size of the particles. The chemical heterogeneity involved the patterned or randomly distributed and exposed charged functional groups on particle and collector surfaces.

SPECIFIC OBJECTIVES

1. To determine the role of bacterial/colloidal type and size on the kinetics of adhesion utilizing a radial stagnation point flow system and a parallel plate flow chamber system. Experiments were conducted under typical marine and groundwater solution chemistry conditions using both well defined bacteria and polystyrene colloids.

2. To evaluate the influence of collector surface chemical heterogeneity on colloid deposition by systematically varying the zeta potential at microelectrodes with remotely applied electric potentials in a parallel plate flow chamber system. These experiments sought to establish the role of the surface charge heterogeneity on particle deposition behavior.

3. To determine the role of collector surface physical and chemical heterogeneity on the kinetics of microbial deposition utilizing a parallel plate flow chamber system. Experiments were conducted using a model bacterial cell or colloid and collector surfaces of bare and zeolite coated stainless steel and aluminum alloy.

1.3 STRUCTURE OF THE DISSERTATION

Following the Introduction (Chapter 1), the second chapter of the dissertation, "Role of Solution Chemistry and Ion Valence on the Adhesion Kinetics of Groundwater and Marine Bacteria", was published in *Langmuir* **2007**, 23: 7162-7169. The purpose of the work was to evaluate the role of microbial heterogeneity on bacterial deposition to solid surfaces in water solutions simulating various aquatic environments. The deposition kinetics of a groundwater bacterium, *Burkholderia cepacia* G4g and a marine bacterium, *Halomonas pacifica* g, were determined experimentally in a radial stagnation point flow cell system. Comparable adhesion trends were observed, however, the deposition kinetics of *H. pacifica* g appeared to be much more sensitive to solution chemistry than that of *B. cepacia* G4g. Additionally,

enhanced bacterial adhesion behavior was observed in the presence of Ca^{2+}, which is attributed to Ca^{2+} binding bacterial surface polymers and altering the polymer conformation.

Chapter 3, "Colloidal and Bacterial Deposition: Role of Gravity", has been recently submitted to the journal *Langmuir*. The objective of this work was to further investigate the effect of "heterogeneity" from the perspective of particle size. Adhesion studies were conducted with polystyrene microspheres of various sizes (0.5, 1.1 and 1.2 μm) and *B. cepacia* G4g in a parallel plate flow chamber system. Experimental results demonstrated that particle size had a considerable effect on the deposition of micron-sized colloids and bacteria and confirmed that size contributes to particle transport and interaction with surfaces. It was found that smaller colloids seem to be more sensitive to hydrodynamic interactions compared to larger colloids and bacterial cells. Moreover, results suggested that gravity is a significant force to transport micron scale particles, validated by calculations using the Smoluchowski-Levich approximation and the experimental observations in a $D_2O/H_2O/KCl$ (heavy water) mixture.

Chapter 4, "Colloidal Deposition on Remotely Controlled Charged Micropatterned Surfaces in a Parallel Plate Flow Chamber", was published in *Langmuir* **2008**, 24: 9381-9385. This work described a method to create collector surface "chemical heterogeneity" by varying the zeta potential at microelectrodes with remotely applied electric potentials. Colloid deposition kinetics was determined in a

parallel plate flow chamber system and it was found that remotely controlled zeta potential changes on microelectrode induced by an external potential gave predictable adhesion trends. We further proposed colloidal particles respond to local variation in surface potential through electrostatic interactions, altering particle streamlines flowing along the surface, and ultimately the extent of deposition.

Chapter 5, "Initial Bacterial Deposition on Bare and Zeolite-Coated Aluminum and Stainless Steel", was published in *Langmuir* **2009**, 25: 1620-1626. This work presents a critical evaluation of the physical and chemical mechanisms controlling bacterial deposition onto bare versus zeolite-coated stainless steel and aluminum alloy in a parallel plate flow chamber system. Experimental results for the attachment behavior of the marine species, *H. pacifica* g, confirmed that in flowing aquatic environments zeolite coatings reduce the extent of initial bacterial attachment across the range of solution chemistry and hydrodynamic conditions tested, which could lower the possible level of biofilm formation. Complementary cell and collector surface characterization suggested a combination of two chemical mechanisms – hydrophobic and electrostatic interactions – contribute to the antifouling nature of the zeolite surface.

Finally, to compliment the previously mentioned work with collector surface roughness, adhesion studies were conducted with polystyrene colloids. The metal collector surfaces were systematically polished to alter the surface roughness from nanoscale to microscale. Chapter 6, "Initial Colloid Deposition on Bare and

Zeolite-Coated Stainless Steel and Aluminum: Influence of Surface Roughness", has been recently submitted to the journal *Langmuir*. The work describes experiments conducted to evaluate the collector surface roughness on colloid deposition and to further elucidate the mechanisms contributing zeolite coatings reducing the extent of initial particle attachment in flowing aquatic environments. The relative importance of surface roughness versus contributions of electrostatic interactions and hydrophobicity to the colloid deposition was discussed thoroughly.

The findings from this doctoral research are summarized in Chapter 7, "Conclusions". Below is a list of the publications which have resulted from this research:

1. G. Chen, and S.L. Walker. 2007. "Role of solution chemistry and ion valence on the adhesion kinetics of groundwater and marine bacteria" *Langmuir* 23:7162-7169.

2. G. Chen, Y. Hong, and S.L. Walker. "Colloidal and bacterial deposition: Role of gravity" *Langmuir*, submitted in August 2009.

3. T.R. Kline, G.X. Chen, and S.L. Walker. 2008. "Colloidal deposition on remotely controlled charged micropatterned surfaces in a parallel-plate flow chamber" *Langmuir* 24:9381-9385.

4. G. Chen, D.E. Beving, R.S. Bedi, Y.S. Yan, and S.L. Walker. 2009. "Initial bacterial deposition on bare and zeolite-coated aluminum alloy and stainless steel" *Langmuir* 25:1620-1626

5. G. Chen, R.S. Bedi, Y.S. Yan, and S.L. Walker. "Initial colloidal deposition on bare and zeolite-coated stainless steel and aluminum alloy: Influence of surface roughness" *Langmuir*, submitted in July 2009.

1.4 REFERENCES

1. Ginn, T. R.; Wood, B. D.; Nelson, K. E.; Scheibe, T. D.; Murphy, E. M.; Clement, T. P. *Adv. Water Resour.* **2002,** 25, (8-12), 1017-1042.

2. Albinger, O.; Biesemeyer, B. K.; Arnold, R. G.; Logan, B. E. *FEMS Microbiol. Lett.* **1994,** 124, (3), 321-326.

3. van der Mei, H. C.; Engels, E.; de Vries, J.; Busscher, H. J. *Caries Res.* **2008,** 42, (1), 19-27.

4. Adoue, M.; Bacchin, P.; Lorthois, S.; Combes, D.; Schmitz, P.; Mercier-Bonin, M. *Chem. Eng. Res. Des.* **2007,** 85, (A6), 792-799.

5. Speth, T. F.; Gusses, A. M.; Summers, R. S. *Desalination* **2000,** 130, (1), 31-44.

6. Speth, T. F.; Summers, R. S.; Gusses, A. M. *Environ. Sci. Technol.* **1998,** 32, (22), 3612-3617.

7. Li, Q.; Logan, B. E. *Water Res.* **1999,** 33, (4), 1090-1100.

8. Borges, M. T.; Nascimento, A. G.; Rocha, U. N.; Totola, M. R. *Braz. J.Microbiol.* **2008,** 39, (3), 457-463.

9. Grasso, D.; Smets, B. F. *J. Disper. Sci. Technol.* **1998,** 19, (6-7), 1081-1106.

10. Chen, J. H.; Czajka, D. R.; Lion, L. W.; Shuler, M. L.; Ghiorse, W. C. *Environ. Health Perspect.* **1995,** 103, 53-58.

11. O'Toole, G.; Kaplan, H. B.; Kolter, R. *Annu. Rev. Microbiol.* **2000,** 54, 49-79.

12. Melo, L. F.; Bott, T. R. *Exp. Therm. Fluid Sci.* **1997,** 14, (4), 375-381.

13. Ross, J. *Smithsonian* **1994,** 24, (11), 40-&.

14. Coetser, S. E.; Cloete, T. E. *Crit. Rev. Microbiol.* **2005,** 31, (4), 213-232.

15. He, Y. L.; Xu, P.; Li, C. J.; Zhang, B. *Water Res.* **2005,** 39, (17), 4110-4118.

16. Goto, Y. *Water Sci. Technol.* **2002,** 46, (11-12), 45-50.

17. Shi, Z.; Neoh, K. G.; Zhong, S. P.; Yung, L. Y. L.; Kang, E. T.; Wang, W. *J. Biomed. Mater. Res. A* **2006,** 76A, (4), 826-834.

18. Yao, K. M.; Habibian, M. T.; O'Melia, C. R. *Environ. Sci. Technol.* **1971,** 5, 1105-1112.

19. Gregory, J. *J. Colloid Interf. Sci.* **1981,** 83, (1), 138-145.

20. Hogg, R.; Healy, T. W.; Fuerstenau, D. W. *T. Faraday Soc.* **1966,** 62, (522P), 1638-1651.

21. Elimelech, M., Gregory, J., Jia, X., Williams, R.A., *Particle Deposition and Aggregation: Measurement, Modeling and Simulation*. Butterworth-Heinemann: 1995; p 441.

22. Vanloosdrecht, M. C. M.; Lyklema, J.; Norde, W.; Zehnder, A. J. B. *Microb. Ecol.* **1989,** 17, (1), 1-15.

23. Boyd, R. D.; Verran, J.; Jones, M. V.; Bhakoo, M. *Langmuir* **2002,** 18, (6), 2343-2346.

24. Smets, B. F.; Grasso, D.; Engwall, M. A.; Machinist, B. J. *Colloid. Surface. B* **1999,** 14, (1-4), 121-139.

25. Truesdail, S. E.; Lukasik, J.; Farrah, S. R.; Shah, D. O.; Dickinson, R. B. *J. Colloid Interf. Sci.* **1998,** 203, (2), 369-378.

26. Rijnaarts, H. H. M.; Norde, W.; Lyklema, J.; Zehnder, A. J. B. *Colloid. Surface. B* **1999,** 14, (1-4), 179-195.

27. Lawler, D. F.; Nason, J. A. *Water Sci. Technol.* **2006,** 53, (7), 1-7.

28. Kuznar, Z. A.; Elimelech, M. *Environ. Sci. Technol.* **2004,** 38, (24), 6839-6845.

29. Chen, J. Y.; Klemic, J. F.; Elimelech, M. *Nano Lett.* **2002,** 2, (4), 393-396.

30. Kalasin, S.; Santore, M. M. *Langmuir* **2008,** 24, (9), 4435-4438.

31. Yiantsios, S. G.; Karabelas, A. J. *Chem. Eng. Sci.* **2003,** 58, (14), 3105-3113.

32. Zhuang, J.; Qi, J.; Jin, Y. *Environ. Sci. Technol.* **2005,** 39, (20), 7853-7859.

33. Busscher, H. J.; Weerkamp, A. H. *FEMS Microbiol. Rev.* **1987,** 46, (2), 165-173.

34. Walker, S. L. *Colloid. Surface. B* **2005,** 45, 181-188.

35. Walker, S. L.; Hill, J. E.; Redman, J. A.; Elimelech, M. *Appl. Environ. Microbiol.* **2005,** 71, 3093-3099.

36. van Loosdrecht, M. C. M.; Lyklema, J.; Norde, W.; Schraa, G.; Zehnder, A. J. B. *Appl. Environ. Microbiol.* **1987,** 53, (8), 1893-1897.

37. Schafer, A.; Harms, H.; Zehnder, A. J. B. *Environ. Sci. Technol.* **1998,** 32, (23), 3704-3712.

38. Gross, M.; Cramton, S. E.; Gotz, F.; Peschel, A. *Infect. Immun.* **2001,** 69, (5), 3423-3426.

39. Kuznar, Z. A.; Elimelech, M. *Langmuir* **2005,** 21, (2), 710-716.

40. Bowen, W. R.; Lovitt, R. W.; Wright, C. J. *J. Mater. Sci.* **2001,** 36, (3), 623-629.

41. Ma, H.; Winslow, C. J.; Logan, B. E. *Colloid. Surface. B* **2008,** 62, (2), 232-237.

42. Zhao, Q.; Liu, Y.; Wang, C.; Wang, S.; Peng, N.; Jeynes, C. *Med. Eng. Phys.* **2008,** 30, (3), 341-349.

43. Shellenberger, K.; Logan, B. E. *Environ. Sci. Technol.* **2002,** 36, (2), 184-189.

44. Mitik-Dineva, N.; Wang, J.; Truong, V. K.; Stoddart, P.; Malherbe, F.; Crawford, R. J.; Ivanova, E. P. *Curr. Microbiol.* **2009,** 58, (3), 268-273.

45. Bhattacharjee, S.; Ko, C. H.; Elimelech, M. *Langmuir* **1998,** 14, (12), 3365-3375.

46. Otto, K.; Elwing, H.; Hermansson, M. *Colloid. Surface. B* **1999,** 15, (1), 99-111.

47. Czaczyk, K.; Bialas, W.; Myszka, K. *Pol. J. Microbiol.* **2008,** 57, (4), 313-319.

48. Li, J.; McLandsborough, L. A. *Int. J. Food Microbiol.* **1999,** 53, (2-3), 185-193.

49. Bos, R.; van der Mei, H. C.; Gold, J.; Busscher, H. J. *FEMS Microbiol. Lett.* **2000,** 189, (2), 311-315.

50. Vanhaecke, E.; Remon, J. P.; Moors, M.; Raes, F.; Derudder, D.; Vanpeteghem, A. *Appl. Environ. Microbiol.* **1990,** 56, (3), 788-795.

51. Taylor, R. L.; Verran, J.; Lees, G. C.; Ward, A. J. P. *J. Mater. Sci.-Mater. M.* **1998,** 9, (1), 17-22.

52. Tang, H. Y.; Cao, T.; Liang, X. M.; Wang, A. F.; Salley, S. O.; McAllister, J.; Ng, K. Y. S. *J. Biomed. Mater. Res. A* **2009,** 88A, (2), 454-463.

53. Emerson, R. J.; Bergstrom, T. S.; Liu, Y. T.; Soto, E. R.; Brown, C. A.; McGimpsey, W. G.; Camesano, T. A. *Langmuir* **2006,** 22, (26), 11311-11321.

54. Barnes, L. M.; Lo, M. F.; Adams, M. R.; Chamberlain, A. H. L. *Appl. Environ. Microbiol.* **1999,** 65, (10), 4543-4548.

55. Gubjornsdottir, B.; Einarsson, H.; Thorkelsson, G. *Food Technol. Biotechnol.* **2005,** 43, (1), 55-61.

56. Song, L. F.; Johnson, P. R.; Elimelech, M. *Environ. Sci. Technol.* **1994,** 28, (6), 1164-1171.

57. Elimelech, M.; Nagai, M.; Ko, C. H.; Ryan, J. N. *Environ. Sci. Technol.* **2000,** 34, (11), 2143-2148.

58. Litton, G. M.; Olson, T. M. *J. Colloid Interf. Sci.* **1994,** 165, 522-525.

59. Kihira, H.; Matijevic, E. *Langmuir* **1992,** 8, 2855-2862.

60. Feick, J. D.; Velegol, D. *Langmuir* **2000,** 16, (26), 10315-10321.

61. Feick, J. D.; Velegol, D. *Langmuir* **2002,** 18, (9), 3454-3458.

CHAPTER 2

ROLE OF SOLUTION CHEMISTRY AND ION VALENCE ON THE ADHESION KINETICS OF GROUNDWATER AND MARINE BACTERIA

ABSTRACT

The role of solution chemistry on bacterial adhesion has been investigated using a radial stagnation point flow (RSPF) system. This experimental system utilized an optical microscope and an image-capturing device to directly observe the deposition kinetics of a groundwater bacterium, *Burkholderia cepacia* G4g, and a marine bacterium, *Halomonas pacifica* g. Experiments were carried out under well-controlled hydrodynamic and solution chemistry conditions, allowing for the sensitivity of bacterial adhesion behavior to be examined under a range of ionic strength and valence (KCl vs. $CaCl_2$) simulating groundwater and marine environments. Complimentary cell characterization techniques were conducted to evaluate the electrophoretic mobility, hydrophobicity, surface charge density and viability of the bacteria under the same range of conditions. Solution chemistry was found to have a marked effect on the electrokinetic and surface properties of bacteria and the quartz collector – and on the resulting rate of bacterial deposition. Comparable adhesion trends were observed for *B. cepacia* G4g and *H. pacifica* g. Specifically, the deposition rates of the two bacteria species in both KCl and $CaCl_2$ solutions increased with ionic strength, a trend consistent with traditional Derjaguin-Landau-Verwey-Overbeek (DLVO) theory which considers the combination of van der Waals and electrostatic double layer interaction forces. However, in some cases, experimental results showed bacterial deposition behavior to deviate from DLVO predictions. Based on the systematic investigation of bacterial

cell characteristics, it was found that Ca^{2+} ions play a distinct role on bacterial surface charge, hydrophobicity and deposition behaviors. It is further suggested that bacterial adhesion is determined by the combined influence of DLVO interactions, electrosteric interactions associated with solution chemistry, and the hydrodynamics of the deposition system.

2.1 INTRODUCTION

Biofouling is the undesired attachment of organisms to surfaces within an aquatic environment[1]. In biofouling the "modification" of the structure does not occur spontaneously but rather in stages. Initially, bacteria and extracellular polymeric substances (EPS) attach to the surface and form a conditioning film[2, 3]. Once microorganisms are attached to a substratum surface, a multi-step process starts leading to the formation of a complex, adhering microbial community that is termed a "biofilm"[4, 5]

Biofouling of solid surfaces submerged in aqueous environments has compromised efficient operation of military equipments and industrial processes[6, 7] due to increased biomass on boats and marine structures, and the clogging of water pipes (e.g. in cooling installation). Huge sums of money are spent annually to combat the consequences of biological fouling in marine and freshwater environments. It is estimated that damage from zebra mussels, *Dreissena polymorpha*, cost more than 5 billion dollars through the year 2000 in the Great Lakes alone[6] as a result of mature biofouling of surfaces.

Biofouling begins with the adhesion of individual microbial cells on solid surfaces. The physical, chemical and biological factors governing this critical step in aquatic systems have been studied extensively and attributed to cell type[8], growth phase[9, 10], collector heterogeneity[11], solution chemistry[12, 13], hydrophobic interactions[14-16], surface charge characteristics[16, 17] and surface macromolecules[18]. These factors have been found to affect many of the interaction forces that govern the approach and adhesion of

a bacterial cell to the surface, such as electrostatic, van der Waals, hydrophobic, hydration, and other specific forces[19]. Hence, if fouling is to be controlled, it is the initial stage of microbial adhesion that must be inhibited and these interaction mechanisms well understood.

Classic Derjaguin-Landau-Verwey-Overbeek (DLVO) theory may be utilized to predict the interaction forces between microorganisms and surfaces. In this theory, the total interaction energies existing between a particle (in this case a bacterium) and a collector surface, is quantified as the sum of van der Waals and electrostatic interactions, both of which decay with separation distance[20]. This approach has proven merits for predicting microbial adhesion under well-controlled environments for certain bacterial species and strains; however, it fails to yield a universally applicable description[21].

The effect of solution chemistry on adhesion is of particular interest for understanding microbial adhesion. It is well known that solution ionic strength (IS) influences the extent of bacterial adhesion to a surface. Increasing the IS leads to a decrease in the thickness of the electrostatic double layer surrounding a bacterium and a surface. As a result, the bacterial cell may approach to a surface to a sufficient proximity such that van der Waals attraction may overcome the repulsive energy barrier between two negatively charged surfaces and result in the bacterium adhering to the surface. Several laboratory studies of bacterial transport through porous media have shown that the higher the IS of the solution, the reduced effect of electrostatic

forces and thus enhanced the retention of bacteria[9, 22, 23]. However, this is not always the case for microbial systems[13, 24]. Kuznar[13] found that no measurable *Cryptosporidium* oocyst deposition was observed up to an IS of 177 mM in the presence of KCl solution, despite the absence of an energy barrier based on DLVO predictions, indicating the involvement of additional non-DLVO incorporated interactions. Similarly, Rijnaarts et al[24] noted at low ionic strengths DLVO-type interactions controlled the extent of bacterial deposition; however, at 0.1M and above steric interactions dominated.

Cation valence in the salt solution is another solution chemistry parameter which can influence the deposition behavior of bacteria in aquatic environments. Huysman and Verstraet[25] concluded that divalent cations increased the attachment of bacteria to the surface compared to monovalent cations. Whereas, Tan[26] observed that there was no significant difference between cell attachment in the presence of $CaCl_2$ or KCl at the same IS. This behavior was attributed to hydrophobic interactions being the dominate interaction force controlling attachment. These conflicting results on the role of ion valence suggest that the mechanisms by which mono- and di-valent cations influence deposition are still not fully understood.

Despite the efforts discussed above, few have focused specifically on the differences of the role of solution chemistry on both marine and groundwater bacterial adhesion. Therefore, to better explain the mechanism of bacterial cell deposition to solid surfaces in different aquatic environment this study was developed. Specifically, the role of solution IS and the presence of mono- versus di-valent cations

on the adhesion kinetics of a model groundwater and marine bacterial species was investigated using a radial stagnation point flow (RSPF) cell. This experimental system has a well-defined flow field, and utilizing a fluorescent microscope and an image-capturing device, the adhesion kinetics of the marine and groundwater bacteria onto the quartz surface was determined in solutions containing either monovalent (KCl) or divalent ($CaCl_2$) salts.

2.2 Materials and Methods

2.2.1 Bacterial cell growth and preparation.

Burkholderia cepacia G4, a groundwater bacterium, and *Halomonas pacifica* ATCC 27122, a marine bacterium, were selected for this study. *B. cepacia* has been reported to be a non-motile, rod-shaped, Gram-negative bacteria[27]. *B. cepacia* G4 has the capacity to degrade chlorinated ethenes and was originally isolated from an industrial waste facility[28, 29]. *H. pacifica* was obtained from ATCC (American Type Culture Collection, Rockville, MD). *H. pacifica* is a non-motile rod-shaped, Gram-negative cell[30]. The strain of *H. pacifica* was identified as Se (IV) reducer[31] and having the capacity to cause serious fouling problems in the marine environment[32, 33].

For visualization of the cells in the experimental system, a plasmid coding for an enhanced green fluorescent protein (EGFP) and gentamicin resistance[34] was introduced into the native *H. pacifica* cells by electroporation[35]. The resulting transformed cell line is referred to as *H. pacifica* g. *B. cepacia* G4 was previously labeled with EGFP and

this cell line is referred to *B. cepacia* G4g[8]. *B. cepacia* G4g cells were incubated in Luria-Bertani broth (LB) (Fisher Scientific, Fair Lawn, NJ) at 37 ºC in the presence of 0.03 g/L gentamicin (Sigma, St. Louis, MO). *H. pacifica* g cells were grown in artificial seawater (Sea Salts, 38.5 $g \cdot l^{-1}$, Sigma), supplemented with bacteriological peptone (Sigma, 5 $g \cdot l^{-1}$) and yeast extract (Sigma, 1 $g \cdot l^{-1}$) at 30 ºC with 0.03 g/L gentamicin. Cells were grown until reaching mid-exponential growth phase (5 hours and 10.25 hours for *B. cepacia* G4g and *H. pacifica* g respectively), at which time they were harvested for use in adhesion and characterization studies. Cells were pelleted by centrifugation (Fisher accuSpin* 3R Centrifuge) for 15 min at 3689 × *g* (Swing Bucket Rotor 7500 4394). The growth medium was decanted and the pellet was resuspended in a KCl or $CaCl_2$ solution (IS of 10 mM). The centrifugation and rinsing step with fresh electrolyte solution was repeated two additional times to remove traces of the growth medium. All electrolyte solutions utilized in cell preparation and experiments were prepared with deionized water (Millipore, Billerica, MA) and reagent-grade KCl or $CaCl_2$ (both Fisher Scientific) with no pH adjustment (pH 5.6–5.8).

2.2.2 Bacterial cell characterization.

Viability tests for the *B. cepacia* G4g and *H. pacifica* g cells were performed using the Live/Dead BacLight® kit (L-7012, Molecular Probes, Eugene, OR) in both KCl and $CaCl_2$ solutions (IS ranging from 1 to 1000mM). The direct counting of the stained live and dead cells was done using an inverted microscope (IX70, Olympus, Japan)

operating in fluorescent mode with a green fluorescence filter set (Chroma Technology Corp., Brattleboro, VT). The viability of the *B.* cepacia G4g and *H. pacifica* g cell cultures both averaged 89% when suspended in KCl and 96% and 95% in $CaCl_2$ solution over the range of IS condition tested, respectively.

The electrophoretic mobility of the bacterial cells was determined using freshly harvested cells suspended in 10 mM electrolyte at an optical density of 0.2-0.25 measured at 546 nm (BioSpec-mini Spectrophotometer, Shimadzu Corp., Kyoto, Japan). Electrophoretic mobility measurements were conducted for cells suspended in either KCl and $CaCl_2$ electrolyte solutions from 1-100mM (the upper limit of the machine) at 25 ºC using a ZetaPALS analyzer (Brookhaven Instruments Corporation, Holtsville, NY) and were repeated at least three times using freshly rinsed cells. The experimentally determined electrophoretic mobility values were converted to zeta potential (ξ) using the Smoluchowski equation[20].

In order to analyze the size of the bacterial cells, an inverted microscope (IX70, Olympus, Japan) operating in phase contrast mode was used to take images of *B. cepacia* G4g and *H. pacifica* g cells. The cells were suspended in an electrolyte solution at an approximate concentration of 10^8 cells/mL in 10 mM KCl and 3.33 mM $CaCl_2$. The images were imported into an image processing program (SimplePCI, Precision Instruments, Inc., Minneapolis, MN) and the individual cell lengths and widths were measured. The average length and width for *B. cepacia* G4g was found to be 2.41±0.13 μm and 1.26±0.08 μm, respectively. For *H. pacifica* g, the average

length and width were 3.08±0.43 μm and 1.28±0.06 μm. The resulting equivalent spherical radius of the *B. cepacia* G4g cell was determined to be 0.88 μm and the *H. pacifica* g cell radius was 0.97 μm.

The relative hydrophobicity of the *B. cepacia* G4g and *H. pacifica* g cells was measured using the semi-quantitative microbial adhesion to hydrocarbons (MATH) test[36]. Samples were prepared by transferring 4 mL of a cell solution (optical density of 0.2–0.25 in 10 mM KCl or 3.33 mM $CaCl_2$ at 546 nm) to a test tube containing 1 mL of *n*-dodecane (laboratory grade, Fisher Scientific). Test tubes were vortexed (AutoTouch Mixer Model 231, Fisher) for 2 min, followed by a 15 min rest period. After this time, allowing for phase separation, the optical density of the cells in the aqueous phase was measured spectroscopically at 546 nm (BioSpec-mini, Shimadzu Corp.) to determine the extent of bacterial cell partitioning between the *n*-dodecane and the electrolyte. The hydrophobicity of each cell type is reported as the percent of total cells partitioned into the hydrocarbon[36].

Potentiometric titrations of *B. cepacia* G4g and *H. pacifica* g cells were conducted to determine the relative acidity of the bacterial surfaces. A microtitrator (798 Titrino, Metroohm, Switzerland) was used with an electrolyte solution first purged with N_2 gas (to remove any dissolved carbon dioxide present) and then with bacterial suspensions (concentration between 4×10^7 and 1×10^8 cells/mL) in 10 mM KCl or 3.33 mM$CaCl_2$. Based upon the total amount of NaOH consumed during the

titration between pHs 4 and 10, the resulting acidity and the corresponding surface charge were determined[37].

The extracellular polymeric substances (EPS) composition, specifically the protein and polysaccharide content, was analyzed after isolating the EPS by an established extraction method[38]. Based on the extraction method, the pellet of concentrated bacterial cells was suspended in a solution containing 0.22% of formaldehyde (ACS grade, Fisher Scientific) and 8.5% of NaCl, and kept at 4°C for two hours. This suspension was centrifuged to re-concentrate the cellular material, and the resulting pellet was rinsed with distilled water and re-centrifuged into pellet form. One gram of the resulting pellet was resuspended in 50 mL of distilled water, lyophilized, and re-suspended in 10 mL of distilled water for further compositional analysis. The analysis of protein was performed by using the Lowry method[39] with Bovine Serum Albumin (BSA, 1 mg/mL) (Fisher BioReagents, Fisher Scientific) as the standard and measured spectroscopically (BioSpec-mini, Shimadzu Corp., Kyoto, Japan) at a wavelength of 500 nm. The analysis of sugars was performed by using the phenol-sulfuric acid method according to Dubois et al.[40] and Xanthan gum (Practical Grade, Fisher Scientific) as the standard. The total carbohydrate content was measured at a wavelength of 488 nm.

2.2.3 Bacterial adhesion experimental setup.

Bacterial deposition experiments were conducted in a RSPF system[23, 41, 42] which consists of a specially blown glass flow chamber installed on the stage of an inverted

fluorescent microscope (IX70, Olympus). Fluid stream enters the chamber from a capillary tube (2mm inner diameter) and impinges upon a quartz microscope cover slip (located 2mm from the end of the tube) at a right angle and flows away in all directions. Fluorescently labeled cells depositing on the quartz were imaged by a 40x objective (UPlanFI, Olympus) focused on the inner surface of the cover slip and using a fluorescent filter set with an excitation wavelength of 480 nm and emission wavelength of 510 nm (Chroma Technology Corp., Brattleboro, VT).

All quartz microscope cover slips (Electron Microscopy Sciences, Ft. Washington, PA) were cleaned by a surfactant, ethanol, and deionized water rinse, followed by submersion in NOCHROMIX® solution (Godax Laboratories, Inc., Takoma Park, MD). After removal from NOCHROMIX® solution and rinsing with de-ionized water, cover slips were mounted in the RSPF flow cell. To achieve favorable, non-repulsive electrostatic conditions, the slides were chemically modified[43] to exhibit a net positive zeta potential of 3.3 mV. This was achieved by exposure of the quartz to a 0.2% (v/v) mixture of (aminoethylaminomethyl)–phenethyltrimethoxysilane (Gelest, Inc., Tullytown, PA) in ethanol for 3–5 min at room temperature and then curing for 90 min at 130 ºC[11]. The electrokinetic properties of the quartz cover slides were determined by a streaming potential analyzer (EKA, Brookhaven Instruments Corp.) with an asymmetric clamping cell[43]. Measurements were obtained in KCl and $CaCl_2$ over the range of ISs used in the deposition experiments. The instrument was first rinsed with 1 L of deionized water followed by 0.5 L of the electrolyte solution used

in the measurement. Prior to the streaming potential measurements being taken, the quartz slide was equilibrated with the corresponding fresh electrolyte solution for 10 min. The zeta potential was calculated from the measured streaming potential as described elsewhere[43].

2.2.4 Determination of bacterial adhesion rate and adhesion efficiency.

Deposition of bacterial cells was recorded with a digital camera (Retiga 1300 Mono Cooled, QImaging) acquiring images every 20 seconds over the course of a 20 min injection and analyzed with the supplied software (SimplePCI, Precision Instruments, Inc., Minneapolis, MN). The number of deposited bacteria was determined for each time interval by comparing the changes between successive images. Inlet concentrations for experiments were maintained at 10^7–10^8 cells/mL. The injected cell concentration was determined for each experiment by directly visualizing and enumerating cells in a counting chamber (Bürker-Türk chamber, Marienfield Laboratory Glassware, Lauda-Konigshofen, Germany). A flow rate of 6.25 mL/min was employed, corresponding to an average capillary flow velocity of 3.32 cm/s. In this system, the Reynolds number is 33.2 and the corresponding Peclet numbers are 3.01 and 2.04 for *H. pacifica* g and *B. cepacia* G4g, respectively. Bacterial cell deposition experiments were conducted using *B. cepacia* G4g and *H. pacifica* g cells, over a range of IS conditions (10 to 1000 mM KCl and 3.33 to 333.3 Mm $CaCl_2$) at ambient pH (5.6–5.8) and temperature (22–25 ºC). The solution chemistry

conditions tested was selected to be representative of the ions and range of ionic strength found in groundwater and seawater[44, 45].

The kinetics of bacterial adhesion in the RSPF system was quantified by calculating the bacterial transfer rate coefficient, k_{RSPF}, which is related to the bacterial deposition flux (number of cells per area per time), J, and the bulk bacterial cell concentration, C_0, via

$$k_{RSPF} = \frac{J}{C_0} \qquad (1)$$

The deposition flux (J) was determined by normalizing the initial slope of the number of deposited cells versus time curve by the microscope viewing area (211 μm × 168 μm).

Theoretical deposition rates under chemically favorable, transport-limited conditions can only be predicted for spherical particles[46]. Hence, these favorable deposition rates cannot be predicted accurately for non-spherical bacteria. Therefore, values for the favorable deposition rate in the RSPF system ($k_{RSPF, fav}$) were determined experimentally for the *B. cepacia* G4g and *H. pacifica* g in 10mM KCl. Favorable, non-repulsive conditions were achieved in the RSPF system by using a quartz microscope slide with a net positive zeta potential, achieved by modifying the microscope slides with aminosilane (described earlier). The average bacterial transfer rate coefficient under favorable conditions for the *B. cepacia* G4g cells is 4.26×10^{-7} m/s and 3.87×10^{-7} m/s for *H. pacifica* g. The reported k_{RSPF} and $k_{RSPF, fav}$ values represent

the average of a minimum of three different runs, each utilizing a fresh cell suspension.

The corresponding adhesion (attachment) efficiency in the RSPF system, α, was calculated by normalizing the bacterial transfer rate coefficient at each IS by the transfer rate coefficient determined under favorable electrostatic conditions:

$$\alpha = \frac{k_{RSPF}}{k_{RSPF,fav}} \qquad (2)$$

α is indicative of the success of a cell attaching to the quartz surface. Theoretically, α should be between 0 and 1[46].

2.3 RESULTS AND DISCUSSION

2.3.1 Electrokinetic properties of *B. cepacia* G4g and *H. pacifica* g cells.

The zeta potentials of the B. cepacia G4g and H. pacifica g cells are presented in Figure 2.1. The results indicate that both the groundwater and marine bacteria used in this study are negatively charged over the range of IS and pH (5.6–5.8) conditions tested. For both strains, the absolute magnitude of the cell zeta potential decreased with an increase in salt concentration (in either KCl or $CaCl_2$) as expected from electrostatic double layer compression which occurs in the presence of either 1:1 or 2:1 electrolytes. The microbes in KCl solutions exhibited a much more negative zeta potential than those in $CaCl_2$ solutions. Figure 2.1 also shows that the cell type with the least negative zeta potential is *H. pacifica g* in $CaCl_2$ solution, while the most

negative potential is found for *B. cepacia* G4g in KCl solution. Although slightly less negative, the zeta potentials of *B. cepacia G4g* in $CaCl_2$ solution are close to *H. pacifica* g in $CaCl_2$ solution. This is likely due to Ca^{2+} complexing with bacteria surface proteins resulting in charge neutralization[47]. Therefore, the much less negative zeta potentials of cells are observed at the corresponding IS in presence of Ca^{2+} ions. These zeta potential values were used to calculate the DLVO interaction energy profiles between the bacteria and the quartz surfaces which are presented later in this paper.

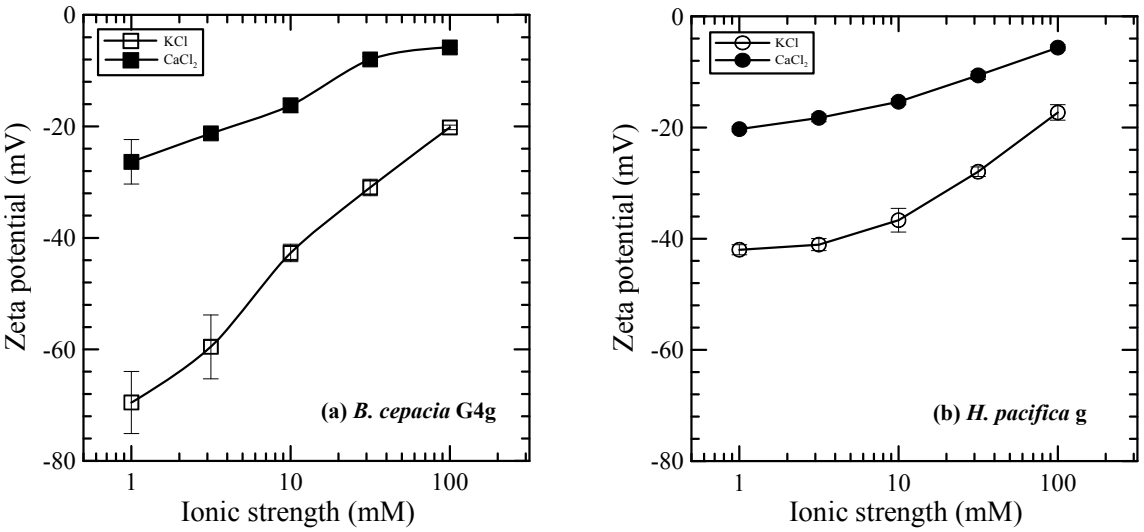

Figure 2.1 Zeta potential of *B. cepacia* G4g and *H. pacifica* g cells as a function of IS (either KCl or $CaCl_2$ solution). Experiments were carried out at ambient pH (5.6-5.8) and temperature (22-25 ºC). Error bars indicate one standard deviation.

2.3.2 Adhesion behavior of *B. cepacia* G4g and *H. pacifica* g.

The adhesion characteristics of the bacteria suspended in either KCl or $CaCl_2$ solutions is shown in Figure 2.2, where values of the attachment efficiency (α) are plotted as a function of solution IS. It is evident from this figure that IS and presence of

$CaCl_2$ have a marked effect on the adhesion kinetics for both bacteria. General trends are similar for both species, with increasing adhesion with IS; after which the attachment efficiencies approach a maximum and plateau. The IS above which deposition was insensitive to further changes in solution chemistry was distinct for each cell type. Additionally, there was no measurable deposition below a certain IS. However, IS below which deposition was immeasurable was also specific to cell type and the presence of K^+ or Ca^{2+} ions. Figure 2.2 (a) indicates that the attachment efficiencies of *B. cepacia* G4g were determined as 0.26 and 0.08 in 100 mM KCl and 10 mM $CaCl_2$, respectively; and below these IS, there was no measurable cell adhesion. With further increase in IS to approximately 316 mM, α value appears to reach a maximum value of 0.89 in KCl and approaches unity in $CaCl_2$. *H. pacifica* g displays subtly different deposition behavior (Fig. 2b). The attachment efficiency of *H. pacifica* g is 0.12 at an IS of 180 mM in KCl, and increases up to a value of 0.72 at 1M. Above this point the adhesion efficiency does not increase further even at notably higher IS conditions; rather the adhesion efficiency effectively plateaus. When *H. pacifica g* cells were suspended in $CaCl_2$ solution, α was determined to be 0.26 at IS of 31.6 mM and reaching a maximum value near unity at approximately 56 mM. For the marine species, no measurable bacterial deposition was observed at IS conditions below 180 mM in KCl solution and 31.6 mM in $CaCl_2$ solution. Generally speaking, the *H. pacifica* g suspended in $CaCl_2$ exhibited higher attachment efficiency values as compared with cells suspended in the KCl solution, with the only exception occurring

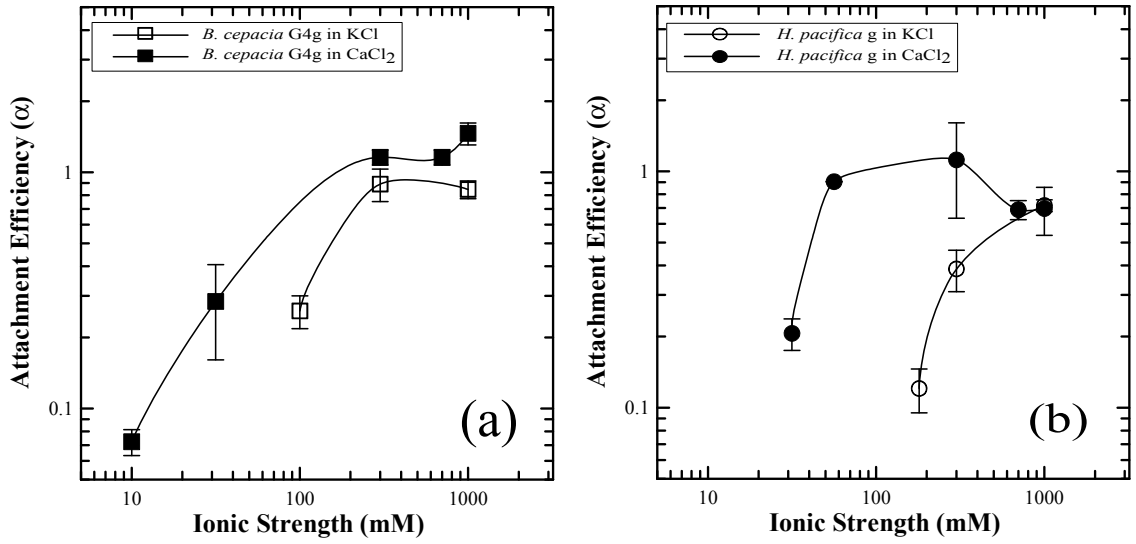

Figure 2.2 Adhesion (attachment) efficiency, α, of *B. cepacia* G4g and *H. pacifica* g onto quartz collector surface in RSPF system, determined as a function of IS (KCl and $CaCl_2$). Experiments were carried out at ambient pH (5.6-5.8) and temperature (22-25ºC). Error bars indicate one standard deviation.

at the highest IS conditions tested where the cells reached a transport-limited deposition regime. This shows that Ca^{2+}, a divalent cation known to complex with bacterial surface polymers[47], has a significant effect on deposition kinetics.

To understand better the observed deposition behavior, particularly the difference of the attachment efficiencies in KCl and $CaCl_2$ solutions for both bacteria, the classic DLVO theory for colloidal stability[48] has been applied and these interaction energy calculations are described here. To calculate the DLVO interaction energy profile, the repulsive electrostatic interaction energy was obtained using the constant surface potential interaction expression of Hogg et al.[49], and the expression of Gregory[50] was used to determine the retarded van der Waals attraction energy. Sphere-plate geometry was assumed when calculating the interaction energies between the bacteria and

surface. In the calculation, a value of Hamaker constant of 6.5×10^{-21} J was chosen, similar to which has been reported for other microbial particles interacting with quartz in an aqueous media[8, 51, 52]. Finally, the experimentally determined zeta potentials of both the bacteria and the quartz (see Figure 2.1 and Table 2.1) were used in the place of surface potentials in these calculations. The resulting calculated energy barriers are presented in Table 2.1. There were no energy barriers (Table 2.1) existing for the *B. cepacia* G4g cells in 31.6 mM KCl solution and for the *H. pacifica* g cells in 31.6 mM KCl solution and 3.33 mM $CaCl_2$ solution (IS is 10 mM); however, no measurable deposition was observed at these conditions in the RSPF experiments, which suggests the limitations of theoretical DLVO predictions in the experimental system.

Table 2.1 Energy Barrier Height (kT) as a function of IS for *B. cepacia* G4g and *H. pacifica* g as Calculated by DLVO Theory [a]

IS (mM)	Quartz zeta potential (mV)[c]		*B.cepacia*	*B.cepacia*	*H. pacifica* g in	*H. pacifica* g in
	KCl	$CaCl_2$	G4g in KCl	G4g in $CaCl_2$	KCl	$CaCl_2$
1	-24.7	-16.05	1061	341	1005	301
3.16	-25.2	-12.75	1024	162	950	151
10	-19.8	-5.6	510	0.8	503	NB
31.6	-4.2	-4.91	NB b	NB	NB	NB
100	-3.41	1.05	NB	NB	NB	NB

[a] Calculations were done assuming a Hamaker constant of 6.5×10^{-21}J and using the bacterial size values reported in Table 2.2.

[b] NB: no energy barrier.

[c] Measured zeta potentials of quartz in solutions of KCl and $CaCl_2$ (1-100 mM)

2.3.3 Characterization of *B. cepacia* G4g and *H. pacifica* g cells.

To better understand what factors caused the deviation between the experimental deposition behavior and the predicted from DLVO theory for both bacteria, further

characterization techniques were employed. The first distinction between the groundwater and marine cells was observed in the measurement of cell size. Under the microscope, it was confirmed that both bacteria strains were rod-shape. The equivalent spherical radius was calculated from the experimentally measured lengths and widths of cells. *H. pacifica* g cells were found to be approximately 10% larger than *B. cepacia* G4g cells. The size difference between the two cell types may have contributed to the transport and subsequent adhesion behavior. This was determined to be the case through experiments conducted under chemically favorable, transport-limited conditions. The resulting transfer rate coefficient under favorable conditions ($k_{RSPF,fav}$) for *B. cepacia* G4g was found to be approximately 10% greater than that of *H. pacifica* g in KCl solution (refer to Table 2.2 for $k_{RSPF,fav}$ values). This relationship suggests that size is involved somewhat in the extent of transport of bacterial cells to the collector surface. However, it was observed that the size of cells was unaffected by the presence of either K^+ or Ca^{2+} (Table 2.2). This suggests that cell size cannot be credited with causing the variation in adhesion trends observed between cells in presence of the monovalent versus divalent ions.

Analysis of the cell hydrophobicity employing the MATH test established 56.5% of *B. cepacia* G4g cells in KCl solution partitioned into n-dodecane, whereas only 17.6% of the *H. pacifica* g in KCl solution partitioned into the hydrocarbon. Similarly, for cells suspended in $CaCl_2$ solution, 70.6% of *B. cepacia* G4g and 23.8% of *H. pacifica* g cells partitioned into n-dodecane. When cells were suspended in $CaCl_2$ solution, both

bacteria were more hydrophobic as compared with cells suspended in KCl solution. A similar trend has been observed previously in the literature[47]. Overall, the data reported in Table 2.2 indicates that more *B. cepacia* G4g cells partitioned into hydrocarbon compared with *H. pacifica* g cells in solutions suggesting *B. cepacia* G4g is the more hydrophobic of the two bacterial species.

Table 2.2 Characterization of *B. cepacia* G4g and *H. pacifica* g cells

Cell Strain	Radius (μm)[a]	$k_{RSPF,fav}$ (x 10^{-7}m/s)	Acidity (meq/10^8 cell)[b]	Surface charge (μC/cm^2)[c]	MATH[d] (%)	Live[e] (%)
B. cepacia G4g in KCl	0.88±0.08	4.26±0.32	3.4×10^{-5}	443	56.5±0.005	89±2
B. cepacia G4g in $CaCl_2$	0.88±0.08		3.0×10^{-5}	389	70.6±0.002	96±1
H. pacifica g in KCl	0.97±0.03	3.87±0.30	2.6×10^{-5}	182	17.6±0.002	89±2
H. pacifica g in $CaCl_2$	0.97±0.03		1.8×10^{-5}	150	23.8±0.003	95±1

[a] Value for equivalent spherical radius calculated from experimentally measured length and width of individual cells.

[b] Acidity determined from the amount of NaOH consumed during a titration between pH 4 and 10 for cells suspended in 10 mM electrolyte (KCl or $CaCl_2$) solution.

[c] Indicates the density of charged functional groups across the cell surface. Value determined from the experimentally measured acidity, and accounting for the exposed surface area of the cells (calculated for a spherical cell) and Faraday's constant of 96,485 C/mol.

[d] Microbial adhesion to hydrocarbon (MATH) indicates the relative hydrophobicity of the cell as the percent of cells partitioned in dodecane versus 10mM electrolyte (KCl or $CaCl_2$).

[e] Percent of cell population determined to be viable based on the Live/Dead BacLight® kit at 10 mM (KCl or $CaCl_2$). Values are the average of viability measured in triplicate.

The results of the potentiometric titrations are presented in Table 2.2 as the acidity and titrated surface charge density. Acidity (in units of milliequivalents per 10^8 cells) indicates the amount of NaOH consumed by suspended whole cells during a titration

between pH value of 4 and 10[37]. The surface charge density was calculated from the acidity and accounting for the surface area of a cell and provides a measure of the total charged functional groups not only on the outer membrane surface, but within the extracellular polymeric matrix as well. This characterization method indicates that *B. cepacia* G4g and *H. pacifica* g exhibit a considerable difference in surface chemistry. Specifically, *B. cepacia* G4g has almost 2.5 times the number of charged groups as *H. pacifica* g in KCl solution. As indicated in Table 2.2, the titrated surface charge densities are 443 and 182 $\mu C/cm^2$ for *B. cepacia* G4g and *H. pacifica* g in KCl solutions, respectively. When bacteria suspended in KCl solution, the bacteria exhibits a slightly higher charge density than the same bacteria cells suspended in $CaCl_2$ solution.

The viability measurement showed that the *B. cepacia* G4g and *H. pacifica* g exhibited almost equal viability in the identical solution chemistry. Specifically, the viability of cells in KCl solution averaged 89%, whereas 96% for *B. cepacia* G4g in $CaCl_2$ solution and 95% for *H. pacifica* g in $CaCl_2$ solution. Interestingly, both cells suspended in $CaCl_2$ solution were more viable than those in KCl solution likely due to a favorable metabolic response of cells to the presence of Ca^{2+} [53-55]. These results are summarized in Table 2.2.

The experimentally determined values for bacterial EPS presence and composition (Table 2.3) indicate that *B. cepacia* G4g has greater amount of total EPS, as well as relative amounts of protein and polysaccharide than *H. pacifica* g. The total EPS,

protein and polysaccharide content for 10^{11} cells of *B. cepacia* G4g cells are 93.3 mg, 20.63 mg and 10.38 mg, respectively, while corresponding values for *H. pacifica* g are 22.6 mg, 6.9 mg and 4.95 mg. It is important to note the relative content of the protein as compared to sugar was substantially higher for *B. cepacia* G4g than for *H. pacifica* g. This higher total and relative protein content is likely responsible for the greater surface charge density observed via titration. Additionally, the higher hydrophobicity of the groundwater bacteria may be attributed to the polysaccharide content being greater than the marine strain.

Table 2.3 EPS presence and composition of *B. cepacia* G4g and *H. pacifica* g cells

	EPS (mg) [a]	Protein (mg) [b]	Polysaccharide (mg) [c]
B. cepacia G4g	93.3±10.3	20.6±0.7	10.4±0.6
H. pacifica g	22.6±6.0	4.2±2.4	4.9±4.4

[a] based on 10^{11} cells

[b] based on Bovine Serum Albumin (BSA) as the standard.

[c] based on Xanthan gum as the standard.

2.3.4 Adhesion mechanisms of *B. cepacia* G4g and *H. pacifica* g in RSPF system.

Bacterial adhesion to a collector surface is controlled by two major factors: the bacterial cell transport to a collector surface and the subsequent interactions between the cell and surface that occur upon close approach. The size of the cell and hydrodynamics of the system control the transport of the bacteria, meanwhile the adhesion is determined by the near surface interactions, including such forces as

DLVO-type (electrostatic and van der Waals), electrosteric, hydrophobic, and hydration. The observed sensitivity of both groundwater and marine bacteria adhesion to IS (Figure 2.2) indicates that electrostatic forces dominate interactions between bacterial cells and quartz surface. As indicated by measured zeta potentials (Figure 2.1 and Table 2.1), both bacterial cells and quartz surfaces were negatively charged under measured solution conditions, suggesting that repulsive interactions should dominate cell deposition. The magnitude of repulsive electrostatic interactions are sensitive to the solution IS, with an increase in the IS resulting in a decrease of electrostatic repulsive force and a higher bacterial attachment efficiency (α). This is the case for the interactions between bacteria and quartz under unfavorable conditions.

As mentioned in section 3.2, deviation was observed between DLVO predictions and experimental results. If DLVO type interactions, dominated by electrostatic repulsion, were the only mechanisms involved, bacteria cells should adhere to the quartz surface under the conditions indicated as having no energy barrier to deposition in Table 2.1. This was obviously not the case from Figure 2.2, suggesting additional interaction mechanisms must play a role in the deposition of the cells which are not incorporated with traditional DLVO theory. In the RSPF system, bacterial cells interacting with quartz also experience hydrodynamic, electrosteric, and hydration forces when approaching the surface, which are not accounted for the DLVO theory. These factors can decrease the bacterial attachment efficiency[13, 46, 56, 57]. Therefore, the

adhesion behavior of both species was dependent on a combination of DLVO and non-DLVO type interactions between the cell surfaces and the quartz.

2.3.5 Influence of solution chemistry and valence on bacterial deposition kinetics.

Over the range of conditions evaluated, bacteria suspended in $CaCl_2$ solutions exhibited higher attachment efficiency as compared with the same cell type suspended in the KCl solution for both marine and groundwater species, except at the highest ISs where bacteria reach the transport-limited deposition regime. The adhesion efficiency trends also suggest that the effect of solution chemistry is more pronounced for *H. pacifica* g than for *B. cepacia* G4g. These observations suggest an underlying distinction in how groundwater versus the marine cells respond to solution chemistry and subsequently how their fate in aquatic environments may differ. Such characteristics as electrokinetic properties, cell viability, cell size, EPS production, surface charge, and cell hydrophobicity may explain the variations in deposition behavior; however, the deposition behavior may also be attributed to other local-scale cell characteristics which were often overlooked in bacteria transport studies[9, 58].

Kuznar[13, 18] and Chen[59] previously reported that Ca^{2+} has a substantial effect on particle interactions and found significantly lower deposition and aggregation rates in the presence of a monovalent salt (KCl) compared to a divalent salt ($CaCl_2$). Similar to these studies, the sensitivity to ion valence was observed and the deposition behavior attributed to the binding of bacterial surface polymers by Ca^{2+} ions. It has been noted in the literature that calcium ions can bind the surface polymers of bacteria and alter the

conformation of these polymers – ultimately influencing which functional groups remain exposed[60]. This causes variation in polymer conformation and results in a change in the degree of the forces acting between the surface and the approaching bacteria. The presence of calcium also impacts the bacterial surface characteristics, which experimentally determined values of surface charge and hydrophobicity confirmed (Table 2.2). The surface charge decreased by 18% and the hydrophobicity increased by 35% for *H. pacifica* g when suspended in $CaCl_2$ versus KCl; whereas, the corresponding decrease in surface charge and increase in hydrophobicity were 12% and 25% for *B. cepacia* G4g, respectively.

Previous work has demonstrated the affinity of bacteria for a surface increases with IS up to 0.1M[61, 62]. Above this point there often is a decrease in bacterial attachment to a surface at high salt concentrations (>0.1 M). These current results and earlier studies[8] also point toward this phenomenon. The data in Figure 2.2 indicate that the attachment efficiencies for *B. cepacia* G4g (KCl and $CaCl_2$) and *H. pacifica* g ($CaCl_2$) slightly decrease after α reaching a plateau, except for *H. pacifica* g in KCl which reaches a maximum value a the highest IS tested. (1 M). This is likely because of electrosteric forces occurring between bacterial surface polymers (EPS) and the quartz surface at high IS conditions. Steric interactions between outer cell surface macromolecules and the substratum surface can be repulsive or attractive, depending on the ionic strength of the suspending medium[20]. At lower ionic strengths, steric interactions promote cell deposition due to the cell surface polymers "bridging"

between the cell and collector surface[20]. However, at these lower ionic strength conditions electrostatic repulsion will dominate and minimize cell-surface interactions. Above a certain ionic strength (dependent upon the solution chemistry and the functionality of the cell polymers), steric interactions can overcome the electrostatic repulsion and contribute to cell deposition[20]. Finally, based upon the polymers and solution chemistry, steric interactions can become repulsive and inhibit further deposition[24]. This is due to the presence of ions suspended among the polymers, which lead to the polymers being more rigid. This rigidity minimizes the ability of the polymers to re-conform and interact directly with the quartz surface. In the experiments discussed herein, the electrosteric forces are likely repulsive when the ionic strength is greater than 300 mM, as demonstrated by the attachment efficiency decreasing at these higher ionic strength conditions (Figure 2.2).

In section 2.2.4 it was noted that the attachment efficiency (α) value theoretically should be between 0 and 1. However, Figure 2.2 indicates that our experimentally determined α values exceed unity when bacteria were suspended in $CaCl_2$ solution. This suggests that the bacterial transfer rate coefficients (k_{RSPF}) under such conditions are greater than the coefficients achieved under chemically favorable, mass transport-limited conditions ($k_{RSPF,\,fav}$). A possible reason for this phenomenon is that aminosilane modified quartz is highly positively charged and the bacteria are near neutral. This may result in electrostatic repulsion, decreasing the resulting $k_{RSPF,\,fav}$ even under conditions otherwise considered transport limited. Under the same solution

chemistry (high IS $CaCl_2$), quartz is near neutral or negatively charged and repels the microorganisms to a lesser degree. This can result in values of $k_{RSPF}>k_{RSPF,fav}$ and subsequently values of α greater than one.

2.3.6 Distinction of bacterial deposition kinetics between groundwater and marine bacteria.

It has been observed that solution chemistry has a more significant effect on the adhesion behavior of the marine bacteria investigated. Additional evidence of this can be found in Figure 2.2 in which the data indicates that the IS at which bacterial adhesion efficiency approaches a plateau is much higher for *H. pacifica* g than for *B. cepacia* G4g in presence of KCl. This trend does not hold in the presence of $CaCl_2$. Other pieces of evidence are found in the analysis of the cells in the presence of Ca^{2+} versus K^+. The surface charge density decreased by 18% and the hydrophobicity increased by 35% for *H. pacifica* g, when suspended in KCl versus $CaCl_2$, whereas the corresponding values are 12% and 25% for *B. cepacia* G4g. The likely reason for these trends is that Ca^{2+} ions neutralize the surface polymer function groups outside bacteria and bind the surface polymer as discussed in section 3.5. Notably, it was observed that the *Halomonas* cells were much more sensitive to the Ca^{2+} ions as evident by the variation of key cell characteristics such as surface charge and hydrophobicity as noted above.

Cellular deposition and the strengthening of attachment have been attributed to the presence of EPS[9, 63, 64]. The amount of EPS, specifically the protein and polysaccharide

content, was analyzed and is shown in Table 2.3. This data provides another indication of the subtle local-scale differences between the groundwater and marine species which can contribute to the extent of interactions between the cells and quartz surfaces. Based on theoretical and experimental studies to date, the presence of surface charge heterogeneity can decrease electrostatic repulsion at the local scale and increase the rate of irreversible particle attachment [65-70]. *B. cepacia* G4g has greater amount of total EPS, protein and sugar than *H. pacifica* g (Table 2.3). The groundwater species has higher acidity and surface charge likely because of its greater protein content, and is more hydrophobicity because of its greater sugar content. Therefore the EPS appears to enhance the heterogeneity of the *B. cepacia* G4g surface and results in greater attachment.

In this study, the equivalent spherical radius of *H. pacifica* g and *B. cepacia* G4g cells were slightly smaller than 1 μm. In this size range a combination of transport mechanisms. interception and diffusion, dominates the bacterial transport process[71]. The magnitude of the Peclet number can indicate which of the mechanisms (convection versus diffusion) dominates in the process of particle transport. Specifically, $Pe<1$ suggests diffusion-dominated and $Pe\geq10$ implies convection-dominated flow regimes[20]. As noted in section 2.4, in our system the Peclet numbers are 3.01 and 2.04 for *H. pacifica* g and *B. cepacia* G4g, respectively. Both Peclet numbers are very small and indicate a combination of transport phenomena; however, suggesting diffusion likely plays a substantial role in the bacterial transport process. The diffusion

coefficient of suspended *B. cepacia* G4g cells will be 10% greater than that of *H. pacifica* g cells, based on the Stokes-Einstein relationship ($D_\infty=kT/(6\pi\mu a_p)$)[20], where D_∞ is the diffusion coefficient of a spherical particle of radius a_p subject to a flow characterized by fluid viscosity μ; k is the Boltzmann constant and T is temperature. This is due to the groundwater cells being 10% larger than their marine counterpart. Based upon traditional filtration theory, this will result in a greater value of single collector efficiency[72] for *B. cepacia* G4g than *H. pacifica* g under the same solution chemistry conditions. In fact, this was observed experimentally with the bacterial transfer rate coefficiency ($k_{RSPF,\ fav}$) of *B. cepacia* G4g under chemically favorable, transport-limited conditions in KCl solution was 10% greater than that of *H. pacifica* g. We also observed that the adhesion efficiencies of *H. pacifica* g were lower than those of *B. cepacia* G4g cells in the presence of the monovalent salt across the same range of experimental conditions tested. However, this is not the case when bacteria were suspended in $CaCl_2$ solution likely due to ion valence having a significant effect on the bacterial adhesion behavior as discussed previously.

2.4 CONCLUSION

The radial stagnation point flow (RSPF) experimental system was employed to thoroughly investigate the role of solution chemistry and ion valence on the adhesion kinetics of groundwater and marine bacteria, *B. cepacia* G4g and *H. pacifica* g respectively. The experiment results indicate that the adhesion properties of both

groundwater and marine microorganisms are markedly sensitive to solution IS and valence. Deposition trends suggest both marine and groundwater bacterial species adhesion kinetics are governed by the combination of DLVO and non-DLVO type interactions.

The solution chemistry and valence have marked influence on the cell deposition kinetics for both groundwater and marine species; however, the deposition kinetics of marine species *H. pacifica* g appears to be much more sensitive to solution chemistry than that of groundwater species *B. cepacia* G4g. Combined with extensive cell characterization, further insight into bacterial deposition kinetics was obtained regarding the presence of the divalent ion Ca^{2+}. Calcium can bind the surface polymers of bacteria and alter the conformation of these polymers, and it is by this mechanism that Ca^{2+} ions are responsible for the distinct adhesion behavior of the cells under the solution chemistry conditions.

2.5 REFERENCES

(1) Cooksey, K. E.; Wigglesworthcooksey, B. *Aquat. Microb. Ecol.* **1995,** 9, (1), 87-96.

(2) Sreekumari, K. R.; Nandakumar, K.; Kikuchi, Y. *Biofouling* **2001,** 17, (4), 303-316.

(3) Kerr, A.; Cowling, M. J. *Philos. Mag.* **2003,** 83, (24), 2779-2795.

(4) O'Toole, G.; Kaplan, H. B.; Kolter, R. *Annu. Rev. Microbiol.* **2000,** 54, 49-79.

(5) Melo, L. F.; Bott, T. R. *Exp. Therm. Fluid Sci.* **1997,** 14, (4), 375-381.

(6) Ross, J. *Smithsonian* **1994,** 24, (11), 40-&.

(7) Coetser, S. E.; Cloete, T. E. *Crit. Rev. Microbiol.* **2005,** 31, (4), 213-232.

(8) Walker, S. L. *Colloid. Surface. B* **2005,** 45, (3-4), 181-188.

(9) Walker, S. L.; Redman, J. A.; Elimelech, M. *Environ. Sci. Technol.* **2005,** 39, (17), 6405-6411.

(10) Walker, S. L.; Hill, J. E.; Redman, J. A.; Elimelech, M. *Appl. Environ. Microbiol.* **2005,** 71, (6), 3093-3099.

(11) Chen, J. Y.; Klemic, J. F.; Elimelech, M. *Nano Lett.* **2002,** 2, (4), 393-396.

(12) Li, Q.; Logan, B. E. *Water Res.* **1999,** 33, (4), 1090-1100.

(13) Kuznar, Z. A.; Elimelech, M. *Environ. Sci. Technol.* **2004,** 38, (24), 6839-6845.

(14) Vanloosdrecht, M. C. M.; Lyklema, J.; Norde, W.; Schraa, G.; Zehnder, A. J. B. *Appl. Environ. Microbiol.* **1987,** 53, (8), 1893-1897.

(15) Schafer, A.; Harms, H.; Zehnder, A. J. B. *Environ. Sci. Technol.* **1998,** 32, (23), 3704-3712.

(16) Vanloosdrecht, M. C. M.; Lyklema, J.; Norde, W.; Schraa, G.; Zehnder, A. J. B. *Appl. Environ. Microbiol.* **1987,** 53, (8), 1898-1901.

(17) Gross, M.; Cramton, S. E.; Gotz, F.; Peschel, A. *Infect. Immun.* **2001,** 69, (5), 3423-3426.

(18) Kuznar, Z. A.; Elimelech, M. *Langmuir* **2005,** 21, (2), 710-716.

(19) Busscher, H. J.; Weerkamp, A. H. *FEMS Microbiol. Rev.* **1987,** 46, (2), 165-173.

(20) Elimelech, M., Gregory, J., Jia, X., Williams, R.A., *Particle Deposition and Aggregation: Measurement, Modeling and Simulation*. ed.; Butterworth-Heinemann: 1995; 'Vol.' p 441.

(21) Vanloosdrecht, M. C. M.; Lyklema, J.; Norde, W.; Zehnder, A. J. B. *Microb. Ecol.* **1989,** 17, (1), 1-15.

(22) Rijnaarts, H. H. M.; Norde, W.; Bouwer, E. J.; Lyklema, J.; Zehnder, A. J. B. *Environ. Sci. Technol.* **1996,** 30, (10), 2877-2883.

(23) Redman, J. A.; Walker, S. L.; Elimelech, M. *Environ. Sci. Technol.* **2004,** 38, (6), 1777-1785.

(24) Rijnaarts, H. H. M.; Norde, W.; Lyklema, J.; Zehnder, A. J. B. *Colloid. Surface. B* **1999,** 14, (1-4), 179-195.

(25) Huysman, F.; Verstraete, W. *Biol. Fertil. Soils* **1993,** 16, (1), 21-26.

(26) Tan, Y.; Bond, W. J.; Griffin, D. M. *Soil Sci. Soc. Am. J.* **1992,** 56, (5), 1331-1340.

(27) Camesano, T. A.; Logan, B. E. *Environ. Sci. Technol.* **1998,** 32, (11), 1699-1708.

(28) Steffan, R. J.; Sperry, K. L.; Walsh, M. T.; Vainberg, S.; Condee, C. W. *Environ. Sci. Technol.* **1999,** 33, (16), 2771-2781.

(29) MunakataMarr, J.; McCarty, P. L.; Shields, M. S.; Reagin, M.; Francesconi, S. C. *Environ. Sci. Technol.* **1996,** 30, (6), 2045-2052.

(30) Dobson, S. J.; Franzmann, P. D. *Int. J. Syst. Bacteriol.* **1996,** 46, (2), 550-558.

(31) Siddique, T.; Zhang, Y. Q.; Okeke, B. C.; Frankenberger, W. T. *Bioresour. Technol.* **2006,** 97, (8), 1041-1049.

(32) Bakker, D. P.; Busscher, H. J.; van Zanten, J.; de Vries, J.; Klijnstra, J. W.; van der Mei, H. C. *Microbiol.-SGM* **2004,** 150, 1779-1784.

(33) Bakker, D. P.; Huijs, F. M.; de Vries, J.; Klijnstra, J. W.; Busscher, H. J.; van der Mei, H. C. *Colloid. Surface. B* **2003,** 32, (3), 179-190.

(34) Stuurman, N.; Bras, C. P.; Schlaman, H. R. M.; Wijfjes, A. H. M.; Bloemberg, G.; Spaink, H. P. *Mol. Plant-Microbe Interact.* **2000,** 13, (11), 1163-1169.

(35) Sambrook, J.; Fritsch, E. F.; Maniatis, T., *Molecular Cloning, A Laboratory Manual*. 2nd ed.; Cold Spring Harbor Laboratory Press: Cold Spring Harbor, New York, 1989; 'Vol.' 3, p.

(36) Pembrey, R. S.; Marshall, K. C.; Schneider, R. P. *Appl. Environ. Microbiol.* **1999,** 65, (7), 2877-2894.

(37) Shim, Y.; Lee, H. J.; Lee, S.; Moon, S. H.; Cho, J. *Environ. Sci. Technol.* **2002,** 36, (17), 3864-3871.

(38) Azeredo, J.; Lazarova, V.; Oliveira, R. *Water Sci. Technol.* **1999,** 39, (7), 243-250.

(39) Switzer, R.; Garrity, L., *Experimental Biochemistry*. ed.; W.H. Freeman Publishing: 1999; 'Vol.' p.

(40) Dubois, M.; Gilles, K. A.; Hamilton, J. K.; Rebers, P. A.; Smith, F. *Anal. Chem.* **1956,** 28, (3), 350-356.

(41) Walker, S. L.; Redman, J. A.; Elimelech, M. *Langmuir* **2004,** 20, (18), 7736-7746.

(42) Adamczyk, Z.; Zembala, M.; Siwek, B.; Czarnecki, J. *J. Colloid Interf. Sci.* **1986,** 110, (1), 188-200.

(43) Walker, S. L.; Bhattacharjee, S.; Hoek, E. M. V.; Elimelech, M. *Langmuir* **2002,** 18, (6), 2193-2198.

(44) Deutsch, W. J., *Groundwater geochemistry: fundamentals and applications to contamination*. ed.; Lewis publishers: New York, 1997; 'Vol.' p 29.

(45) Goldberg, E. D., *Chemistry- The oceans as a chemical system*. ed.; Wiley-Interscience: New York, 1963; 'Vol.' p 2-25.

(46) Brow, C. N.; Li, X. Q.; Ricka, J.; Johnson, W. P. *Colloid. Surface. A* **2005,** 253, (1-3), 125-136.

(47) Khemakhem, W.; Ammar, E.; Bakhrouf, A. *World J. Microbiol. Biotechnol.* **2005,** 21, (8-9), 1623-1631.

(48) Derjaguin, B. V.; Landau, L. *Acta Physicochim U.S.S.R.* **1941,** 14, 733-763.

(49) Hogg, R.; Healy, T. W.; Fuerstenau, D. W. *T. Faraday Soc.* **1966,** 62, (522P), 1638-1651.

(50) Gregory, J. *J Colloid Interf. Sci.* **1981,** 83, (1), 138-145.

(51) Truesdail, S. E.; Lukasik, J.; Farrah, S. R.; Shah, D. O.; Dickinson, R. B. *J. Colloid Interf. Sci.* **1998,** 203, (2), 369-378.

(52) Simoni, S. F.; Bosma, T. N. P.; Harms, H.; Zehnder, A. J. B. *Environ. Sci. Technol.* **2000,** 34, (6), 1011-1017.

(53) Dilworth, M. J.; Rynne, F. G.; Castelli, J. M.; Vivas-Marfisi, A. I.; Glenn, A. R. *Microbiol.-UK* **1999,** 145, 1585-1593.

(54) Norris, V.; Grant, S.; Freestone, P.; Canvin, J.; Sheikh, F. N.; Toth, I.; Trinei, M.; Modha, K.; Norman, R. I. *J. Bacteriol.* **1996,** 178, (13), 3677-3682.

(55) Turakhia, M. H.; Characklis, W. G. *Biotechnol. Bioeng.* **1989,** 33, (4), 406-414.

(56) Dabros, T.; Vandeven, T. G. M. *Physicochem. Hydrodynam.* **1987,** 8, (2), 161-172.

(57) McWhirter, M. J.; McQuillan, A. J.; Bremer, P. J. *Colloid. Surface. B* **2002,** 26, (4), 365-372.

(58) Waar, K.; van der Mei, H. C.; Harmsen, H. J. M.; Degener, J. E.; Busscher, H. J. *Microbiol.-SGM* **2002,** 148, 1863-1870.

(59) Chen, K. L.; Mylon, S. E.; Elimelech, M. *Environ. Sci. Technol.* **2006,** 40, (5), 1516-1523.

(60) Rose, R. K. *Biochim. Biophys. Acta-General Subjects* **2000,** 1475, (1), 76-82.

(61) Marshall, K. C.; Stout, R.; Mitchell, R. *J. Gen. Microbiol.* **1971,** 68, (NOV), 337-&.

(62) Gordon, A. S.; Millero, F. J. *Appl. Environ. Microbiol.* **1984,** 47, (3), 495-499.

(63) Frank, B. P.; Belfort, G. *J. Membr. Sci.* **2003,** 212, (1-2), 205-212.

(64) Olofsson, A. C.; Hermansson, M.; Elwing, H. *Appl. Environ. Microbiol.* **2003,** 69, (8), 4814-4822.

(65) Song, L. F.; Johnson, P. R.; Elimelech, M. *Environ. Sci. Technol.* **1994,** 28, (6), 1164-1171.

(66) Elimelech, M.; Nagai, M.; Ko, C. H.; Ryan, J. N. *Environ. Sci. Technol.* **2000,** 34, (11), 2143-2148.

(67) Litton, G. M.; Olson, T. M. *J. Colloid Interf. Sci.* **1994,** 165, 522-525.

(68) Kihira, H.; Matijevic, E. *Langmuir* **1992,** 8, 2855-2862.

(69) Feick, J. D.; Velegol, D. *Langmuir* **2000,** 16, (26), 10315-10321.

(70) Feick, J. D.; Velegol, D. *Langmuir* **2002,** 18, (9), 3454-3458.

(71) Tufenkji, N.; Elimelech, M. *Environ. Sci. Technol.* **2004,** 38, (2), 529-536.

(72) Yao, K. M.; Habibian, M. M.; Omelia, C. R. *Environ. Sci. Technol.* **1971,** 5, (11), 1105-&.

CHAPTER 3

COLLOIDAL AND BACTERIAL DEPOSITION: ROLE OF GRAVITY

ABSTRACT

The role of gravitational force on the deposition of 0.5, 1.1, 1.8 μm carboxylate-modified polystyrene latex (CML) microspheres and bacterium *Burkholderia cepacia* G4g has been evaluated using a parallel plate flow chamber system. This experimental system utilized an inverted and an upright optical microscope attached with image-capturing devices to directly observe and determine the deposition kinetics onto glass surfaces located at the top and bottom of the flow chamber. Deposition kinetics was quantified at 10 mM KCl under electrostatically unfavorable and favorable attachment conditions and at two flow rates (0.06 and 3 mL/min), simulating the range of flow velocities from groundwater to rapid granular filtration. Comparing the particle deposition kinetics onto the top and bottom surfaces under identical flowing exposure time, fluid chemistries and hydrodynamic conditions, results showed that significant differences were observed between the two surfaces, suggesting that gravity was a significant driving force for the initial stages of deposition of particles that were larger than 1 μm size. This was further supported by additional deposition experiments with 1.1 μm microspheres suspended in a deuterium oxide (D_2O)/water mixture (heavy water) where the density of colloid and the suspending heavy water were effectively the same. Under this condition, deposition rates were observed to be identical between the top and bottom surfaces. Results from normal and heavy water solutions indicated that the greater deposition of colloidal particles larger than 1 (m on the bottom in normal water solutions is due to gravity.

Finally, the experimental results were compared with deposition studies using smaller 0.5 (m colloids as well as some theoretical calculations of expected rates of particle deposition.

3.1 Introduction

The phenomena of colloidal particle (e.g. abiotic or biotic) transport and adhesion in flowing suspensions onto solid surfaces are of great significance to many environmental and technological processes. Examples include bacterial pathogen fate and transport in groundwater environments, which is relevant to our drinking water supply safety, and in granular filtration processes for water and wastewater treatment[1]. Understanding and predicting the transport and adhesion of colloidal particles in natural subsurface environments as well as engineered systems is a challenging problem[2] because it involves a combination of physical and chemical factors (as well as biological for biotic colloids) including solution chemistry[3, 4], collector surface heterogeneity[5], hydrodynamic condition[6, 7], particle property[8], etc. acting at the solid/water interface which may affect the interaction forces governing the approach and adhesion of a particle to the surface, such as gravitational, electrostatic, van der Waals, hydrophobic, hydration, and other specific forces[9].

Traditionally, colloidal deposition is considered the outcome of two consecutive steps: (i) particle transport from the bulk of a flowing suspension to the collector surface and (ii) attachment. The first step for which the basic mechanisms include diffusion, interception, and sedimentation is primarily governed by physical factors. The second step is controlled by physicochemical interactions between colloids and collector surface such as electrostatic interactions and van der Waals forces. In porous media, particle transport is quantified by the collection efficiency (η), the ratio of

particles striking the collector to particles flowing toward the collector. There are a few analytical correlation equations available to calculate η by integrating individual contributions of each transport mechanism (diffusion, interception, and sedimentation).[10-12] Practically, colloidal transfer rate coefficient (k)[13, 14] or Sherwood number (Sh)[15, 16] are often determined experimentally or theoretically to characterize the transport and attachment of particles in porous media[13, 14], parallel plate flow chamber[15, 16], and radial stagnation point flow cell[13, 14] systems. Due to the complex nature of porous media, the parallel plate flow chamber[17-21] is a technique widely used to investigate the fundamental mechanisms governing colloid and bacterial transport and adhesion in aqueous environments, which simulates when flow is parallel to the collector surface in porous media. The advantages of this system include direct observation of the model particle deposition process by a microscopy technique and a well-defined hydrodynamic flow fieldas would exist in porous media.

Micron-sized colloids are of particular interest as the classical filtration theory predicts a minimum removal efficiency existing for colloids with size about 1 μm under typical conditions where particle transport is dominated by diffusion.[10] The relative importance of diffusion and sedimentation contributing to particle deposition can be evaluated by the dimensionless group $G = \frac{4\pi a^4(\rho_p - \rho)g}{3k_B T}$, where a is particle radius, ρ_p is the specific density of the particle, ρ is the specific density of fluid, g is the acceleration due to gravity, k_B is Boltzmann constant, and T is temperature; which

represents the ratio of the gravitational potential of a particle located one particle radius above the collector to the thermal energy that drives diffusion[22]. A value of unity would be the transition point from diffusion to sedimentation dominance[22]. For instance, in the case of polystyrene particles (ρ_p = 1.055 g/cm^3) with diameter of 1.1 μm suspended in water at 25°C the value of G would be 0.05, which suggests diffusion dominating particle deposition. This is in agreement with the calculations of the collection efficiency predicted by the correlation equations proposed by Tufenkji and Elimelech[12]. Notably, for 1.1 μm diameter colloids when representative groundwater fluid velocity (1.3×10^{-4} m/s) in porous media is assumed, with porosity of 0.36[23], and collector diameter of 0.3 mm, the diffusion term (η_D) and gravitational term (η_G) are 3.88×10^{-3} and 1.03×10^{-4}, respectively. The diffusion term is one order of magnitude higher than the gravitational term, which also indicates diffusion dominance when utilizing filtration theory to predict colloid transport and removal. This is also the case for larger 1.8 μm polystyrene particles where the diffusion term is still one order of magnitude greater than the settling term as predicted by the correlation equation by Tufenkji and Elimelech[12]. In addition, classical filtration theory is widely used for the predicting bacterial transport and fate in porous media[24, 25] and similar diffusion dominance would be predicted for bacteria under the above conditions assumed. Conversely, bacterial cell deposition studies[26, 27] on an inclined flat plate showed that cell deposition from a suspension on the underside of the surface was

limited, if not negligible, even for favorable conditions, suggesting that gravity dominated cell transport to the surface.

The objective of this study was to quantitatively demonstrate the contribution of gravity on polystyrene colloid and bacterial cell deposition in an aquatic environment. A parallel plate flow chamber system was utilized for this purpose. The flow chamber was mounted on an inverted and an upright optical fluorescent microscope attached with image-capturing devices so that the rate of individual particle transfer to the collector surface could be calculated. This experimental system has a well-defined flow field[16], and allowed for the direct observation and determination of mass transfer rates on test surfaces either on the top or bottom of the flow chamber, where gravity was assumed to minimize or enhance particle deposition, respectively. Deposition was quantified on both chemically unfavorable (glass) and favorable surfaces (modified glass surface). Two representative flow rates, 0.06 and 3 mL/min (i.e. fluid velocities 1.3×10^{-4} and 6.6×10^{-3} m/s), simulating the range of flow velocities in groundwater and in rapid granular filtration, respectively, were utilized for the study. Additionally, experiments were conducted in a deuterium oxide/water mixture with identical specific density to polystyrene microspheres using 1.1 μm colloids, eliminating the effect of gravitational force. These experimental results have been compared with theoretical calculations to determine the magnitude of the gravitational contribution.

3.2 MATERIALS AND METHODS

3.2.1 Colloid and bacterial cell selection and preparation.

Fluorescent carboxylate-modified polystyrene latex microspheres (Invitrogen, Eugene, OR) were utilized as model colloids for the deposition experiments. The monodispersed colloids had a mean diameter of 0.5, 1.1 and 1.8 μm, respectively. The specific density of colloids was 1.055 g/cm^3.

Burkholderia cepacia G4, a groundwater bacterium was selected for this study. *B. cepacia* has been reported to be a non-motile, rod-shaped, Gram-negative bacteria[28]. For visualization of the cells in the experimental system, a plasmid coding for an enhanced green fluorescent protein (EGFP) and gentamicin resistance[29] was previously introduced into the native *B. cepacia* G4 cells by electroporation[30]. The resulting transformed cell line is referred to *B. cepacia* G4g[31]. *B. cepacia* G4g cells were incubated in Luria-Bertani broth (LB) (Fisher Scientific, Pittsburgh, PA) at 37 ºC in the presence of 0.03 g/L gentamicin (Sigma, St. Louis, MO). Cells were grown until reaching mid-exponential growth phase (5 hours), at which time they were harvested for use in deposition and characterization studies. Cells were pelleted by centrifugation (Fisher accuSpin* 3R Centrifuge) for 15 min at 3689 × *g* (Swing Bucket Rotor 7500 4394). The growth medium was decanted and the pellet was resuspended in a 10 mM KCl solution. The centrifugation and rinsing step with fresh electrolyte solution was repeated two additional times to remove traces of the growth medium. All electrolyte solutions utilized in cell preparation and experiments were prepared with

deionized water (Millipore, Billerica, MA) and reagent-grade KCl (Fisher Scientific) with no pH adjustment (pH 5.6–5.8).

3.2.2 Colloid and bacterial cell characterization.

The electrophoretic mobility of the colloids and bacterial cells was determined using freshly suspended colloids and harvested cells in 10mM KCl electrolyte solutions at 25 °C. Measurements were made using a ZetaPALS analyzer (Brookhaven Instruments Corporation, Holtsville, NY) and were repeated at least three times. The Smoluchowski equation[32] was used to convert the experimentally determined electrophoretic mobility values to zeta potentials.

In order to analyze the size of the bacteria, an inverted microscope (IX70, Olympus, Japan) operating in phase contrast mode was used to take images of the *B. cepacia* G4g cells. Cells were suspended in an electrolyte solution at an approximate concentration of 10^8 cells/mL in 10 mM KCl. The images were imported into an image processing program (SimplePCI, Precision Instruments, Inc., Minneapolis, MN), and the individual cell lengths and widths were measured. The average length and width for *B. cepacia* G4g were found to be 2.41±0.13 μm and 1.26±0.08 μm, respectively. The resulting equivalent spherical diameter of the *B. cepacia* G4g cell was 1.76 μm.

3.2.3 Deposition experiments.

Colloidal and bacterial deposition experiments were conducted in a rectangular parallel plate flow chamber system (Product number: 31-010, GlycoTech, Rockville,

MA) installed on the stage of an inverted fluorescent microscope (IX70, Olympus, Center Valley, PA) or an upright fluorescent microscope (BX-52, Olympus, Center Valley, PA). The parallel plate flow chamber (inner dimensions of 6 cm × 1 cm × 0.762 mm) consisted of a Plexiglass block, a flexible silicon elastomer gasket, and a microscope glass slide. Chambers were sealed with a thin film of vacuum grease on the gasket. The deposition of fluorescently labeled colloids and bacterial cells onto the glass surfaces were imaged by an infinity corrected 40x objective (Olympus UPlanFI, N.A. 0.75) focused near the center on the inner surface of the test surface. Imaging was done using a Xe lamp with a fluorescent filter set, excitation of 480 nm and emission of 510 nm (Chroma Technology Corp., Brattleboro, VT).

In order to decouple the effect of gravity and hydrodynamic interaction and justify theoretical calculations, select deposition experiments for 1.1 μm CML colloids were carried out in a mixture of deuterium oxide (Sigma-Aldrich Co., St. Louis, MO) / water / KCl (ionic strength of 10 mM) having a density of 1.06 g/cm^3 determined by a specific gravity hydrometer (Fisher Scientific, Pittsburgh, PA) under favorable conditions. Suspending the colloids into such a mixture and centrifuging the suspension at 14,000 g for 30 minutes, no sedimentation was observed. In this way, the contribution of particle sedimentation on deposition measurements was eliminated.

All microscope glass slides (Fisher Scientific, Pittsburgh, PA) were cleaned by a surfactant, ethanol, and deionized water rinse before deposition experiments and characterization[15]. To achieve favorable, non-repulsive electrostatic conditions, the

slides were chemically modified to exhibit a net positive zeta potential[33]. This was achieved by exposure of the glass slide to a 0.2% (v/v) mixture of (aminoethylaminomethyl)–phenethyltrimethoxysilane (Gelest, Inc., Tullytown, PA) in ethanol for 3–5 min at room temperature and then curing for 90 min at 130 ºC[5]. The electrokinetic properties of the glass slides were determined by a streaming potential analyzer (EKA, Brookhaven Instruments Corp.) with an asymmetric clamping cell[33] at 10 mM KCl, as was used in the deposition experiments. The zeta potential was calculated from the measured streaming potential as described previously[33].

3.2.4 Quantification of colloid deposition onto test surfaces.

Colloidal and bacterial deposition were recorded with digital cameras attached to the inverted fluorescent microscope (Retiga 1300 Mono Cooled, Qimaging, British Columbia) and the upright fluorescent microscope (Demo Retiga EXI Monochrome, QImaging) acquiring images every 20 seconds for 30 min time period (length of experiment) and then analyzed with the supplied software (SimplePCI, Precision Instruments, Inc., Minneapolis, MN). Data acquisition and analysis methods have been previously reported.[34] Briefly, the number of deposited colloids was determined for each time interval by accounting for changes in particle deposition between successive images. Colloid and bacterial cell injection concentrations were maintained at 5×10^7 particles/mL over the course of the experiment. Flow rates of 3 mL/min and 0.06 mL/min were employed, corresponding to average flow velocities of 23.6 m/h, which is in the range of typical fluid rates in a rapid granular filtration bed, and 37.2

feet/day which is in the range of groundwater flow, respectively. The Reynolds number of the colloids and bacterial cells was between 6.56×10^{-5} and 0.012, corresponding to Peclet numbers in the range of 2.4×10^{-5} and 0.22, both indicative of a diffusion-dominated transport regime at these respective velocities. All experiments were conducted at ionic strength of 10 mM KCl, and an ambient pH (5.5-5.8) and temperature (22–25 ºC).

The kinetics of colloidal and bacterial adhesion in the parallel plate flow chamber system was quantified by calculating the particle transfer rate coefficient, k, which is related to the particle deposition flux (number of particles per area per time), J, and the bulk particle concentration, C_0, via

$$k = \frac{J}{C_0} \qquad (1)$$

The deposition flux (J) was determined by normalizing the initial slope of the number of deposited particles versus time curve by the microscope viewing area (211 μm × 168 μm). A transfer rate coefficient was calculated for both test surfaces located at the top and bottom of the flow chamber, which were expressed in terms of k_{Top} and k_{Bottom}, respectively.

Deposition rates under chemically favorable, transport-limited conditions can only be predicted for spherical particles[35], not for rod-shaped bacteria. Therefore, values for the favorable deposition rate in the parallel plate flow chamber system (k_{fav}) were determined experimentally for both the colloids and *B. cepacia* G4g on the top and

bottom surfaces separately. Favorable, non-repulsive conditions were achieved in the parallel plate flow chamber system by using a microscope glass slide with a net positive zeta potential, achieved by modifying the microscope slides with aminosilane as described earlier.

3.3 RESULTS AND DISCUSSION

3.3.1 Characterization of surfaces.

To determine the extent of electrostatic interactions between particles (colloids and bacteria) and collector surfaces, zeta potential measurement was employed. The colloids exhibited zeta potentials of -84.10 ± 1.43, -118.17 ± 0.98 and -96.39 ± 2.38 mV for 0.5, 1.1 and 1.8 μm colloids, respectively, when suspended in an aqueous 10 mM KCl solution. Meanwhile, the zeta potential of *B. cepacia* G4g cells suspended in the same electrolyte solution was -43.2 ± 1.23 mV. The results indicate that both the colloids and bacterial cells used in this study are highly negatively charged at pH 5.6–5.8, with the 1.1 μm colloids possessing the most negative zeta potentials in 10 mM KCl. This is likely due to the colloids having the greatest density of carboxylate on the latex microsphere surface[36]. Note that the colloids exhibited a much more negative zeta potential than the bacterial cells.

The glass slide exhibited a negative zeta potential (-42.5±0.2 mV) and the amine-terminated silane coated glass was positively charged (+3.3 mV)[34] at 10 mM KCl. Hence, repulsive electrostatic conditions should exist between the particles and

bare glass and chemically favorable conditions achieved between the positively charged coated glass and particles. These zeta potential values were used to calculate the DLVO interaction energy profiles between the colloids and the glass surfaces[34]. The profiles showed 800–3100 kT energy barriers existing for model colloids and bacterial cells when these particles approaching a bare glass surfaces, which indicated highly "unfavorable" conditions (DLVO profiles not shown).

3.3.2 Colloid and bacterial deposition trends in 10 mM KCl.

The deposition behavior of the colloids and bacteria suspended in KCl solutions is reported in Table 3.1 and Figure 3.1, where the values of particle transfer rate coefficient (k) onto the top and bottom surfaces of the parallel plate flow chamber are plotted as a function of particle size and surface chemistry. It is evident from this figure that particle size, collector surface location and surface chemistry have a marked influence on the deposition kinetics for the three model colloids and bacteria at both flow conditions.

General trends of deposition are similar for all particles at both flow rates. For bottom surfaces, greater deposition was observed under favorable versus unfavorable conditions, colloid deposition increased with particle size, and bacterial deposition was more than the colloids even though the diameter of bacterial cells are slightly less than 1.8 μm. For top surfaces, significantly less deposition was observed than on the bottom for either unfavorable or favorable conditions. For instance, the deposition rates on top versus bottom surfaces were $(1.17 \pm 0.12) \times 10^{-9}$ and $(2.37 \pm 0.14) \times 10^{-9}$, respectively,

under unfavorable conditions for 0.5 μm colloids at the lower flow rate. The one exception to this was that under unfavorable conditions, statistically similar values of k were observed for 0.5 μm colloids on the top and bottom surfaces at the higher flow rate. Deposition onto the top surface for these smaller colloids was measurable under these conditions, whereas it was immeasurable under the same favorable conditions for 1.8 μm colloids and bacterial cells. Under favorable conditions, particle transfer rates on bottom surfaces were greater at 3 mL/min (Figure 3.1b) than 0.06 mL/min (Figure 3.1a) for all particles tested in the current study. This is likely attributed to greater mass transport to the surface, even though particles may experience larger hydrodynamic forces at the higher velocity. However, the difference between deposition on the top and bottom surfaces was more significant at the lower flow rate (0.06 mL/min). For example, 603 ± 21% greater deposition was observed at 10 mM for 1.1 μm colloids on the bottom surface than the top under favorable conditions at the lower flow rate, while the number increased to122 ± 5% at 3 mL/min. Therefore, the difference in particle transfer rates between top and bottom surfaces was more pronounced at the lower flow rate in which particles experienced longer residence times in the parallel plate flow chamber.

Table 3.1 The particle transfer rate coefficients determined for the bottom and top flow channel surfaces under favorable conditions for 0.5, 1.1, 1.8 μm colloids and *B. cepacia*, G4g. Theoretical values of particle transfer rate coefficients obtained from equation 2 are reported as k_{Ideal}. The particle settling velocities (v_s) were calculated by Stoke's Law for colloids and bacteria. Experimental results and theoretical values are reported for both flow rates

Particle	Flow rate (mL/min)	k_{Bottom} (m/s)	k_{Ideal} (m/s)	k_{Top} (m/s)	v_s (m/s)
0.5 μm colloids	0.06	$7.00 \pm 0.40 \times 10^{-9}$	1.59×10^{-8}	$4.64 \pm 0.24 \times 10^{-9}$	7.71×10^{-9}
1.1 μm colloids		$3.34 \pm 0.10 \times 10^{-8}$	9.43×10^{-9}	$4.75 \pm 0.66 \times 10^{-9}$	3.73×10^{-8}
1.8 μm colloids		$6.36 \pm 0.15 \times 10^{-8}$	6.72×10^{-9}	0	1.03×10^{-7}
B. cepacia G4g		$8.21 \pm 0.36 \times 10^{-8}$	6.89×10^{-9}	0	1.71×10^{-7}
0.5 μm colloids	3	$3.40 \pm 0.16 \times 10^{-8}$	5.88×10^{-8}	$2.58 \pm 0.04 \times 10^{-8}$	7.71×10^{-9}
1.1 μm colloids		$6.29 \pm 0.14 \times 10^{-8}$	3.47×10^{-8}	$2.83 \pm 0.10 \times 10^{-8}$	3.73×10^{-8}
1.8 μm colloids		$7.50 \pm 0.12 \times 10^{-8}$	2.53×10^{-8}	0	1.03×10^{-7}
B. cepacia G4g		$9.30 \pm 0.69 \times 10^{-8}$	2.54×10^{-8}	0	1.71×10^{-7}

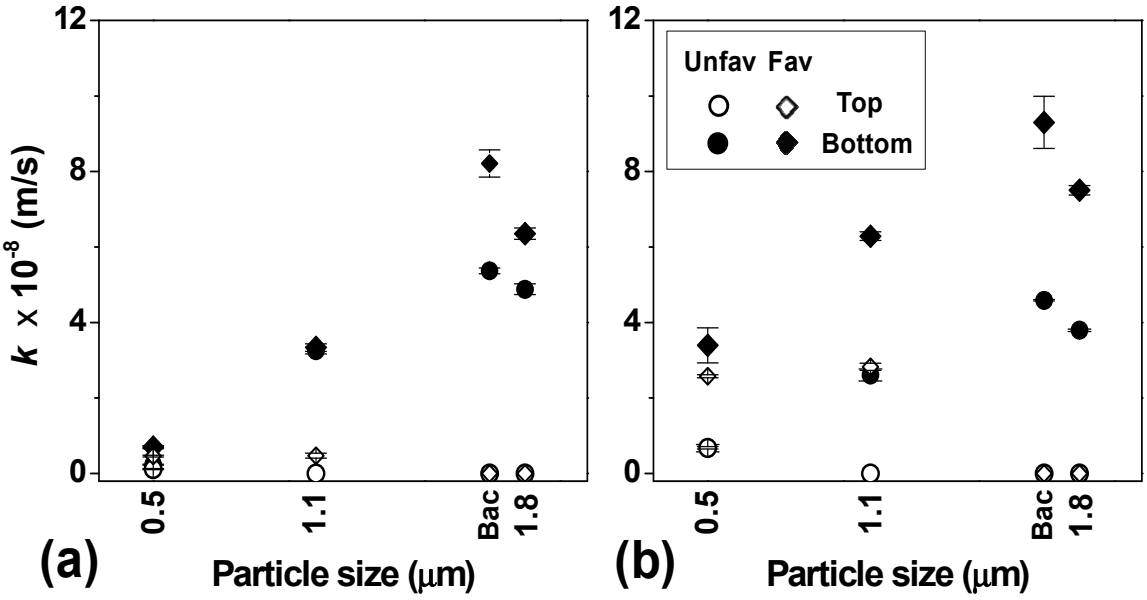

Figure 3.1 Colloidal and bacterial transfer rate coefficients determined for the bottom and top flow channel surfaces for 0.5, 1.1, 1.8 μm colloids and *B. cepacia*, G4g in 10 mM KCl. Data reported for glass and aminosilane modified-glass to achieve unfavorable and favorable electrostatic interactions, respectively. Experiments were conducted at A) 0.06 mL/min and B) 3 mL/min. Error bars indicate one standard deviation.

3.3.3 Colloid deposition trends in heavy water (10 mM KCl).

The adhesion kinetics of 1.1 μm colloids suspended in a D_2O/H_2O/KCl mixture under favorable conditions is shown in Table 3.2. Results indicate that colloidal deposition trends in this suspension were completely different than the aqueous solution at either flow rate. Notably, in the heavy water in which the density of the colloids and that of the suspending fluid are virtually the same, similar deposition rates were observed between the top and bottom surfaces. This confirmed that in the absence of gravity and sedimentation forces particle transfer to these surfaces are virtually identical. Interestingly, 6-10% higher deposition rates on the top surfaces versus the bottom surfaces were observed at both flow rates, which may be attributed to colloidal buoyancy as the density of the D_2O/H_2O/KCl mixture (1.06 g/cm^3) was slightly greater than the polystyrene colloids (1.055 g/cm^3). Specifically, 10.7 ± 1.1% more of the 1.1 μm colloids adhered on the top versus bottom surfaces at the lower flow rate (0.06 mL/min), whereas the number became to 6.2 ± 0.8% at 3 mL/min. This is a similar trend with the 1.1 μm colloids in the normal water solution where the greater deposition difference between the bottom and top surfaces takes place at the lower flow rate due to the longer residence times. These results also further suggest that the greater deposition observed on the bottom as opposed to the top surfaces for the model particles in normal aqueous solutions is due to gravity (section 3.2). The gravitational force enhanced the mass transfer of model particles to the bottom surface, while reducing deposition on the top surface.

Table 3.2 Colloidal transfer rate coefficients determined for the bottom and top flow channel surfaces for 1.1 μm colloids under electrostatically favorable conditions in a 10 mM D_2O/H_2O/KCl mixture. Theoretical values calculated from equation 2 are reported as k_{Ideal} for comparison with experimental results

Particle	Flowrate (mL/min)	k_{Bottom} (m/s)	k_{Ideal} (m/s)	k_{Top} (m/s)
1.1 μm colloids	0.06	$9.55 \pm 0.12 \times 10^{-9}$	9.43×10^{-9}	$1.07 \pm 0.04 \times 10^{-8}$
1.1 μm colloids	3	$3.47 \pm 0.03 \times 10^{-8}$	3.47×10^{-8}	$3.70 \pm 0.04 \times 10^{-8}$

3.3.4 Theoretical calculations of particle transfer rate coefficients.

Traditionally, the convection-diffusion equation has been used to describe colloidal particle transport and deposition from flowing suspensions onto collector surfaces in systems such as granular filtration[10, 12] and a parallel plate flow chamber[16, 37]. However, an analytical solution for such an equation is difficult to achieve. Instead, numerical and approximate solutions such as Smoluchowski-Levich (SL) approximation have been suggested.[12, 16] In the SL approximation, it is assumed that all particles adhere irreversibly (favorable conditions) when sufficiently close to a collector surface, and any external forces including gravity and hydrodynamic corrections are neglected. In this case, the local particle transfer rate coefficient (k_{Ideal}) can be expressed as[16]:

$$k_{Ideal} = \frac{J}{C_0} = \frac{Sh_{Ideal} D_\infty}{a_p} = \frac{D_\infty}{\Gamma(4/3) a_p} \left(\frac{2Pe}{9x/b}\right)^{1/3} \qquad (2)$$

where Sh_{Ideal} is the dimensionless Sherwood number, a_p is the particle radius, D_∞ (= $k_B T/(6\pi\mu a_p)$) is the bulk diffusion coefficient calculated from the Stokes-Einstein equation, μ is fluid dynamic viscosity, Pe is the Peclet number that is equal to $3ua_p^3/(2b^2D_\infty)$ in the parallel plate configuration[32], u is the fluid velocity, x is equal to

half of the flow chamber length, b is midway depth of the parallel plate flow channel, and the gamma function $\Gamma(4/3)$ is equal to 0.893[20].

The calculations of the particle transfer rate coefficients as obtained from the SL approximation (k_{Ideal}) are presented in Table 3.1 and 3.2. As suggested by Equation 2 that k_{Ideal} is proportional to $a_p^{(-2/3)}$, the particle transfer rate coefficients decrease with particle size (Table 3.1). Notably, the theoretical calculations agreed with the experimental observations of 1.1 μm colloids in heavy water experiments ($k_{Top} \cong k_{Ideal} \cong k_{Bottom}$) for both flow rates (Table 3.2). Considering the assumption of the SL approximation that gravity and hydrodynamic corrections are insignificant, the observation of the relationship ($k_{Top} \cong k_{Ideal} \cong k_{Bottom}$) for both flow rates confirms this point for 1.1 μm colloids suspended in heavy water.

Table 3.1 compares the particle transfer rate coefficients as obtained from the SL approximation (k_{Ideal}) and the experimentally determined particle transfer rate coefficients for both the bottom (k_{Bottom}) and top (k_{Top}) surfaces (also plotted in Figure 3.1) for the colloids and bacterial cells under favorable conditions. For 0.5 μm colloids, a relationship of $k_{Top}<k_{Bottom}<k_{Ideal}$ was observed at two flow rates. This is consistent with Wit's observation[37] for 814 nm polystyrene microspheres, in which experimentally determined initial particle deposition rates were smaller than those obtained from the SL approximation. The larger (1.1 and 1.8 μm) colloids and bacterial cells followed a consistent trend of $k_{Top}<k_{Ideal}<k_{Bottom}$. The difference between k_{Ideal} and

k_{Bottom} increased with particle size at both flow rates. k_{Bottom} was a full order of magnitude greater than k_{Ideal} for the bacterial cells at the low flow rate.

The observed and calculated transfer rates followed a different trend for the smallest (0.5 μm) colloids. Notably, $k_{Top}<k_{Bottom}$ for 0.5 μm colloids obtained under the same chemical and hydrodynamic conditions, suggesting that gravitational force enhanced transport of the particles to the lower surface and reduced transfer to the upper plate simultaneously. However, both k_{Top} and k_{Bottom} were less than k_{Ideal}. This suggests at this smaller particle size, hydrodynamic interactions prevent such colloids from depositing and gravity is not a substantial contributor to deposition, otherwise the relationship $k_{Bottom}\geq k_{Ideal}$ would have been observed due to the contribution from gravity.

The relationship of $k_{Top}<<k_{Bottom}$ of the larger colloids and bacterial cells indicates an enhanced particle transfer to the bottom surfaces and dramatically reduced transfer to the top surfaces, which suggests that gravity is much more important for the particles greater than 1 μm in diameter (i.e., 1.1 and 1.8 μm colloids and bacteria) than previously predicted by the classical filtration theory presented in the introduction section. In addition, as suggested by the experimental observations in the $D_2O/H_2O/KCl$ mixture, in which similar transfer rates were observed between top, bottom surfaces and theoretical calculations ($k_{Top}\cong k_{Ideal}\cong k_{Bottom}$) for both flow rates, hydrodynamic interactions were insignificant in influencing larger colloids and bacterial cell deposition under our experimental conditions.

3.3.5 Role of sedimentation on colloidal and bacterial deposition kinetics.

Based on the momentum balance for a spherical particle suspended in a fluid, the particle settling velocity (Re < 1) derived from Stokes's law can be expressed as [38]:

$$\frac{dv_s}{dt} = \left(\frac{\rho_p - \rho}{\rho_p}\right) g - \frac{18\mu v_s}{d_p{}^2 \rho_p} \qquad (3)$$

where v_s is the particle settling velocity, ρ_p is the specific density of the particle, ρ is the specific density of fluid, μ is fluid dynamic viscosity, d_p is particle diameter, g is the acceleration due to gravity and t is the elapsed time.

After reaching steady state, the particle settling velocity can be calculated by the following equation[38]:

$$v_s = \frac{g(\rho_p - \rho) d_p{}^2}{18\mu} \qquad (4)$$

Ignoring the interaction between particles and the collector wall in the vicinity of the wall[39], the calculated particle settling velocities for each particles at 0.06 mL/min are the same as those for the corresponding particles at 3.0 mL/min, as shown in Table 3.2, since the Reynolds numbers for two velocities range from 6.6×10^{-5} and 0.012, which are less than 1[1]. 1.055 g/cm^3 was used for specific gravity (ρ_p) of polystyrene colloids. Specific gravities of bacteria have been reported[40-45] to range between 1.04 and 1.13 g/cm^3 with a mean of 1.10 g/cm^3. This mean value was utilized as the bacterial cell density when calculating bacterial cell settling velocities.

In the parallel plate flow chamber system, mechanisms contributing to particle transport to a collector surface include convective diffusion and sedimentation. Under

favorable conditions, the contribution to the experimental particle deposition flux by diffusion can be obtained from equation 2, which equals to $k_{Ideal}C_0$. The particle deposition flux by gravitational forces can be estimated as v_sC_0 when gravity controls the deposition process[46]. Table 3.1 showed that $k_{Ideal} > v_s$ for 0.5 μm colloids at both flow rates, which suggests that convection and diffusion are dominating in the transport of 0.5 μm colloids. The opposite relation ($k_{Ideal} < v_s$) was observed for larger model particles, which suggests gravity plays more pronounced role on these particles' transport. This postulate was confirmed by experimental observations, where much larger values of k_{Bottom} than k_{Top} (Table 3.1) implies that gravitational forces dramatically enhance particle deposition onto the bottom surfaces. Meanwhile, gravity minimizes particle deposition onto the top surfaces (no measurable deposition onto top surfaces of 1.8 μm colloids and bacterial cells). This trend becomes more pronounced with lower flow rates. This is attributed to the particles experiencing longer residence times at lower flow rates before reaching the midway in the parallel plate flow chamber, allowing a greater period of time in which gravity may influence the particles trajectory away from the top surface. The settling velocities (v_s) of 1.8 μm colloids and bacterial cells were of the same order of magnitude as k_{Bottom}, both a full order of magnitude greater than k_{Ideal} at the low flow rate. This indicates that deposition was not primarily diffusion-based, and is further evidence for gravitational dominance over the convective and diffusive transport of the colloidal particles greater than 1 μm in diameter.

Interestingly, k_{Bottom} and v_s of the bacterial cells were greater than those of 1.8 μm colloids, even though the size of the bacterial cells was slightly smaller. This may be due to the greater density of bacterial cells than that of the CML colloids. Similarly, McClaine[20] observed significantly higher attachment rate of nonmotile bacterial species to the bottom plate of the parallel plate flow chamber than theoretical calculations. They concluded that the attachment was not diffusion-limited and the augmented attachment was attributed to the result of bacterial settling after comparing the bacterial transfer rates (k) to the bacterial settling velocities (v_s). Based on these observations, sedimentation of micron-sized colloids and bacterial cells under the influence of gravity is deemed an important transport mechanism contributing to the rate of collisions between particles and collector surfaces[47-49]. This is more pronounced at lower fluid velocities such as those typical for groundwater.

3.4 CONCLUSION

Our results show that gravitational forces can have a considerable effect on the deposition of micron-sized colloids and bacterial cells. Using a parallel plate flow chamber system, we quantitatively examined the role of gravity on colloidal and bacterial deposition. Experimental observations confirmed that the gravitational force enhanced the mass transfer of model particles to the bottom surface, while dramatically reducing deposition on the top surface. This was the case even for 0.5 μm colloids where diffusion forces dominate. Results suggest gravity is a significant force,

validated by calculations using the Smoluchowski-Levich approximation and the experimental observations in a D_2O/H_2O/KCl mixture. Meanwhile, smaller colloids seem to be more sensitive to hydrodynamic interactions compared to larger colloids and bacterial cells. It is therefore not adequate to assume a negligible contribution from gravitational forces just based on a particle size criterion[25]. In many cases, gravity should be explicitly taken into account, particularly as in the case of bacterial transport and lower velocity conditions.

Our results show that gravitational forces can have a considerable effect on the deposition of micron-sized colloids and bacterial cells. Using a parallel plate flow chamber system, we quantitatively examined the role of gravity on colloidal and bacterial deposition. Experimental observations confirmed that the gravitational force enhanced the mass transfer of model particles that were especially larger than 1 μm in diameter to the bottom surface, while dramatically reducing deposition on the top surface. Results suggest gravity is a significant force, validated by calculations using the Smoluchowski-Levich approximation and the experimental observations in a D_2O/H_2O/KCl mixture. Meanwhile, smaller colloids less than 1 μm size are more sensitive to hydrodynamic interactions as compared to larger colloids and bacterial cells. Therefore, gravity should not be assumed negligible, but rather should be explicitly taken into account, particularly as in the case of bacterial transport and lower velocity conditions.

3.5 REFERENCES

1. MWH, *Water treatment principles and design*. 2nd ed.; John Wiley & Sons, Inc.: 2005; p 1948.

2. Lawler, D. F.; Nason, J. A. *Water Sci. Technol.* **2006,** 53, (7), 1-7.

3. Li, Q.; Logan, B. E. *Water Res.* **1999,** 33, (4), 1090-1100.

4. Kuznar, Z. A.; Elimelech, M. *Environ. Sci. Technol.* **2004,** 38, (24), 6839-6845.

5. Chen, J. Y.; Klemic, J. F.; Elimelech, M. *Nano Lett.* **2002,** 2, (4), 393-396.

6. Kalasin, S.; Santore, M. M. *Langmuir* **2008,** 24, (9), 4435-4438.

7. Yiantsios, S. G.; Karabelas, A. J. *Chem. Eng. Sci.* **2003,** 58, (14), 3105-3113.

8. Zhuang, J.; Qi, J.; Jin, Y. *Environ. Sci. Technol.* **2005,** 39, (20), 7853-7859.

9. Busscher, H. J.; Weerkamp, A. H. *Fems Microbiol. Rev.* **1987,** 46, (2), 165-173.

10. Yao, K. M.; Habibian, M. T.; O'Melia, C. R. *Environ. Sci. Technol.* **1971,** 5, 1105-1112.

11. Rajagopalan, R.; Tien, C. *AIChE J.* **1976,** 22, 523-533.

12. Tufenkji, N.; Elimelech, M. *Environ. Sci. Technol.* **2004,** 38, (2), 529-536.

13. Walker, S. L.; Redman, J. A.; Elimelech, M. *Langmuir* **2004,** 20, (18), 7736-7746.

14. Walker, S. L.; Redman, J. A.; Elimelech, M. *Environ. Sci. Technol.* **2005,** 39, (17), 6405-6411.

15. Kline, T. R.; Chen, G. X.; Walker, S. L. *Langmuir* **2008,** 24, (17), 9381-9385.

16. Adamczyk, Z.; Vandeven, T. G. M. *J. Colloid Interf. Sci.* **1981,** 80, (2), 340-356.

17. Bowen, B. D.; Epstein, N. *J. Colloid Interf. Sci.* **1979,** 72, (1), 81-97.
18. Sjollema, J.; Busscher, H. J.; Weerkamp, A. H. *J. Microbiol. Meth.* **1989,** 9, (2), 73-78.

19. Unni, H. N.; Yang, C. *Canadian J. Chem. Eng.* **2007,** 85, (5), 609-616.

20. McClaine, J. W.; Ford, R. M. *Biotechnol. Bioeng.* **2002,** 78, (2), 179-189.

21. Mohamed, N.; Rainier, T. R.; Ross, J. M. *Biotechnol. Bioeng.* **2000,** 68, (6), 628-636.

22. Prieve, D. C.; Ruckenst.E. *AICHE J.* **1974,** 20, (6), 1178-1187.

23. Logan, B. E.; Jewett, D. G.; Arnold, R. G.; Bouwer, E. J.; Omelia, C. R. *J. Environ. Eng.-ASCE* **1995,** 121, (12), 869-873.

24. Harvey, R. W.; Garabedian, S. P. *Environ. Sci. Technol.* **1991,** 25, (1), 178-185.

25. Tufenkji, N. *Adv. Water Resour.* **2007,** 30, (6-7), 1455-1469.

26. Walt, D. R.; Smulow, J. B.; Turesky, S. S.; Hill, R. G. *J. Colloid Interf. Sci.* **1985,** 107, (2), 334-336.

27. Marmur, A.; Ruckenstein, E. *J. Colloid Interf. Sci.* **1986,** 114, (1), 261-266.

28. Camesano, T. A.; Logan, B. E. *Environ. Sci. Technol.* **1998,** 32, (11), 1699-1708.

29. Stuurman, N.; Bras, C. P.; Schlaman, H. R. M.; Wijfjes, A. H. M.; Bloemberg, G.; Spaink, H. P. *Mol. Plant-Microbe Interact.* **2000,** 13, (11), 1163-1169.

30. Sambrook, J.; Fritsch, E. F.; Maniatis, T., *Molecular Cloning, A Laboratory Manual*. 2nd ed.; Cold Spring Harbor Laboratory Press: Cold Spring Harbor, New York, 1989; Vol. 3.

31. Walker, S. L. *Colloid Surf. B* **2005,** 45, (3-4), 181-188.

32. Elimelech, M., Gregory, J., Jia, X., Williams, R.A., *Particle Deposition and Aggregation: Measurement, Modeling and Simulation*. Butterworth-Heinemann: 1995; p 441.

33. Walker, S. L.; Bhattacharjee, S.; Hoek, E. M. V.; Elimelech, M. *Langmuir* **2002,** 18, (6), 2193-2198.

34. Chen, G. X.; Walker, S. L. *Langmuir* **2007,** 23, (13), 7162-7169.

35. Brow, C. N.; Li, X. Q.; Ricka, J.; Johnson, W. P. *Colloid Surf. A* **2005,** 253, (1-3), 125-136.

36. El-Gholabzouri, O.; Cabrerizo, M. A.; Hidalgo-Alvarez, R. *J. Colloid Interf. Sci.* **1999,** 214, (2), 243-250.

37. Wit, P. J.; Poortinga, A.; Noordmans, J.; van der Mei, H. C.; Busscher, H. J. *Langmuir* **1999,** 15, (8), 2620-2626.

38. Crittenden, J. C., Trussell, R.R., Hand, D.W., Howe, K.J., Tchobanoglous, G., *Water treatment: Principles and design*. 2nd ed.; John Wiley & Sons, Inc.: 2005; p 1948.

39. Brown, P. P.; Lawler, D. F. *J. Environ. Eng.-ASCE* **2003,** 129, (3), 222-231.

40. Scherer, P. *J Appl. Bacteriol.* **1983,** 55, (3), 481-486.

41. Kubitschek, H. E.; Baldwin, W. W.; Graetzer, R. *J. Bacteriol.* **1983,** 155, (3), 1027-1032.

42. Kubitschek, H. E.; Baldwin, W. W.; Schroeter, S. J.; Graetzer, R. *J. Bacteriol.* **1984,** 158, (1), 296-299.

43. Kuhn, A. H. U.; Jutte, H.; Kellenberger, E. *J. Virol.* **1983,** 47, (3), 540-552.

44. Baldwin, W. W.; Kubitschek, H. E. *J. Bacteriol.* **1984,** 159, (1), 393-394.

45. Dicker, D. T.; Higgins, M. L. *J. Bacteriol.* **1987,** 169, (3), 1200-1204.

46. Yiantsios, S. G.; Karabelas, A. J. *Int. J. Multiphas. Flow* **1998,** 24, (2), 283-293.

47. Korber, D. R.; Lawrence, J. R.; Zhang, L.; Caldwell, D. E. *Biofouling* **1990,** 2, (4), 335-350.

48. Roosjen, A.; Boks, N. P.; van der Mei, H. C.; Busscher, H. J.; Norde, W. *Colloid Surf. B* **2005,** 46, (1), 1-6.

49. Wan, J. M.; Tokunaga, T. K.; Tsang, C. F. *Water Resour. Res.* **1995,** 31, (7), 1627-1636.

CHAPTER 4

COLLOIDAL DEPOSITION ON REMOTELY CONTROLLED CHARGED MICROPATTERNED SURFACES IN A PARALLEL PLATE FLOW CHAMBER

ABSTRACT

This paper describes a method to influence colloid deposition by varying the zeta potential at microelectrodes with remotely applied electric potentials. Deposition experiments were conducted in a parallel plate flow chamber for bulk substrates of glass, indium tin oxide (ITO), and ITO-glass microelectrodes in 10 mM and 60 mM potassium chloride solutions. Colloid deposition is shown to be a function of solution chemistry and the small locally delivered electric surface potentials. Electric fields and physical surface heterogeneity are ruled out as cause of the observed deposition. Results are reported using experimentally determined Sherwood numbers, and compared to the predictions of the previously developed patch model. Minor deviation between predicted and experimental Sherwood numbers implies a combination of physical and chemical interactions occurring. Specifically, we propose colloidal particles respond to local variation in surface potential through electrostatic interactions, altering particle streamlines flowing along the surface, and ultimately the extent of deposition.

4.1 INTRODUCTION

This paper describes on a method to influence colloid deposition by varying the zeta potential at microelectrodes with remotely applied electric potentials. We hypothesize that externally applied potentials will influence adhesion of colloids undergoing diffusion-dominated transport. Such dynamic methods to study particle transport are important to fully understand the fate of problematic particles and bacteria in complex aquatic environments such as groundwater.[1-4] Efforts are ongoing to theoretically model bacterial adhesion with simple models.[5, 6]

There are a variety of straightforward experimental approaches available to simulate various physical and chemical elements of subsurface environments.[7, 8] Such systems are designed to capture transport and deposition behavior of particles in porous media around a single soil particle. For example, the radial stagnation point system (also referred to as the impinging jet), allows for measurement of colloid deposition in the forward stagnation region of a single collector as would exist in porous media.[9-13] Another system, the parallel plate (PP) flow chamber, captures particle deposition when the flow is parallel to the collector surface, simulating the flow regime as the fluid streamline goes around parallel to a collector.[14-19] The RSPF and PP systems are ideal for investigating the microscopic deposition behavior as the flow cells are mounted on a microscope stage and individual particles can be visualized and rates of colloid transfer to the test surface can be measured. There are other experimental approaches that simulate the subsurface which involve porous media; these include micromodels and

packed-bed columns.[6, 20-23] Microscopic visualization and quantification of individual particles can be more difficult in the RSPF and PP systems; however, complex transport phenomena within porous media is incorporated. More recently complexity has been added in these systems, attempting to establish the extent to which physical and chemical heterogeneity impact particle deposition.[14, 15, 24-28] These studies have shown a considerable influence of both physical and chemical heterogeneity on colloid attachment. To have a role, physical heterogeneity requires comparable size scales to colloids[25, 27] while chemical heterogeneity has been reported to impact deposition at remarkably smaller size regimes.[29-31]

Outside of the issue of heterogeneity, research efforts have investigated the influence of bacteria shape, leachates in model soil systems, particle size, and surface properties amongst others.[32-34] However a component missing from the above experimental systems is a controlled chemical process[3, 4] – notably what happens when there are chemical reactions, ion gradients, etc. occurring that may locally influence surface potential, subsequent chemical interactions, and ultimately particle deposition. These local changes in surface potential or zeta potential can render chemical conditions either more or less favorable to particle deposition on a length-scale comparable in magnitude to the size of an individual colloid or bacterial cell.[35, 36] In order to simulate zeta potential in microscopic processes, we have altered the zeta potential using a microelectrode at a length-scale relevant to a colloid. The influence of a macroscopic electrode on reversibly deposited colloids has been

experimentally reported for alternating current electric fields but to our knowledge no experimental work has been done utilizing an electrode at the size scale of a particle to apply a range of electric potentials without generating a current.[37-41] However, theoretical consideration of influence of DC electric field on zeta potential at an electrode has been reported.[42] To simulate what occurs when the localized zeta potential changes in a complex, charged system we have used optically transparent electrodes to exert small external potentials that can change the local zeta potential, perturbing the microscale system, and ultimately alter the extent of colloid attachment. To provide insight into our results and the localized phenomena observed, we have compared our results with a patch model which accounts for a distribution of chemically favorable and unfavorable regions for colloid deposition.[27]

4.2 Materials and Methods

4.2.1 Particle and test surface selection, preparation, and characterization.

Test surfaces utilized in the parallel plate flow chamber for deposition experiments included bulk glass, indium tin oxide (ITO), and ITO-patterned glass slides. Prior to their use in experimentation or characterization, a thorough cleaning of all glass, and ITO slides was performed via sonication in a surfactant (2% RBS 35; Fisher Scientific, Pittsburgh, PA), followed by alternately rinsing with ethanol and deionized (DI) water. The ITO -patterned microscope slides were cleaned by sonication in DI water to avoid the surfactant altering the surface chemistry of the ITO electrodes. After

this washing step with either DI or surfactant, the microscope slides were dried and attached to the parallel plate flow chamber.

To achieve favorable, non-repulsive electrostatic conditions, glass slides were chemically modified to exhibit a net positive zeta potential at the ionic strength of interest.[43] First, the unmodified glass microscope slide was immersed in a 0.2% (v/v) mixture of (aminoethylaminomethyl)–phenethyltrimethoxysilane (Gelest, Inc., Tullytown, PA) in ethanol for 3–5 min at room temperature and then cured for 90 min at 130 ºC.[25] After modification slides were rinsed with DI and attached to the parallel plate chamber system.

To produce the micropatterned surfaces, ITO slides with thickness of 60 nm and resistivity of 30-60 Ω/m^2 (Sigma-Aldrich Inc., St. Louis, MO) were coated with a positive photoresist, Shipley 1813 (Rohm and Haas, Philadelphia, PA), at 3000 rpm for 40 seconds. Samples were soft-baked for 1 minute at 95 ºC, then exposed for 10 seconds (Quintel Q-4000, Morgan Hill, CA or Karl Suss MA6, Garching, Germany) in hard contact mode using platinum microelectrodes on glass as a mask (Abteck Scientific, Richmond, VA). The pattern was developed for ~1 minute (CD26 Rohm and Haas), dried under nitrogen and complete development was confirmed with conductivity and profilometry (Veeco Dektak, Plainview, NY) measurements.[44] Then the ITO film was etched where it was exposed (no photoresist) with an inductively coupled plasma (Oxford Instruments Plasmalab System 100, Concord, MA) at 50 sccm CH_4, 15 sccm H_2, and 30 sccm N_2 for 5 minutes, 3.6 mT pressure, 120 W RF power, and

1000 W ICP power. Inductively coupled plasmas are generated by coupling radio frequency (RF) energy into a low pressure gas ($CH_4/H_2/N_2$ in our system) by an inductive coil. Reactive plasmas comprised of hydrocarbon gas mixtures have been reported to etch ITO.[45] Completely etched ITO was confirmed with profilometry, conductivity, and optical microscopy (**Figure 4.1**), as ITO is less transparent than glass. After micropatterning, slides were rinsed with DI and installed in the parallel plate chamber system.

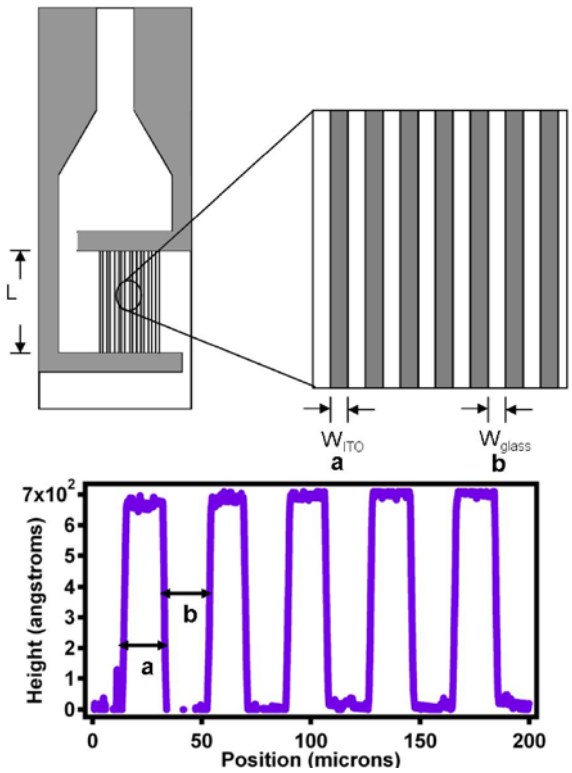

Figure 4.1 Schematic of interdigitated microelectrodes patterned on ITO coated glass slides with inset showing (a) width of each microelectrode, and (b) spacing between each microelectrode. (top) and the profile across obtained with Veeco Daktek profilometer showing the relative uniform microelectrode height in angstroms from bulk glass slide and width. (bottom).

Surface zeta potentials of glass, ITO, and patterned surfaces were determined by a streaming potential analyzer (EKA, Brookhaven Instruments Corp., Holtsville, NY) with an asymmetric clamping cell at ionic strengths of 10 and 60 mM KCl and compared to previously reported surface zeta potentials for aminosilane modified surfaces.[43] The EKA was thoroughly rinsed with water and KCl electrolyte before the zeta potential measurements. Then the surface was equilibrated with electrolyte in the EKA for 10 minutes prior to measurement. Zeta potential measurements and calculations were done using previously reported procedures.[46]

Fluorescent carboxylate-modified polystyrene latex microspheres (Invitrogen, Eugene, OR) were used as model colloids for the deposition experiments. The monodispersed colloids had a mean diameter of 1.1 μm. Electrophoretic mobility measurements were conducted for colloids suspended in KCl electrolyte solutions at 10 and 60 mM at 25 ºC using a ZetaPALS analyzer (Brookhaven Instruments Corporation, Holtsville, NY). The Smoluchowski equation was used to convert electrophoretic mobility to zeta potential.[47]

4.2.2 Deposition experiments.

Colloidal deposition experiments were conducted in a rectangular parallel plate flow chamber system (Product number: 31-010, GlycoTech, Rockville, MA) installed on the stage of an inverted fluorescent microscope (IX70, Olympus, Center Valley, PA). The parallel plate flow chamber (inner dimensions of 6 cm × 1 cm × 0.254 mm) consisted of a Plexiglass block, a flexible silicon elastomer gasket, and a microscope

slide. Chambers were sealed with a thin film of vacuum grease on the gasket. The deposition of fluorescently labeled colloids onto the surfaces were imaged by an infinity corrected 40x objective (Olympus UPlanFI, N.A. 0.75) focused near the center on the inner surface of the test surface. Imaging was done with a Xe lamp with a filter, excitation of 480 nm and emission of 510 nm (Chroma Technology Corp., Brattleboro, VT).

Colloid deposition was recorded with a digital camera (Retiga 1300 Mono Cooled, Qimaging, British Columbia) acquiring images every 20 seconds for 30 min time period (time for deposition study) and then analyzed with the supplied software (SimplePCI, Precision Instruments, Inc., Minneapolis, MN). Data acquisition and analysis methods have been previously reported.[46] Briefly, the number of deposited colloids was determined for each time interval by accounting for changes in particle deposition between successive images. Colloid injection concentrations were maintained at 7.5×10^6 particles/mL over the course of the experiment. Flow rates of 0.01 mL/min were employed, corresponding to an average flow velocity of 2.2×10^{-5} m/s. The Reynolds number was 0.017 and the corresponding Peclet number was 0.0001, both indicative of diffusion-dominated transport regime. Experiments were conducted at ionic strength of 10 and 60 mM KCl, and an ambient pH (5.5-5.8) and temperature (22–25 ºC).

4.2.3 Quantification of colloid deposition onto test surfaces.

The kinetics of colloidal deposition in the parallel plate flow chamber system were measured by calculating the dimensionless Sherwood number (Sh).[47] The Sherwood number correlates particle deposition flux (number of colloids per area per time), *J*; the colloid radius, a_p; the bulk colloidal particle concentration, C_0; and the bulk diffusion coefficient,[47] D_∞ as follows,

$$Sh = \frac{Ja_p}{C_0 D_\infty} \qquad (1)$$

The deposition flux (*J*) was found by determining the initial slope of the number of deposited colloids versus time. This slope, normalized by the microscope viewing area (209 μm × 166 μm) resulted in the deposition flux. This was calculated for all test surfaces: glass, ITO, micro-patterned ITO, and modified glass microscope slides, which were expressed in terms of Sh_{glass}, Sh_{ITO} Sh_{exp}, and Sh_{fav}, respectively. The experimental results were compared with predictions from the patch model, Sh_{patch}, which the overall colloidal deposition rate is a linear combination of the glass (Sh_{glass}) and ITO (Sh_{ITO}) slides deposition rates. The predicted Sherwood number for the patch model was determined from equation 2:

$$Sh_{patch} = \lambda Sh_{glass} + (1-\lambda) Sh_{ITO} \qquad (2)$$

where λ is the area fraction of glass patches. For our system, λ=0.5.[24, 47]

Externally applied potentials were applied to bulk and micropatterned surfaces with a potentiostat (Pine Instruments, Grove City, PA). The working electrode was the bulk

ITO surface or microelectrode ITO surface in the parallel plate flow chamber, a Pt wire served as the counter electrode located in electrolyte reservoir, and Ag/AgCl reference electrode also in electrolyte reservoir, approximately 25 cm from working electrode (all potentials reported are relative to Ag/AgCl reference electrode). A complete electrical circuit is established by tubing that connects flow chamber to the electrolyte reservoir. A potential of –0.2 V, 0 V, or +0.2 V was applied, defined as maximum potential before onset of a measurable current with the potentiostat set to the most sensitive current level, ±1 nA. A measurable current would complicate adhesion studies with electrophoretic and electrosmostic effects.[38, 39, 48-50] Additionally, measurable currents oxidize and corrode indium tin oxide.[51]

4.3 Results and Discussion

4.3.1 Zeta potential measurements.

Solution ionic strength and an applied external potential were found to influence the measured zeta potential of all test surfaces (Figure 4.2). The glass slide exhibited a significantly more negative zeta potential at 10 mM (-35.5±0.3 mV) than at 60 mM ionic strength (-5.9±0.3 mV). The indium tin oxide coated surface exhibited zeta potentials of -32.7±0.2 mV at 10 mM and +1.2±0.4 mV at 60 mM when there was no potential applied. Zeta potentials for titanium dioxide reported previously[52] as a function of ionic strength became more positive with an increased ionic strength because of the compression of the double layer leads to different ions that adsorb to

oxide surface. When a positive external potential (+0.2 V) was applied, the zeta potential was found to be -30±1 mV and +1.6±0.8 mV at 10 mM and 60 mM respectively. Interestingly, when a negative potential was applied (-0.2 V), it resulted in a positive zeta potential (+20±1 mV and +167±7 mV at 10 mM and 60 mM, respectively). These highly positive values were reproducible, but likely both an indication of the positive nature of the material, but also an artifact of the streaming potential equipment which reaches its limit of measurement at higher ionic strength conditions. As can be observed in Figure 4.2, the zeta potential for the carboxylate modified spheres was -64±3 mV and -32±2 mV at 10 and 60 mM, respectively. Hence, regardless of ionic strength, the colloidal zeta potential values were substantially more negative than the test surfaces used in deposition studies, suggesting repulsive electrostatic conditions should exist. "Favorable" conditions were therefore achieved in colloid deposition studies by utilizing a positively charged amine-terminated silane coated glass surface (+20 mV at 10mM KCl),[43] and under these electrostatically favorable conditions the measured Sherwood number (Sh_{fav}) was 0.0261 ± 0.0004.

4.3.2 Experimental Sherwood numbers for bulk substrates.

Deposition did not occur on glass surfaces because electrostatic interaction between colloid and surface were electrostatically unfavorable resulting in a Sherwood number (Sh_{glass}) of zero for both 10 and 60 mM ionic strength. Figure 3 displays Sherwood numbers for bulk ITO surfaces (Sh_{ITO}) without an applied potential, which was 0.0155±0.0003 and 0.020±0.002 at 10 mM and 60 mM, respectively. Applying a

positive potential to the ITO surface resulted in Sh_{ITO} of 0.017±0.001 and 0.023±0.003 at 10 mM and 60 mM, respectively. Applying a negative potential resulted in Sh_{ITO} of 0.012±0.001 at 10 mM and 0.0104±0.0006 at 60 mM. Experimentally, the Sherwood number became more favorable for deposition as voltage is applied (from 0 to +0.2 V) at both 10 mM and 60 mM, in part due to the ITO surface's zeta potential becoming more positive and interactions become more electrostatically favorable. Second, Sh_{ITO} decreased from no applied voltage to a negative applied voltage (-0.2 V) at both ionic strength conditions because materials become more negatively charged and repulsive. However, if predicted deposition behavior was based on surface zeta potentials and electrostatic interactions alone, one would expect significantly higher deposition. It is not evident why our surface zeta potential results indicate a remarkably higher and more positive zeta potential without showing a corresponding influence on the deposition trends. Neither corrosion or other chemical processes(such as production of ions) are likely occurring due to the low applied potential,[51] nor did we observe significant collection or clustering of particles on the microelectrode edges where electric fields were the least-linear. Furthermore, streaming potential measurements are highly reproducible, degradation or chemical change of substrates would yield varying surface potentials. One possible explanation for the highly positive zeta potential measured for the ITO surface with -0.2 V potential applied is strong adsorption of ions onto the electrode due to the high effective nuclear charge of H^+ (pH of solution ~5.7) and K^+ ions relative to the Cl^- that results upon applying a negative potential during

surface zeta potential streaming potential measurement. Our observations are similar to another study which identified that anions present render the zeta potentials of porous membranes more negative during streaming potential measurement.[53] Further studies are warranted to investigate role of outside electrodes during streaming potential measurements.

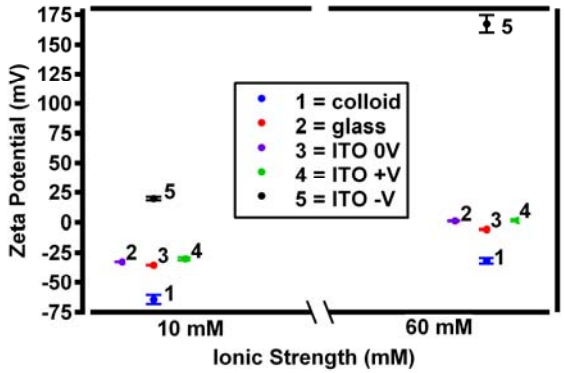

Figure 4.2 Zeta potential of colloid and surfaces at 10 and 60 mM ionic strength with numbers next to each measurement to identify them in legend. In legend ITO 0V is bulk ITO surface without zeta potential, ITO +V is bulk ITO surface with +0.2 V, and ITO –V is bulk ITO surface with -0.2 V.

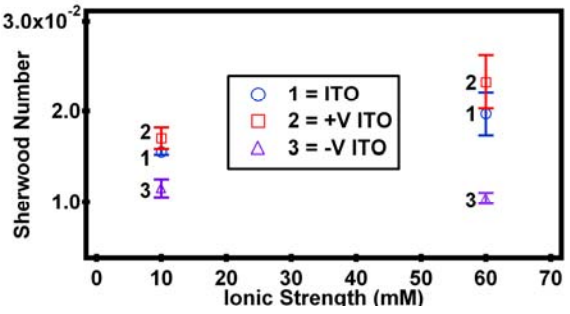

Figure 4.3 Particle deposition rate expressed as Sherwood number at 10 and 60 mM ionic strength on bulk ITO, positive voltage on ITO, and negative voltage on ITO surfaces.

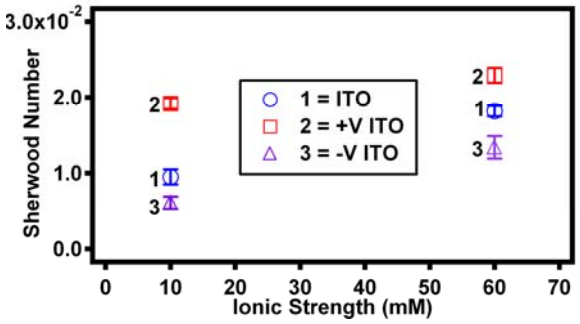

Figure 4.4 Sherwood number for colloid deposition on microelectrodes at three different applied potentials of -0.2 V, 0 V, and +0.2 V for 10 and 60 mM ionic strength. We determined a Sherwood number 0.0261 ± 0.0004 to represent favorable deposition.

4.3.3 Experimental Sherwood numbers for microelectrodes.

The Sherwood numbers for ITO microelectrodes (Sh_{exp}, reported in Figure 4.3) qualitatively agreed with Sh_{ITO} measurements. The Sh_{exp} without an applied potential were 0.001±0.001 and 0.0182±0.0007 for 10 mM and 60 mM respectively. The 60 mM relative to the 10 mM Sh_{exp} indicated an 18x increase in deposition as ionic strength was increased leading to the compression of the double layer between the colloids and the micro-patterned surface and more favorable interactions. A potential of +0.2 V on ITO microelectrodes increased Sh_{exp} to 0.0192±0.0007 and 0.023±0.001 for 10 mM and 60 mM, respectively. The positive applied potential of +0.2 V decreased the sensitivity to ionic strength because the relative Sh_{exp} to 0 V increased by 1.2x at 10 mM and by 1.3x at 60 mM. This increase in Sh_{exp} indicated that only a fraction of the sensitivity between colloid and the substrate can be contributed to ionic strength in the absence of an externally applied potential. A negative external potential of -0.2 V on

the ITO microelectrodes reduced the Sh_{exp} to 0.0061±0.0008 and 0.013±0.001 for 10 mM and 60 mM, respectively with two major relative effects. First, this represented a 2.1x relative increase in overall deposition at -0.2 V as ionic strength increased from 10 mM to 60 mM consistent with double layer compression and greater interaction between colloid and substrate. Second, was a decrease in deposition of 0.7x for +0.2 at 60 mM relative to 0 V at 60 mM suggesting that at a given ionic strength the negative externally applied potential renders the substrate surface less favorable for colloid deposition. In general, we observed that Sh_{exp} when the surface was exposed to a negative applied potential is less than the Sh_{exp} at either zero or positive voltage applied, regardless of the background solution ionic strength when no voltage applied.

The Sherwood number at 60 mM and -0.2 V is ~1/2 of that measured for +0.2 V also at 60 mM ionic strength. The enhanced adhesion is unlikely from the physical height of electrodes because adhesion would likely change uniformly for -0.2 V, 0 V, and +0.2 V which was not observed. The Sherwood numbers less than 0.010 at 10 mM ionic strength for -0.2 V and 0 V on ITO are likely attributed to less double layer attractions or greater electrostatic repulsions. We propose that changes in surface zeta potential brought on by external potential explain the absolute Sherwood numbers.

4.3.4 Adhesion on microelectrodes as described by a "patch" model.

For further mechanistic illumination we turned to a patch model, which accounts for deposition onto distinct favorable and unfavorable patches of the collector surface.[27] This model explains adhesion of colloids onto patterned surfaces and

provides insight into the deposition occurring onto the ITO microelectrodes. Specifically, the patch model accounts for chemically favorable and unfavorable regions on a collector surface – or "patches" – that are alternating 20 μm stripes. In Figure 4.5, the relationship between the idealized, calculated Sherwood number (Sh_{patch}) was compared to the experimentally determined Sherwood number on the micro-patterned electrode (Sh_{exp}). A ratio of 1 Sh_{exp}/Sh_{patch} indicated exact experimental agreement with the patch model. Deposition studies at 10 mM resulted in a ratio of 1.2±0.1, 2.26±0.08, and 1.1±0.1 for 0 V, +0.2 V, and -0.2 V, respectively. Experiments at 60 mM were 1.15±0.04 (0V), 1.33±0.06 (+0.2V), and 1.0±0.1 (-0.2 V). All of the ratios suggested our conditions were in relatively good agreement with theory; however, the only condition where the patch model predicted the deposition trends was at a

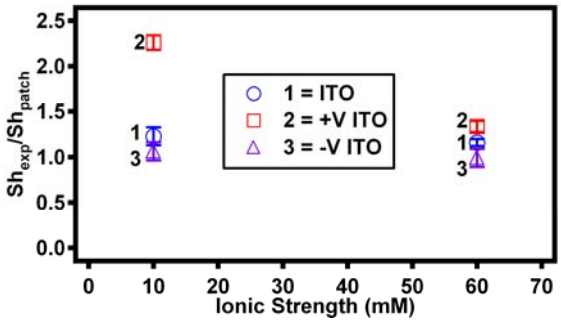

Figure 4.5 The ratio of Sherwood number at 10 mM and 60 mM ionic strength for -0.2 V, 0 V, and +0.2 V that were experimentally measured to theoretical Sherwood number predicted from patch model of alternating patches with a ratio of 1 representing perfect agreement with model.

negatively applied potential (at both ionic strength conditions). When there is a negatively applied potential, we expected the ITO stripes to become more negatively charged relative to ITO stripes at 0 V or +0.2 V, but streaming potential indicated that

they are highly positive (Figure 4.2). However, the bulk glass substrate charge is negative, making interaction with the negatively charged colloid generally unfavorable.

4.3.5 Deviation from the patch model.

Interestingly, except under the negatively applied potential, Sh_{exp}/Sh_{patch} did not follow the patch model based upon bulk surface charge (see Figure 4.2 streaming potential measurements), other than showing sensitivity to ionic strength. This sensitivity suggests electrostatic interactions are involved but not a dominate mechanism controlling colloid deposition. As noted previously, under these conditions electro-osmosis can be ruled out.[39] Electric field effects were ruled out based on an approach presented in a previous study which used similar microelectrodes where electric fields calculated using Ohm's law were used to determine the colloid electrophoretic mobility by the Smoluchowski equation.[54] In our experiments, measured currents were within the noise range of the potentiostat (1 nA), solution conductivity was approximately 300 μS/m, and the separation distance between working microelectrode (~2.0×10^{-6} m^2) and counter/reference electrode (bulk platinum wire) was 25 cm. This results in the calculated effective linear electric field of ~7.0×10^{-7} V/m and an electrophoretic induced velocity of ~0.5 nm/s, which is much too small of a velocity for the colloids to overcome thermal fluctuations. Furthermore, an electric field would result in deposition/aggregation around the electrode as reported previously which was not observed in our experiments[55]. We can also rule out physical roughness because we would have been able to see its effect

on deposition – enhanced in the presence of the electrode – regardless of the applied voltage. We propose that the mechanism involved is a combined physical and chemical response to the charged regions on the collector surface. Likely the particle is responding to local variation in surface potential, and this alters the particle streamlines flowing along the surface. At zero and a positive applied potential $Sh_{exp} > Sh_{patch}$ even though streaming potential measurements suggest a repulsive condition for interactions. This supports our suggested mechanism, but also suggests that the idealized patch model may under-predict deposition consistent with theoretical models for RSPF systems with concentric patches of comparable scale to particle.[28, 56] Trajectory studies with these RSPF patch systems have predicted oscillatory effects when coupled hydrodynamic and colloid forces are considered resulting in a modified patch model.[28] Therefore, it is likely the patch model does not account for how the local positively charged regions attract a negatively charged colloid to a closer proximity to the micro-patterned test surface as would occur near an entirely negatively charged test surface. This would result in the colloid being nearer to the negatively charged "patch", hence leading to a greater amount of interaction overall. The Sh_{exp} value may be larger than Sh_{patch} as it captures colloid deposition which occurs either on the negatively charged region of the micro-patterned surface (as the colloids may approach the negatively charged region closely enough to overcome the energy barrier) *or* overall deposition may be enhanced as the colloids are flowing more closely to the test surface, increasing the transport of the colloid to the

subsequent positively charged stripe. Future experimental studies with parallel plate flow cells containing patches of comparable size to the particle will need to adapt these theoretical modified patch models to produce more accurate predictions.

4.4 CONCLUSION

We have reported an experimental method to vary surface potentials on transparent microelectrodes with an approximate length-scale comparable to the colloid in a diffusion-dominated regime and show its subsequent effect on particle deposition. In general, we found that neither electric fields nor physical heterogeneity contributed to our results. We measured surface zeta potentials to show that remotely controlled zeta potential changes on microelectrode induced by an external potential gave predictable adhesion trends by measuring particle transfer to the surface and calculating a Sherwood number. Our results were adequately described by a patch model consisting of favorable and unfavorable microscopic regions, particularly when a negative potential was applied. However, the patch model was insufficient for explaining deposition trends at 0 V and +0.2 V which suggest future modeling is warranted to account for the coupled hydrodynamic and colloid interaction forces.

4.5 REFERENCES

1. Auckenthaler, A.; Raso, G.; Huggenberger, P. *Water Sci. Technol.* **2002,** 46, 131-138.

2. Duffy, C. J.; Brandes, D. *J. Contam. Hydrol.* **2001,** 48, 151-165.

3. Schoups, G.; Hopmans, J. W.; Tanji, K. K. *Hydrol. Process* **2006,** 20, 2647-2668.

4. Wolf, L.; Klinger, J.; Hoetzl, H.; Mohrlok, U. *J. Soil Sediment* **2007,** 7, 85-95.

5. Simunek, J.; He, C. M.; Pang, L. P.; Bradford, S. A. *Vadose Zone J.* **2006,** 5, 1035-1047.

6. Torkzaban, S.; Bradford, S. A.; Walker, S. L. *Langmuir* **2007,** 23, 9652-9660.

7. Yang, J. L.; Bos, R.; Belder, G. F.; Engel, J.; Busscher, H. J. *J. Colloid Interf. Sci.* **1999,** 220, 410-418.

8. Yang, J. L.; Bos, R.; Poortinga, A.; Wit, P. J.; Belder, G. F.; Busscher, H. J. *Langmuir* **1999,** 15, 4671-4677.

9. Redman, J. A.; Walker, S. L.; Elimelech, M. *Environ. Sci. Technol.* **2004,** 38, 1777-1785.

10. Johnson, P. R.; Elimelech, M. *Langmuir* **1995,** 11, 801-812.

11. Johnson, W. P.; Blue, K. A.; Logan, B. E.; Arnold, R. G. *Water Resour. Res.* **1995,** 31, 2649-2658.

12. Liu, D. L.; Johnson, P. R.; Elimelech, M. *Environ. Sci. Technol.* **1995,** 29, 2963-2973.

13. Johnson, W. P.; Li, X. Q.; Yal, G. *Environ. Sci. Technol.* **2007,** 41, 1279-1287.

14. Wit, P. J.; Poortinga, A.; Noordmans, J.; van der Mei, H. C.; Busscher, H. J. *Langmuir* **1999,** 15, 2620-2626.

15. Suarez, C. G.; Noordmans, J.; van der Mei, H. C.; Busscher, H. J. *Phys. Chem. Chem. Phys.* **1999,** 1, 4423-4427.

16. Suarez, C. G.; Noordmans, J.; van der Mei, H. C.; Busscher, H. J. *Langmuir* **1999,** 15, 5123-5127.

17. Yang, J. L.; Bos, R.; Busscher, H. J. *Colloid. Surface. A* **2000,** 173, 231-234.

18. Gomez-Suarez, C.; van der Mei, H. C.; Busscher, H. J. *Colloid. Surface. A* **2001,** 186, 211-219.

19. McClaine, J. W.; Ford, R. M. *Biotechnol. Bioeng.* **2002,** 78, 179-189.

20. Bradford, S. A.; Torkzaban, S.; Walker, S. L. *Water Res.* **2007,** 41, 3012-3024.

21. Saiers, J. E.; Hornberger, G. M.; Liang, L. Y. *Water Resour. Res.* **1994,** 30, 2499-2506.

22. Keller, A. A.; Sandall, O. C.; Rinker, R. G.; Mitani, M. M.; Bierwagen, B.; Snodgrass, M. J. *Ground Water Monit. R.* **2000,** 20, 114-126.

23. Walker, S. L.; Redman, J. A.; Elimelech, M. *Environ. Sci. Technol.* **2005,** 39, 6405-6411.

24. Song, L. F.; Johnson, P. R.; Elimelech, M. *Environ. Sci. Technol.* **1994,** 28, 1164-1171.

25. Chen, J. Y.; Klemic, J. F.; Elimelech, M. *Nano Lett.* **2002,** 2, 393-396.

26. Bakker, D. P.; Busscher, H. J.; van der Mei, H. C. *Microbiol.-SGM* **2002,** 148, 597-603.

27. Elimelech, M.; Chen, J. Y.; Kuznar, Z. A. *Langmuir* **2003,** 19, 6594-6597.

28. Nazemifard, N.; Masliyah, J. H.; Bhattacharjee, S. *J. Colloid Interf. Sci.* **2006,** 293, 1-15.

29. Elimelech, M.; Nagai, M.; Ko, C. H.; Ryan, J. N. *Environ. Sci. Technol.* **2000,** 34, 2143-2148.

30. Chen, J. Y.; Ko, C. H.; Bhattacharjee, S.; Elimelech, M. *Colloid. Surface. A* **2001,** 191, 3-15.

31. Abudalo, R. A.; Bogatsu, Y. G.; Ryan, J. N.; Harvey, R. W.; Metge, D. W.; Elimelech, M. *Environ. Sci. Technol.* **2005,** 39, 6412-6419.

32. Salerno, M. B.; Flamm, M.; Logan, B. E.; Velegol, D. *Environ. Sci. Technol.* **2006,** 40, 6336-6340.

33. Stoddard, C. S.; Coyne, M. S.; Grove, J. H. *J. Environ. Qual.* **1998,** 27, 1516-1523.

34. Zhuang, J.; Qi, J.; Jin, Y. *Environ. Sci. Technol.* **2005,** 39, 7853-7859.

35. Kaya, A.; Yukselen, Y. *Can. Geotech. J.* **2005,** 42, 1280-1289.

36. Saveyn, H.; Van der Meeren, P.; Hofmann, R.; Stahl, W. *Chem. Eng. Sci.* **2005,** 60, 6768-6779.

37. Kim, J.; Anderson, J. L.; Garoff, S.; Sides, P. J. *Langmuir* **2002,** 18, 5387-5391.
38. Bohmer, M. *Langmuir* **1996,** 12, 5747-5750.

39. Solomentsev, Y.; Bohmer, M.; Anderson, J. L. *Langmuir* **1997,** 13, 6058-6068.

40. Mansouri, A.; Bhattacharjee, S.; Kostiuk, L. W. *J. Phys. Chem. B* **2007,** 111, 12834-12843.

41. Kemps, J. A. L.; Bhattacharjee, S. *Langmuir* **2005,** 21, 11710-11721.

42. Prieve, D. C. *Colloid. Surface. A* **2004,** 250, 67-77.

43. Walker, S. L.; Bhattacharjee, S.; Hoek, E. M. V.; Elimelech, M. *Langmuir* **2002,** 18, 2193-2198.

44. Horiuchi, T.; Niwa, O.; Morita, M. *J. Electrochem. Soc.* **1995,** 142, L146-L149.

45. Meziani, T.; Colpo, P.; Lambertini, V.; Ceccone, G.; Rossi, F. *Appl. Surf. Sci.* **2006,** 252, 3861-3870.

46. Chen, G. X.; Walker, S. L. *Langmuir* **2007,** 23, 7162-7169.

47. Elimelech, M.; Jia, X.; Gregory, J.; Williams, R. *Particle Deposition and Aggregation: Measurement, Modelling and Simulation*. Butterworth-Heinemann: Woburn, MA, 1995; p 448.

48. Vanloosdrecht, M. C. M.; Lyklema, J.; Norde, W.; Schraa, G.; Zehnder, A. J. B. *Appl. Environ. Microbiol.* **1987,** 53, 1898-1901.

49. Litton, G. M.; Olson, T. M. *J. Colloid Interf. Sci.* **1994,** 165, 522-525.

50. Feick, J. D.; Velegol, D. *Langmuir* **2000,** 16, 10315-10321.

51. Folcher, G.; Cachet, H.; Froment, M.; Bruneaux, J. *Thin Solid Films* **1997,** 301, 242-248.

52. Janusz, W.; Sworska, A.; Szczypa, J. *Colloid. Surface. A* **1999,** 152, 223-233.

53. Ariza, M. J.; Benavente, J. *J. Membr. Sci.* **2001,** 190, 119-132.

54. Paxton, W. F.; Baker, P. T.; Kline, T. R.; Wang, Y.; Mallouk, T. E.; Sen, A. *J. Am. Chem. Soc.* **2006,** 128, 14881-14888.

55. Guelcher, S. A.; Solomentsev, Y.; Anderson, J. L. *Powder Technol.* **2000,** 110, 90-97.

56. Nazemifard, N.; Masliyah, J. H.; Bhattacharjee, S. *Langmuir* **2006,** 22, 9879-9893.

CHAPTER 5

INITIAL BACTERIAL DEPOSITION ON BARE AND ZEOLITE-COATED ALUMINUM AND STAINLESS STEEL

ABSTRACT

In this study, the impact of zeolite thin film coatings on bacterial deposition and "biofouling" of surfaces has been investigated in an aqueous environment. The synthesis of two types of zeolite coatings, ZSM-5 coated on aluminum alloy and zeolite A coated on stainless steel, as well as the characterization of the coated and bare metal surfaces, are described. The extent of cell deposition onto the bare and zeolite coated aluminum alloy, and stainless steel surfaces was investigated in a parallel plate flow chamber system under a laminar flow conditions. The initial rates of bacterial transfer to the various surfaces are compared utilizing a marine bacterium *Halomonas pacifica* g under a range of ionic strength conditions. *H. pacifica* g deposited onto bare metal surfaces to a greater extent as compared with cells deposited onto the zeolite coatings. The surface properties found to have the most notable effect on attachment were the electrokinetic and hydrophobicity properties of the metal and zeolite coated surfaces. These results suggest a combination of two chemical mechanisms - hydrophobic and electrostatic interactions - contribute to the antifouling nature of the zeolite surface. Additional observations on the relative role of the hydrodynamic and physical phenomena are also discussed.

5.1 INTRODUCTION

Microbial deposition and biofouling have been recognized as a widespread problem in such fields as material design[1], construction[2], medicine[3], food[4] and aerospace[5]. Biofouling is the undesired attachment of organisms to surfaces within an aquatic environment[6]. All structures in aquatic environments (especially marine environments) are subject to constant, aggressive biofouling phenomena. Biofouling of solid surfaces submerged in aqueous environments has compromised efficient operation of military equipment and industrial processes[7, 8] due to increase of mass on boats and marine structures causing hydrodynamic drag, clogging of water pipes[9] and filters in cooling[10] or desalinization installation[11], etc.. Large sums of money are spent annually to combat the consequences of biofouling in marine and freshwater environments. For example, fouled ship burns up to 40% more fuel in order to maintain the same speed with an annual global cost of extra fuel used reaching $720 million[12]. Therefore, any method of inhibiting biofouling can give rise to substantial cost benefits.

It is widely known that chemically treated zeolite surfaces, such as silver or zinc-containing zeolite[13, 14] and surfactant modified zeolite[15], have been shown to inactivate viruses and bacteria. Zeolite is a crystalline aluminosilicate material with highly uniform molecular sized pores that permits ion exchange of various cationic species (Ag^{+}, Zn^{2+}, etc.) into the zeolite. Previous work showed that silver-ion exchanged zeolite A coatings on stainless steel[5, 16] and silver-ion exchanged zeolite

A-ZSM-5 mixed matrix coatings on aluminum alloys[17] exhibited excellent hydrophilicity and biocidal properties. The silver-zeolite coatings are well suited for use in condensing heat exchangers onboard manned spacecraft[5, 16]. In addition, previous work demonstrated that coatings in their as-synthesized state are extremely corrosion-resistant in strong acid, base, and pitting-aggressive solutions [18, 19]. These properties make zeolite coatings containing silver ions promising for use as antifouling materials. Interestingly, it has been reported that non-silver containing zeolite coating[5] also showed certain antimicrobial property as immediately after bacteria inoculation from the test surface, fewer *E. coli* JM 109 cells were recovered from zeolite A than from the stainless steel surface. Notably, after 24 hours incubation, this trend became quite pronounced, with two orders of magnitude more cells recovered from stainless steel ($10^{7.8}$ colony forming units, cfu) than from zeolite A ($10^{5.7}$ cfu). However, the antifouling properties of zeolite coatings, and the mechanisms by which they impact fouling, have not been explored in a dynamic pattern.

The biofouling process initiates with the adhesion of individual bacterial cells onto solid surfaces, which is followed by a multi-step process leading to the formation of a complex, adhering microbial community referred to as a "biofilm". The physical, chemical and biological factors governing the adhesion step in aquatic systems such as cell type[20], growth phase[21], solution chemistry[22, 23], hydrophobic interactions[24, 25], surface charge characteristics[26] and presence and composition of surface

macromolecules[27] have been studied extensively. These factors have been found to affect many of the interaction forces that govern the approach and adhesion of a bacterial cell to the surface, such as electrostatic, van der Waals, hydrophobic, hydration, and specific chemical forces[28]. Hence, if fouling is to be minimized, it is this initial stage of bacterial adhesion that must be inhibited and these interaction mechanisms understood.

Stainless steel and aluminum are two of the most common metallic materials. In this study, zeolite A and ZSM-5 were coated on stainless steel and aluminum alloy coupons, respectively. The effect of the zeolite coatings in inhibiting bacterial adhesion is evaluated for bacterium *Halomonas pacifica* g in a parallel plate flow chamber mounted on a fluorescent microscope with an image-capturing device. The deposition kinetics of *H. pacifica* g onto the surfaces have been determined in solutions containing KNO_3 salts, simulating the range of ionic strength conditions as would exist in aquatic environments. In addition, various characterization methods were utilized to depict the influence of ionic strength, surface feature, etc. on bacteria-solid surface interaction.

5.2 MATERIALS AND METHODS

5.2.1 Substrate pretreatment.

Aluminum alloy AA-2024-T3 (McMaster-Carr, Robbinsville, NJ) and stainless steel SS-304-2B (McMaster-Carr, Robinsville, NJ) substrates with dimensions 9 x 20

mm were immersed in a 1.3 wt. % solution of Alconox detergent (Alconox Inc., New York, NY) for one hour at 80^{o}C in an oven. The substrates were then rinsed with de-ionized (DI) water and wiped clean with gloved hands. Substrates were dried with compressed air and stored at ambient conditions before use in zeolite synthesis or bacterial deposition experiments.

5.2.2 Preparation of zeolite surfaces.

The ZSM-5 coating on aluminum alloy was prepared by an in situ hydrothermal crystallization method. The in situ crystallization process is a simple low temperature (e.g. 175 °C) one-step process that can coat surfaces with zeolite ZSM-5 of complex geometry and in confined space[18]. First, a clear synthesis solution with a molar composition of Al : NaOH : TPAOH : TEOS : H_2O = 0.0018 : 0.64 : 0.16 : 1.0 : 92.0 was prepared by dissolving aluminum powder (200 mesh, 99.95+ wt%, Aldrich) in sodium hydroxide (NaOH, 99.99 wt%, Aldrich) and double de-ionized (DDI) water followed by drop-by-drop addition of tetraproylammonium hydroxide (TPAOH, 40 wt%, aqueous solution, SACHEM) and tetraethylorthosilicate (TEOS, 98 wt%, Aldrich) under stirring. The clear solution was aged at room temperature for about 4 hours under stirring before use. A 45 mL Teflon-lined Parr autoclave (Parr Instrument Co., Moline, IL) was used as the synthesis vessel and the AA-2024-T3 substrate was fixed vertically inside the synthesis solution using a Teflon holder. Crystallization was carried out in a convection oven (Lindberg Blue, Charleston, SC) at 175°C for 16 hours. The autoclave was then removed and cooled down. The coated samples were

rinsed with DI water and dried at room temperature for at least 12 hours before characterization or cell deposition experiments.

The process of zeolite A coating on stainless steel began with the preparation of a synthesis solution with molar composition of $Na_2O : Al_2O_3 : SiO_2 : H_2O = 10.0 : 0.2 : 1.0 : 200$. The synthesis solution was prepared by first combining aluminum powder (200 mesh, 99.95+%, Aldrich) and double de-ionized (DDI) water in a 250mL wide-mouth polypropylene bottle and stirred for about 10 minutes. Next, sodium hydroxide (pellet 97+%, Aldrich) was added under a fume hood, with the cap loosely fastened to allow for the escape of gases. After stirring for a minimum of 30 minutes, Ludox® LS30 colloidal silica (30 wt. %, silica, Aldrich) was added drop-by-drop to the stirring solution. The synthesis solution was stirred until it became clear. Hollow polypropylene balls (2 cm diameter) (Fisher Scientific, Hanover Park, IL) were slit with a razor blade and an edge of clean SS-304-2B substrates were individually inserted into the slits. The assemblies were then floated in the zeolite A synthesis solution, and heated at 65^{o}C for 12 hours. After the samples were removed from the synthesis solution, they were washed thoroughly under DI water, and blown dry with compressed air before characterization or cell deposition experiments.

5.2.3 Zeolite surface characterization.

The X-ray diffraction (XRD) patterns were obtained on Siemens D-500 diffractometer using Cu K_α radiation. Zeolite coated samples (zeolite A and ZSM-5) were fixed and aligned in the sample holder to minimize shifts in 2-theta angles[29] and

analyzed. Scanning electron microscope (SEM) micrographs and elemental analysis of the coating using energy dispersive analysis of X-ray (EDAX) were obtained on a Philips XL30-FEG scanning electron microscope operated at 20 kV for each type of zeolite coating and bare metal sample. An Au/Pd coating was applied to zeolite by sputtering for 45 seconds prior to SEM imaging.

The hydrophilicity of zeolite coated and non-coated surfaces (aluminum alloy and stainless steel) was determined by contact angle measurements using VCA-Optima (AST Products Inc., Billerica, MA). This was performed by placing the substrates of interest on the sample stage and dispensing a 0.5 μL droplet of DDI water that remained suspended from the tip of an automatic syringe. The sample was raised to make contact with the water droplet and transfer it to substrates, and then lowered so that the contact angle could be measured using VCA-Optima image analysis software. The coating is considered to be hydrophilic if the resulting water contact angle is below 30^{o}. A total of 12 measurements were made on each sample. The data is reported as average with the standard deviation for each substrate (see Table 5.1).

5.2.4 Bacterial cell growth and preparation.

Halomonas pacifica ATCC 27122, a marine bacterium obtained from ATCC (American Type Culture Collection, Rockville, MD), was selected for this study. As previously reported, *H. pacifica* is a nonmotile, rod-shaped, Gram-negative cell[30] with the capacity to cause serious fouling problems in the marine environment[31, 32]. For visualization of the cells in the experimental system, a plasmid coding for an

enhanced green fluorescent protein (EGFP) and gentamicin resistance was previously introduced into the native *H. pacifica* cells by electroporation[33] and the resulting transformed cell line is referred to as *H. pacifica* g[34].

H. pacifica g cells were grown in artificial seawater (Sea Salts, 38.5 g/L, Sigma), supplemented with bacteriological peptone (Sigma, 5 g/L) and yeast extract (Sigma, 1 g/L) at 30 °C with 0.03 g/L gentamicin. Cells were harvested at mid-exponential growth phase (10.25 h) for use in characterization and adhesion studies. Cells were pelleted by centrifugation (Fisher accuSpin* 3R Centrifuge) for 15 min at 3689 g (Swing Bucket Rotor 7500 4394). The growth medium was decanted, and the pellet was resuspended in a 10 mM KNO_3 solution. The centrifugation and rinsing steps with fresh electrolyte solution were repeated two additional times to remove traces of the seawater growth medium. All electrolyte solutions utilized in cell preparation and experiments were prepared with DI water (Millipore, Billerica, MA) and reagent-grade KNO_3 (Fisher Scientific, Pittsburgh, PA) with no pH adjustment (5.6-5.8).

5.2.5 Bacterial cell characterization.

In order to analyze the size of the bacterial cells, an inverted microscope (IX70, Olympus, Japan) operating in phase contrast mode was used to take images of the *H. pacifica* g cells. Cells were suspended in an electrolyte solution at an approximate concentration of 10^8 cells/mL in 10 mM KNO_3. The images were imported into an image processing program (SimplePCI, Precision Instruments, Inc., Minneapolis,

MN), and the individual cell lengths and widths were measured. The average length and width for *H. pacifica* g were found to be 2.77 ± 0.18 μm and 0.69 ± 0.03 μm, respectively. The resulting equivalent spherical radius of the *H. pacifica* g cell was 0.61 ± 0.02 μm.

The electrophoretic mobility of the bacterial cells was determined using freshly harvested cells suspended in KNO_3 electrolyte solutions from 1 to 100 mM (the upper limit of the machine) at 25 °C using a ZetaPALS analyzer (Brookhaven Instruments Corporation, Holtsville, NY) and was repeated at least three times using freshly rinsed cells. The Smoluchowski equation[35] was used to convert the experimentally determined electrophoretic mobility values to zeta potential using the calculated equivalent radius of the cell.

The relative hydrophobicity of the *H. pacifica* g cells was measured using the semi-quantitative microbial adhesion to hydrocarbons (MATH) test[36] which indicates the relative hydrophobicity of the cells as they partition between n-dodecane and an electrolyte (10 mM KNO_3). Samples were prepared by transferring 4 mL of a cell solution (optical density of 0.2-0.25 in 10 mM KNO_3 at 546 nm) to a test tube containing 1 mL of n-dodecane (laboratory grade, Fisher Scientific). Test tubes were vortexed (AutoTouch Mixer Model 231, Fisher) for 2 min, followed by a 15 min rest period. After this time, allowing for phase separation, the optical density of the cells in the aqueous phase was measured spectroscopically at 546 nm (BioSpec-mini,

Shimadzu Corp). The hydrophobicity of cells is reported as the percent of total cells partitioned into the hydrocarbon.

Viability tests for the *H. pacifica* g cells were performed using the Live/Dead BacLight kit (L-7012, Molecular Probes, Eugene, OR) in KNO_3 solutions. The direct counting of the stained live and dead cells was done using an inverted microscope (IX70, Olympus, Japan) operating in fluorescent mode with a red/green fluorescence filter set (Chroma Technology Corp., Brattleboro, VT). The viability of the *H. pacifica* g cell cultures was found to be 93 ± 2% based on the Live/Dead BacLight® kit in 10 mM KNO_3.

5.2.6 Cell adhesion study.

Bacterial deposition experiments were conducted in a rectangular parallel plate flow chamber[37] system (Product # 31-010, GlycoTech, Rockville, MA) (see Figure 5.1) installed on the stage of an upright fluorescent microscope (BX-52, Olympus, Japan). The top of the chamber is a microscope glass slide. The bottom of the chamber is a cast acrylic flow deck having flow entrance and exit slits at opposite ends which were connected to inlet and outlet ports and a groove to hold various samples. A clean metal (aluminum alloy or stainless steel) or zeolite (ZSM-5 or zeolite A coated) sample is inserted in the center of a cast acrylic flow deck in possession of a groove with dimensions of 9 × 20 mm to achieve a flat surface. The sample fits snuggly within the groove and is held in place with vacuum grease. The thickness of the chamber is determined by the rubber gasket, which is pressed against

the flow deck so that the holes are directly over the shaped groove, which is in turn connected to the vacuum port. A thin layer of vacuum grease is applied to both sides of the gasket around the chamber to ensure a tight seal. The electrokinetic properties of the sample surfaces were determined by a streaming potential analyzer (EKA, Anton Paar, Graz, Austria) with an asymmetric clamping cell[38]. Measurements were obtained in KNO_3 over the range of ionic strengths used in the deposition experiments. The instrument was first rinsed with 1 L of deionized water followed by 0.5 L of the electrolyte solution used in the measurement. Prior to the streaming potential measurements being taken, the sample surface was equilibrated with the corresponding fresh electrolyte solution for 10 min. The measured streaming potential was utilized to calculate the zeta potential of samples as described elsewhere[38]. The microscope glass slides used in experiments were cleaned with a detergent (2% RBS 35, Fisher Scientific, Pittsburgh, PA), followed by alternately rinsing with ethanol and deionized (DI) water prior to flow chamber assembly. The overall dimensions of the chamber were 6 cm × 1cm × 0.0762 cm. Fluorescently labeled bacteria depositing on the surface was imaged by a 40x objective (UPlanFI, Olympus) focused on the inner surface of the center of the sample and using a fluorescent filter set with an excitation wavelength of 480 nm and emission wavelength of 510 nm (Chroma Technology Corp., Brattleboro, VT).

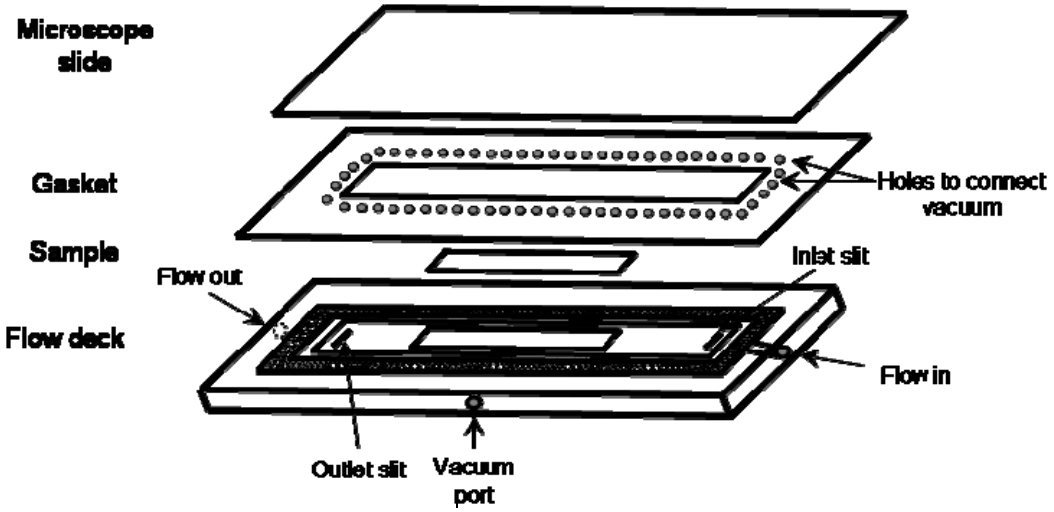

Figure 5.1 Diagram of the parallel plate flow chamber system used in the experiments.

Deposition of cells was recorded with a digital camera (Demo Retiga EXI Monochrome, QImaging) acquiring images every 20 seconds over the course of a 30 minutes injection and analyzed with the supplied software (SimplePCI, Precision Instruments, Inc., Minneapolis, MN). The number of deposited cells was determined for each time interval by comparing the changes between successive images. Inlet concentration for the experiments was maintained at 2×10^7 cells/mL. A flow rate of 2 mL/min was employed, corresponding to an average flow velocity of 0.0044 m/s, a Peclet number of 0.0287 (within the diffusion regime[35, 39]), and a shear rate of 34 s^{-137}. Bacterial deposition experiments were conducted at ionic strength conditions of 1, 10 and 100 mM KNO_3 solution at ambient pH (5.6-5.8) and temperature (22–25 ºC).

The kinetics of bacterial adhesion in the parallel plate flow chamber system was quantified by calculating the dimensionless Sherwood number (*Sh*), which is related to the bacterial deposition flux (number of cells per area per time), *J*, the cell radius, a_p, the bulk cell particle concentration, C_0, and the bulk diffusion coefficient calculated from the Stokes-Einstein equation, D_∞, via[35]

$$Sh = \frac{Ja_p}{C_0 D_\infty} \qquad (1)$$

The deposition flux (*J*) was determined by normalizing the initial slope of the number of deposited cells versus time curve and by the microscope viewing area (205 μm × 153 μm).

The value of deposition rate under chemically favorable, transport-limited conditions in the parallel plate flow chamber system (Sh_{fav}) was determined experimentally for *H. pacifica* g in 10 mM KNO_3. Favorable, non-repulsive conditions were achieved in the parallel plate flow chamber system by using a glass microscope slide with a net positive zeta potential, achieved by modifying the microscope slides with aminosilane[38]. This was done by exposing the plain glass microscope slide to a 0.2% (v/v) mixture of (aminoethylaminomethyl)–phenethyltrimethoxysilane (Gelest, Inc., Tullytown, PA) in ethanol for 3–5 min at room temperature and then curing for 90 min at 130 ºC[40]. The average Sherwood number under favorable conditions (Sh_{fav}) for *H. pacifica* g was 0.029 ± 0.002.

H. pacifica g deposition kinetics were also presented in terms of the attachment efficiency, α, which was calculated by normalizing the Sherwood number at each experimental condition by the Sherwood number determined under favorable electrostatic conditions:

$$\alpha = \frac{Sh}{Sh_{fav}} \qquad (2)$$

α is indicative of the success of a cell attaching to the sample surface[35]. All experimental conditions were tested a minimum of three different times, each utilizing a fresh cell suspension.

5.3 Results and Discussion

5.3.1 Characteristics of test surfaces.

To determine the structure, morphology, and aluminum incorporation, zeolite A coated on SS-304-2B and ZSM-5 coated on AA-2024-T3 were characterized by X-ray diffraction (XRD), scanning electron microscopy (SEM), and energy dispersive analysis of X-ray (EDAX). The XRD patterns for zeolite A and ZSM-5 crystals were in agreement with the patterns reported for zeolite A and ZSM-5 (www.iza-online.org) and confirmed the presence of zeolite A on SS-304-2B and ZSM-5 on AA-2024-T3 (Figure 5.2). No additional diffraction lines were seen and the baseline of the XRD patterns was flat, indicating that the zeolite coatings were essentially free of amorphous materials.

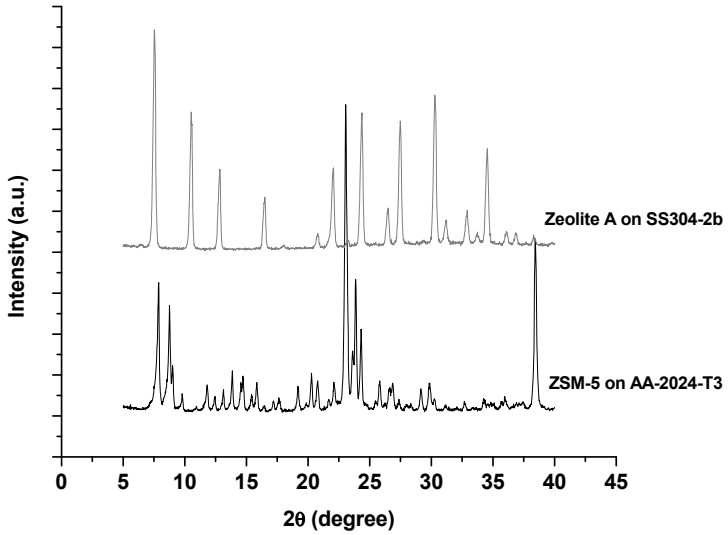

Figure 5.2 X-ray diffraction patterns of ZSM-5 on aluminum and zeolite A on stainless steel.

The morphology of stainless steel, aluminum alloy, zeolite A coated on stainless steel, and ZSM-5 coated on aluminum alloy was examined by scanning electron microscopy (SEM) and the obtained images are shown in Figure 5.3. The SEM images indicate that zeolite A and ZSM-5 coatings have a complete and even coverage over the entire substrate surfaces. The polycrystalline zeolite coatings are fully inter-grown and approximately 5-6 μm thick on top of the base metal. Furthermore, the zeolite coated test surfaces were much rougher than their corresponding bare metal surfaces.

Semi-quantitative elemental analysis by energy dispersive analysis of X-ray (EDAX) spectroscopy presented in Figure 5.4 show that ZSM-5 (Figure 5.4b) has much higher Si/Al ratio than zeolite A (Figure 5.4a). In general, zeolites with lower

Si/Al ratios are more hydrophilic and the contact angle analysis of the coated surfaces confirmed this. The results of zeolite A and ZSM-5 coatings were 0° and 26.3° respectively (refer to Table 5.1). Additionally, the lack of coatings resulted in a more hydrophobic bare metal surface (80° and 64° for aluminum and stainless steel, respectively).

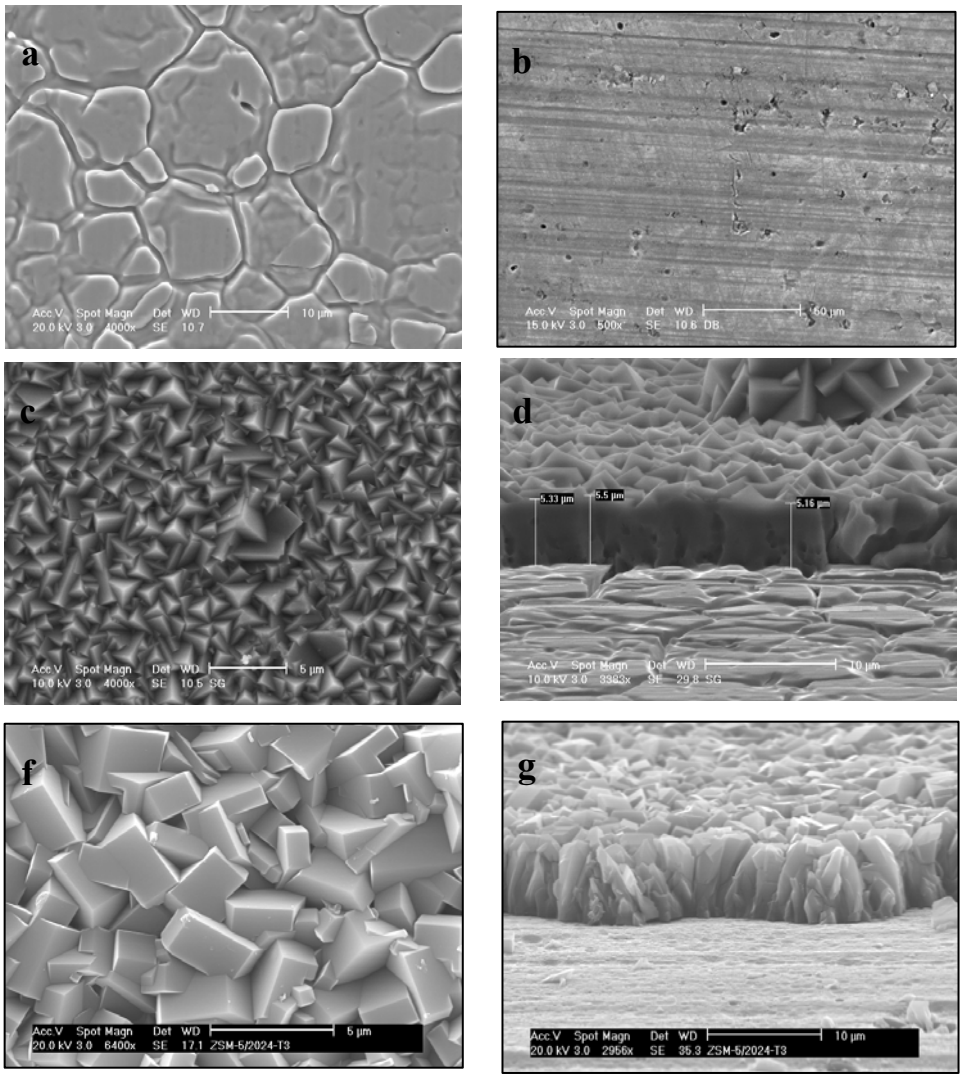

Figure 5.3 SEM images of a) bare stainless steel; b) bare aluminum; c) zeolite A coated on stainless steel; d) zeolite A coated on stainless steel from side-view; e) ZSM-5 coated on aluminum; and f) ZSM-5 coated on aluminum from side view.

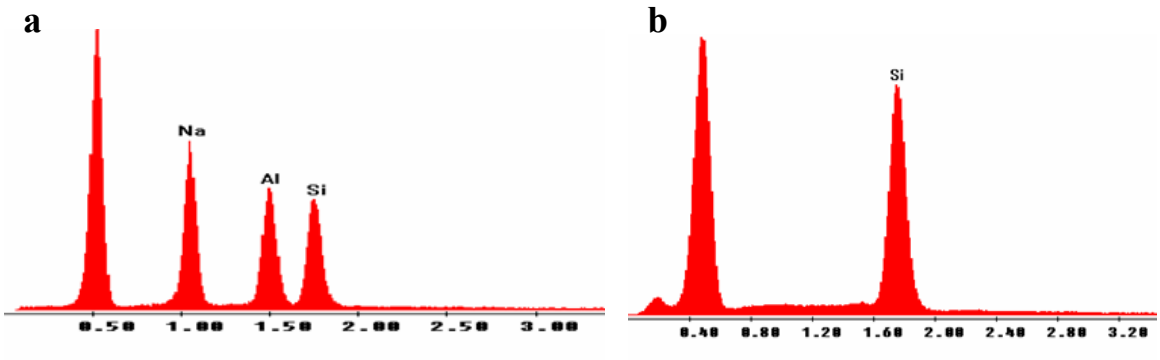

Figure 5.4 Semi-qualitative elemental analysis by EDAX of a) zeolite A coated on stainless steel; b) ZSM-5 coated on aluminum alloy.

Table 5.1 Water contact angles on the bare metal and zeolite coated surfaces

Surface tested	Contact angle (°)
Aluminum	80.0 ± 3.0
Stainless steel	64.0 ± 3.3
Zeolite A on SS	0
ZSM-5 on Al	26.3 ± 2.6

Table 5.2 showed the zeta potentials of four types of surfaces as a function of ionic strength determined by the streaming potential measurements. The four surfaces became less negatively charged with increasing ionic strength as anticipated from electrostatic double layer theory[41]. Specifically, bare stainless steel and aluminum alloy surfaces possessed a positive charge and had similar magnitude of zeta potential over the range of ionic strength conditions tested, while both zeolite coated substrates exhibited a negative charge at 1 mM and a positive charge at 10 mM. Zeolite A

coated on stainless steel showed less negatively charged at 1 mM and more positively charged surface at 10 mM than ZSM-5 at the same solution conditions.

Table 5.2 Zeta potential of surfaces and *H. pacifica* g cells as a function of ionic strength in KNO_3 solution

	1 mM	10 mM	100 mM
Aluminum	4.39 ± 0.16	43.21 ± 1.99	-*
Stainless steel	4.40 ± 0.69	45.40 ± 1.45	-
Zeolite A on SS	-4.14 ± 0.48	48.97 ± 0.81	-
ZSM-5 on Al	-12.57 ± 0.25	25.38 ± 5.54	-
H. pacifica g	-76.47 ± 3.06	-61.21 ± 3.93	-25.20 ± 7.70

* Value not measurable as 100mM is the upper limit for the streaming potential apparatus.

5.3.2 Characteristics of *H. pacifica* g cells.

To understand what factors dominate the interaction between bacteria and surfaces, further cell characterization techniques were employed. The zeta potentials of the *H. pacifica* g cells were presented in Table 5.2. The results indicated that the marine bacteria used in this study were negatively charged over the entire range of ionic strength conditions tested. The absolute magnitude of the cell zeta potential decreased with an increase in salt concentration. The cells exhibited zeta potentials of -76.5 ± 3.1 mV and -61.2 ± 3.9 mV when suspended in an aqueous 1 mM and 10 mM KNO_3 solutions, respectively. The zeta potential decreased to -25.2 ± 7.7 mV with an increase to 100 mM KNO_3. Analysis of the cell hydrophobicity employing the MATH test established 44.9 ± 2.0% of the *H. pacifica* g in 10 mM

KNO_3 solution partitioned into n-dodecane. This suggests the cells are relatively hydrophobic.

5.3.3 Attachment behavior of *H. pacifica* g.

The attachment trends for the bacteria are shown in Figure 5.5, with values of the attachment efficiency (α) plotted as a function of solution ionic strength. It was evident from this figure that ionic strength had a marked effect on the bacterial attachment kinetics, as the general observation for the four surfaces was increasing deposition with ionic strength. Notably, there was no measurable bacterial deposition at 1 mM KNO_3 solution on any of surfaces. The attachment efficiencies of *H. pacifica* g onto stainless steel were determined as 0.33 and 0.60 in 10 mM and 100 mM KNO_3, respectively. The attachment efficiencies of *H. pacifica* g onto zeolite A coating were 0.20 and 0.52 at ionic strength of 10 mM and 100 mM KNO_3. In the case of aluminum alloy, α were determined to be 0.39 and 0.83 at ionic strength of 10 mM and 100 mM. For the corresponding zeolite ZSM-5 coating, the bacterial attachment efficiencies were observed to be 0.14 and 0.60 at ionic strength of 10 mM and 100 mM, respectively. Generally, *H. pacifica* g deposited onto the bare metal at higher attachment efficiency values as compared with cells deposited onto corresponding zeolite coatings.

Further insight can also be gained when considering that bacterial attachment is controlled by cell transport from the bulk solution to the collector surface and the subsequent interactions between the cell and surface occurring upon close approach. Neglecting surface interactions, hydrodynamic and external forces, the Sherwood

number – which is the ideal spherical particle mass transfer number, Sh_{ideal} – under favorable conditions in a parallel plate flow chamber can be expressed as[39]:

$$Sh_{ideal} = \frac{1}{\Gamma(4/3)}\left(\frac{2Pe}{9x/b}\right)^{1/3} \qquad (3)$$

where the Peclet number (Pe) is equal to $3ua_p^3/(2b^2D_\infty)$ in the parallel plate flow chamber, u is the fluid velocity, x is equal to half of the flow chamber length, b is midway depth of the parallel plate channel and the gamma function $\Gamma(4/3)$ is equal to 0.893. The calculated ideal Sherwood number (Sh_{ideal}) was 0.052. This ideal value is almost two times that of the experimentally determined value for favorable conditions (Sh_{fav}, 0.029 ± 0.002), suggesting that *H. pacifica* g under chemically favorable, transport-limited conditions, is not depositing as much as an ideal spherical particle of the same effective size would with the same solution and surface chemistry. The discrepancy indicates that other mechanisms are involved, possibly including the shape of the cells, the physical roughness of the surfaces, and the hydrodynamic interactions imposed on bacteria upon closely approach.

Figure 5.5 shows that the attachment efficiencies (α) of various surfaces were less than unity at the range of all experiment conditions tested. From equation 2, unfavorable Sherwood numbers of various surfaces obtained from experiments were less than Sh_{fav}, 0.029 ± 0.002, determined for *H. pacifica* g. Based upon the zeta potential measurements of the various surfaces, interactions at 10mM KNO_3 should be electrostatically favorable for cell attachment (see Table 5.2), such that any

difference in attachment is likely a function of transport to the surface or a physical-chemical phenomenon at or near the surface. However, care was taken to ensure that transport from the bulk to the surface is uniform in the parallel plate system by maintaining a constant flowrate for all experiments. Thus, transport should not be the cause of the experimentally determined $Sh < Sh_{fav}$. Rather, this observation is the result of subtle surface feature differences between various test surfaces and aminosilane-modified microscope glass slides, likely causing subtle changes in interaction and hydrodynamic forces. Microscope images confirmed the subtle differences in physical appearance, with the aminosilane-modified microscope glass slides appearing smoother than the test sample surfaces (images not shown). The possible interaction and hydrodynamic forces involved are discussed further below.

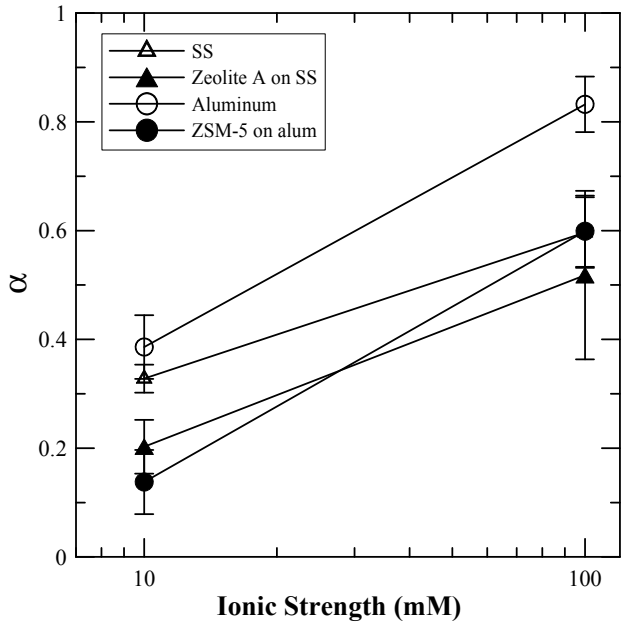

Figure 5.5 Attachment efficiency of *Halamonas pacifica* g onto zeolite coated and metal surfaces.

5.3.4 Influence of coatings on *H. pacifica* g attachment rate.

The present study investigated the initial attachment of *H. pacifica* g to examine the potential antifouling properties of two zeolite coatings. Notably, focus was placed on determining the extent to which zeolite coatings inhibited bacterial attachment onto surfaces compared with the corresponding bare metal surfaces. Evidently, although electrostatic interactions were clearly involved (Figure 5.5) between cells and all of the test surfaces, they are not sufficient to fully explain the observed deposition trends. Interestingly, the presence of a zeolite thin film reduced bacterial deposition for both coated surfaces even though the zeta potential measurements revealed electrostatically "favorable" conditions for bacterial adhesion for the four surfaces tested at 10 mM and 100 mM KNO_3 solutions.

At the lowest salt concentration tested (1 mM) the zeolite coatings on either stainless steel or aluminum alloy resulted in the change of surface charge from positive to negative, as measured by zeta potential. With the negatively zeolite coated surfaces, the bacteria are expected to experience repulsive electrostatic interactions with the bacteria while the positively charged bare metals attract them. However, it was observed that no cells deposited on any of the surfaces at 1 mM. This is likely due to whatever minor attractive forces existed (in particular between the bare substrates and the cells), was overcome by hydrodynamic forces.

Another possible mechanism involved is hydrophobic interaction. It was previously suggested [5] that the addition of a ZSM-5 or zeolite A coating on aluminum

alloy and stainless steel enhances the hydrophilicity, and our contact angle data confirms these trends (see Table 5.1). This current work also observed that the more hydrophilic the surface is (zeolite coating more than the bare metal, the stainless steel more than the bare aluminum alloy and zeolite A coating more than ZSM-5), the less bacterial deposition occurs when experiencing similar electrostatic interactions between bacterial cells and surfaces. This suggests a combination of hydrophobic and electrostatic interactions are contributing to the antimicrobial nature of the test surfaces.

The deposition trends observed under dynamic flow conditions in this study are consistent with previous batch tests [5] which also observed less cell attachment on zeolite A than a bare stainless steel surface. The batch studies showed that immediately after bacteria inoculation from the test surface, fewer *E. coli* JM 109 cells were recovered from zeolite A than from the stainless steel surface. Notably, after 24 hours incubation, this trend became quite pronounced, with two orders of magnitude more cells recovered from stainless steel ($10^{7.8}$ colony forming units, cfu) than from zeolite A ($10^{5.7}$ cfu). In this previous work, the authors attributed these trends to the hydrophilic nature of zeolite A. However, the static batch tests differed substantially from this current study in hydrodynamic and solution chemistry conditions and the extent to which hydrophobicity versus hydrodynamics are involved may be confounded. Nonetheless, both experimental approaches reveal the zeolite

coatings reduce bacterial cell attachment as compared to bare metal surfaces, making these zeolite coatings well-suited for "antifouling" materials.

Finally, the issue of surface roughness must be addressed. As can be observed in the SEM images (Figure 5.2), the zeolite coated test surfaces were much rougher than their corresponding bare metal surfaces. At first one might anticipate a rougher surface resulting in greater attachment because of a higher surface area available for attachment and potentially favorable physicochemical interaction sites[42, 43], but this was not the case. It has been reported that the surface roughness does not affect the number of attaching bacteria under static and flow conditions[44, 45]; however, in this study, it was observed that cell deposition was reduced with greater roughness (with coatings). This is likely due to a combination of both enhanced repulsion with the coated surfaces reducing the bacterial cells' access to the physical asperities, and the fluid flow over the rough surface may be more turbulent leading to greater hydrodynamic forces imposed on bacterial cells upon close approach to the surfaces. Further work to delineate the relative impact of roughness, as compared to these other mechanisms is warranted.

5.4 CONCLUSION

The parallel plate flow chamber experimental system was employed to investigate the influence of zeolite coating onto metal surfaces on the adhesion kinetics of marine bacteria, *H. pacifica* g. The experiment results indicate that the adhesion property of

marine microorganisms is markedly sensitive to collector surface property and solution ionic strength.

Current strategies developing antifouling surfaces and materials emphasize either enhancing the electrostatic repulsion between surfaces and microorganisms (charge modification – either bulk charge, distribution, or density of charge) or increasing the hydrophilic nature of materials. The zeolite coatings containing aluminum, as investigated in this study, enhance the density of charged groups on the material surface both altering the test surface charge and hydrophobicity. Experimental results for the attachment behavior of the marine species, *H. pacifica* g, onto the bare and zeolite coated metal surfaces confirmed that in flowing aquatic environments zeolite coatings reduce the extent of initial bacterial attachment across the range of solution chemistry and hydrodynamic conditions tested, which could lower the possible level of biofilm formation. This provides greater insight into how to design future nontoxic, antifouling surfaces and materials.

5.5 REFERENCES

1. Gademann, K., *Chimia* **2007,** 61, (6), 373-377.

2. Gaylarde, C. C.; Morton, L. H. G., *Rev. Microbiol.* **1997,** 28, (4), 221-229.

3. Norde, W., *Z. Phys. Chemie-Int. J. Res. Phys. Chem. Chem. Phys.* **2007,** 221, (1), 47-63.

4. He, Y. L.; Xu, P.; Li, C. J.; Zhang, B., *Water Res.* **2005,** 39, (17), 4110-4118.

5. McDonnell, A. M. P.; Beving, D.; Wang, A. J.; Chen, W.; Yan, Y. S., *Adv. Funct. Mater.* **2005,** 15, (2), 336-340.

6. Cooksey, K. E.; Wigglesworthcooksey, B., *Aquat. Microb. Ecol.* **1995,** 9, (1), 87-96.

7. Ross, J., *Smithsonian* **1994,** 24, (11), 40-&.

8. Coetser, S. E.; Cloete, T. E., *Crit. Rev. Microbiol.* **2005,** 31, (4), 213-232.

9. Goto, Y., *Water Sci. Technol.* **2002,** 46, (11-12), 45-50.

10. Meesters, K. P. H.; Van Groenestijn, J. W.; Gerritse, J., *Water Res.* **2003,** 37, (3), 525-532.

11. Lu, R. H.; Liu, Q.; Xiao, C. S.; Bai, S.; Chen, H. C.; Wang, F. R., *Acta Microbiologica Sinica* **1984,** 24, (3), 243-249.

12. Townsin, R. L., *Biofouling* **2003,** 19, (1 supp 1), 9 - 15.

13. Cowan, M. M.; Abshire, K. Z.; Houk, S. L.; Evans, S. M., *J. Ind. Microbiol. Biotechnol.* **2003,** 30, (2), 102-106.

14. Rivera-Garza, M.; Olguin, M. T.; Garcia-Sosa, I.; Alcantara, D.; Rodriguez-Fuentes, G., *Microporous Mesoporous Mat.* **2000,** 39, (3), 431-444.

15. Schulze-Mokuch, D.; Bowman, R. S.; Pillai, S. D.; Guan, H. D., *Ground Water Monit. R.* **2003,** 23, (4), 68-74.

16. O'Neill, C.; Beving, D. E.; Chen, W.; Yan, Y. S., *AICHE J.* **2006,** 52, (3), 1157-1161.

17. Beving, D. E.; O'Neill, C. R.; Yan, Y. S., *Microporous Mesoporous Mat.* **2008,** 108, (1-3), 77-85.

18. Cheng, X. L.; Wang, Z. B.; Yan, Y. S., *Electrochem. Solid State Lett.* **2001,** 4, (5), B23-B26.

19. Beving, D. E.; McDonnell, A. M. P.; Yang, W. S.; Yan, Y. S., *J. Electrochem. Soc.* **2006,** 153, (8), B325-B329.

20. Walker, S. L., *Colloid. Surface. B* **2005,** 45, 181-188.

21. Walker, S. L.; Hill, J. E.; Redman, J. A.; Elimelech, M., *Appl. Environ. Microbiol.* **2005,** 71, 3093-3099.

22. Li, Q.; Logan, B. E., *Water Res.* **1999,** 33, (4), 1090-1100.

23. Kuznar, Z.; Elimelech, M., *Environ. Sci. Technol.* **2004,** 38, (24), 6839-6845.

24. van Loosdrecht, M. C. M.; Lyklema, J.; Norde, W.; Schraa, G.; Zehnder, A. J. B., *Appl. Environ. Microbiol.* **1987,** 53, (8), 1893-1897.

25. Schafer, A.; Harms, H.; Zehnder, A. J. B., *Environ. Sci. Technol.* **1998,** 32, (23), 3704-3712.

26. Gross, M.; Cramton, S. E.; Gotz, F.; Peschel, A., *Infect. Immun.* **2001,** 69, (5), 3423-3426.

27. Kuznar, Z. A.; Elimelech, M., *Langmuir* **2005,** 21, (2), 710-716.

28. Ubbink, J.; Schar-Zammaretti, P., *Curr. Opin. Colloid Interface Sci.* **2007,** 12, (4-5), 263-270.

29. Parrish, W.; Wilson, A. J. C., *Acta Crystallographica* **1954,** 7, (10), 622-622.

30. Dobson, S. J.; Franzmann, P. D., *Int. J. Syst. Bacteriol.* **1996,** 46, (2), 550-558.

31. Bakker, D. P.; Busscher, H. J.; van Zanten, J.; de Vries, J.; Klijnstra, J. W.; van der Mei, H. C., *Microbiol.-(UK)* **2004,** 150, 1779-1784.

32. Bakker, D. P.; Huijs, F. M.; de Vries, J.; Klijnstra, J. W.; Busscher, H. J.; van der Mei, H. C., *Colloid. Surface. B* **2003,** 32, (3), 179-190.

33. Sambrook, J.; Fritsch, E. F.; Maniatis, T., *Molecular Cloning, A Laboratory Manual*. 2nd ed.; Cold Spring Harbor Laboratory Press: Cold Spring Harbor, New York, 1989; Vol. 3.

34. Chen, G. X.; Walker, S. L., *Langmuir* **2007,** 23, (13), 7162-7169.

35. Elimelech, M., Gregory, J., Jia, X., Williams, R.A., *Particle Deposition and Aggregation: Measurement, Modeling and Simulation*. Butterworth-Heinemann: 1995; p 441.

36. Pembrey, R. S.; Marshall, K. C.; Schneider, R. P., *Appl. Environ. Microbiol.* **1999,** 65, (7), 2877-2894.

37. McClaine, J. W.; Ford, R. M., *Biotechnol. Bioeng.* **2002,** 78, (2), 179-189.

38. Walker, S. L.; Bhattacharjee, S.; Hoek, E. M. V.; Elimelech, M., *Langmuir* **2002,** 18, (6), 2193-2198.

39. Adamczyk, Z.; Vandeven, T. G. M., *J. Colloid Interf. Sci.* **1981,** 80, (2), 340-356.

40. Chen, J. Y.; Klemic, J. F.; Elimelech, M., *Nano Lett.* **2002,** 2, (4), 393-396.

41. Poortinga, A. T.; Bos, R.; Norde, W.; Busscher, H. J., *Surf. Sci. Rep.* **2002,** 47, (1), 3-32.

42. Pedersen, K., *Water Res.* **1990,** 24, (2), 239-243.

43. Vanhaecke, E.; Remon, J. P.; Moors, M.; Raes, F.; Derudder, D.; Vanpeteghem, A., *Appl. Environ. Microbiol.* **1990,** 56, (3), 788-795.

44. Hilbert, L. R.; Bagge-Ravn, D.; Kold, J.; Gram, L., *Int. Biodeterior. Biodegrad.* **2003,** 52, (3), 175-185.

45. Barnes, L. M.; Lo, M. F.; Adams, M. R.; Chamberlain, A. H. L., *Appl. Environ. Microbiol.* **1999,** 65, (10), 4543-4548.

CHAPTER 6

INITIAL COLLOID DEPOSITION ON BARE AND ZEOLITE-COATED STAINLESS STEEL AND ALUMINUM: INFLUENCE OF SURFACE ROUGHNESS

ABSTRACT

The impact of surface roughness of bare and zeolite ZSM-5 coated stainless steel and aluminum alloy on colloid deposition has been investigated using a parallel plate flow chamber system in an aqueous environment. The metals were systematically polished to alter the surface roughness from nanoscale to microscale, with the subsequent surface roughness of both the bare and coated surfaces varying from 11.2 to 706 nm. The stainless steel and aluminum alloy surfaces are extensively characterized, both as bare and coated surfaces. Experimental results suggest that ZSM-5 coating and surface roughness have a pronounced impact on the kinetics of the colloid deposition. The ZSM-5 coating reduced colloid adhesion compared to the corresponding bare metal surface. In general, the greater surface roughness of like samples resulted in higher colloid deposition. The two exceptions are ZSM-5 coated mirror-polished stainless steel and the unpolished aluminum surfaces, which are rougher than the other two samples of the same metal type, but result in the least deposition. The reasons for these observations are discussed, as well as the effect of surface charge and hydrophobicity on the adhesion. The relative importance of surface roughness versus contributions of electrostatic interactions and hydrophobicity to the colloid deposition is also discussed.

6.1 Introduction

Bacterial attachment and biofilm formation have been widely associated with the problem of the contamination and fouling of different surfaces in such fields as material design[1], construction[2], medicine[3], food processing[4] and aerospace[5]. For instance, biofouling increases the mass on boats and marine structures causing hydrodynamic drag[6, 7], clogs water pipes[8] and filters in cooling or desalinization installation[9, 10], thus has compromised efficient operation of military equipment and industrial processes. Traditionally, antifouling paints containing biocides have been effectively used to control fouling; however, the adverse effects of these compounds in paints (e.g. copper[11] and tributyltin[12]) have resulted in tributyltin-based antifouling paints being banned in the U.S.[13]. Hence, there is considerable interest in the development of new environmentally benign antifouling coatings and surfaces.

Cell surface characteristics (i.e. cell type[14], growth phase[15], hydrophobic interactions[16, 17], surface charge characteristics[18] and presence and composition of surface macromolecules[19]) and collector surface properties (morphology[20], surface chemistry[21, 22], and roughness[23-25]) can influence bacteria adhesion to surfaces. Experimental studies have demonstrated the importance of these properties; however, discrepancies between experimental observations and theoretical simulations exist and the failure of the predictive models is often attributed to the solid collector surface roughness[23, 25, 26] and chemical heterogeneity[27-29].

Contradicting results concerning the influence of surface roughness on bacterial attachment have been reported. Vanhaecke et al.[30] investigated the role of surface roughness (Ra: 0.115 – 0.600 μm) on *Pseudomonas aeruginosa* 27853 attachment to stainless steel and observed ~100 times lower cell deposition on the electropolished plate (the smoothest) versus the 120-grit treated plate (the roughest) surfaces tested. Taylor et al.[31] found that an increase in roughness of polymethyl methacrylate (PMMA) (Ra: 0.04 – 1.24 μm) resulted in significantly greater *Pseudomonas aeruginosa* and *Staphylococcus epidermidis* attachment; however, further increases of roughness (Ra: 1.86 - 7.89 μm) resulted in a decrease in adhesion. They found the underlying topography influenced adhesion even when the PMMA surfaces were coated with protein. Tang et al.[32] showed rougher silicone surfaces promoted *Staphylococcus epidermidis* adhesion and colonization only above a threshold value of the root-mean-square roughness 0.2 μm. Therefore, in the food industry, the German dairy standard (DIN 11480, 1992) states that surface roughness must not exceed Ra of 0.8 μm.[33] Conversely, Mitik-Dineva et al.[24] reported greater *Escherichia coli* K12, *Pseudomonas aeruginosa* (ATCC 9027), and *Staphylococcus aureus* CIP 68.5 adhesion onto smoother glass surfaces for all bacterial species examined. Emerson et al.[34] also observed that the adhesion of *Staphylococcus epidermidis* was inversely proportional to roughness of a variety of chemically and texturally distinct model surfaces including gold, aliphatic and aromatic

self-assembled monolayers, and polymeric and proteinaceous materials ranging from nano- to micron scale roughness.

In many reported cases, surface roughness did not affect bacterial attachment at all[35-37]. Shellenberger and Logan[23] showed roughness of glass beads to contribute to latex microsphere adhesion; however, there was no significant difference between the rough and smooth surfaces for *E. coli*. The authors attributed the lack of sensitivity to roughness to the presence of bacterial surface polymers, which shield influence of roughness. There is clearly disagreement in the literature and an uncertainty as to the mechanisms involved. This is likely due to the wide range of variables in these studies such as surface and bacterial type, as well experimental type (batch versus flowing system).

Our previous work demonstrated that a zeolite-coated stainless steel showed antimicrobial properties[5]. These tests, conducted in batch systems, found two orders of magnitude fewer *E. coli* cells on zeolite versus bare stainless steel after 24 hours. Subsequent experiments tested these observations under flowing, rather than batch systems, using a marine bacterium, *Halomonas pacifica* g.[38] Experimental results showed that bacteria deposited on bare stainless steel and aluminum alloy surfaces to a greater extent than the zeolite coated metals. That study concluded a combination of two mechanisms – hydrophobic and electrostatic interactions – contribute to the antimicrobial, or antifoulding, nature of the zeolite. That work also observed less bacterial deposition on the rougher, coated surfaces. However, the actual

contribution of roughness on bacterial deposition and the relative importance of the impact of roughness as compared to these other mechanisms were unclear.

This study has been designed to directly investigate the contribution of roughness and to better understand the mechanism of deposition on solid surfaces in aquatic environments. Specifically, this study considers surfaces with nanoscale to micron-scale roughness during the initial stage of particle attachment on the metal and zeolite coated surfaces, similar to those utilized in our previous study, in a parallel plate flow chamber system[38]. Latex microspheres are considered surrogates for bacterial cells as their dimensions and non-specific surface interactions are similar to bacteria[20, 39]. This allows the investigation of physicochemical contributions to deposition, avoiding complicated biological factors such as bacterial cell specific ligand-receptor interactions[39], which would differ from one bacterial species to another.

6.2 Materials and Methods

6.2.1 Metal substrates pretreatment.

Two of the most common metallic materials – stainless steel and aluminum alloy were selected for the study. Stainless steel (McMaster-Carr, Robinsville, NJ) samples were purchased with a mirror finish (No. 8 SS-304) and unpolished (SS-304-2B). A sample of the unpolished (SS-304-2B) was polished by an

abrasive paper with 600 grit (3M Co., St. Paul, MN) using a Buehler polisher. This provided collector surfaces with three levels of roughness, which are referred to as mirror finish SS, unpolished SS, and 600-grit SS. Aluminum alloy AA-2024-T3 (McMaster-Carr, Robbinsville, NJ) was polished by abrasive papers (600, 1200 grit, 3M Co., St. Paul, MN) to obtain collector surfaces with three levels of roughness (refer to unpolished Al, 600-grit Al and 1200-grit Al). The substrates (9 x 20 mm samples) were immersed in a 1.3 wt% solution of Alconox detergent (Alconox Inc., New York, NY) for one hour at 80 °C in an oven, then rinsed with de-ionized (DI) water, dried with compressed air and stored at ambient conditions before use in zeolite synthesis or colloid deposition experiments.

6.2.2 Preparation of ZSM-5 coatings on metal substrates.

The ZSM-5 coatings on stainless steel and aluminum alloy with three levels of roughness described above were prepared by an in situ hydrothermal crystallization method[38]. A clear synthesis solution with a molar composition of Al : NaOH : TPAOH : TEOS : H_2O = 0.0018 : 0.64 : 0.16 : 1.0 : 92.0 was made by dissolving aluminum powder (200 mesh, 99.95+ wt%, Aldrich) in sodium hydroxide (NaOH, 99.99 wt%, Aldrich) and double DI water, followed by drop-by-drop addition of tetraproylammonium hydroxide (TPAOH, 40 wt%, aqueous solution, SACHEM) and tetraethylorthosilicate (TEOS, 98 wt%, Aldrich) under stirring. The clear solution was aged at room temperature for 4 hours under stirring and then transferred to a 45 mL Teflon-lined Parr autoclave (Parr Instrument Co., Moline, IL). The metal

substrates described above were fixed vertically inside the synthesis solution using a Teflon holder. Crystallization was carried out in a convection oven (Lindberg Blue, Charleston, SC) at 175°C for 16 hours. The samples were then removed from the autoclave and cooled. The coated samples - referred to ZSM-5 on mirror SS, ZSM-5 on unpolished SS, ZSM-5 on 600-grit SS, ZSM-5 on unpolished Al, ZSM-5 on 600-grit Al and ZSM-5 on 1200-grit Al, respectively - were rinsed with DI water and dried at room temperature for at least 12 hours before characterization or colloid deposition experiments.

6.2.3 Metal and ZSM-5 coated model surfaces characterization.

Siemens D-500 diffractometer using Cu K_α radiation was employed to obtain the X-ray diffraction (XRD) patterns of the bare metal (stainless steel and aluminum alloy) and ZSM-5 coating samples. Samples were fixed and aligned in the sample holder to minimize shifts in 2-theta angles[40] and analyzed. Scanning electron microscope (SEM) micrographs and elemental analysis of the coating using energy dispersive analysis of X-ray (EDAX) were obtained on a Philips XL30-FEG scanning electron microscope operated at 20 kV for each bare metal and ZSM-5 coating sample. An Au/Pd coating was applied to zeolite by sputtering for 45 seconds prior to scanning electron microscopic (SEM) imaging.

Surface roughness measurements were determined as arithmetic average roughness, Ra[41], using a surface profilometer (Veeco Instruments, Inc., Tucson, Arizona) equipped with a stylus of radius equaling 5 μm. The probe of the machine

was oriented perpendicular to the grinding scratches made during sample preparation, so that the values from different sample surfaces could be compared. A tracing length of 0.8 mm was used. The results were presented as averages of seven roughness measurements made on each sample surface.

The hydrophilicity of ZSM-5 coated and non-coated surfaces (stainless steel and aluminum alloy) was analyzed by water contact angle measurements using VCA-Optima (AST Products Inc., Billerica, MA).[38] The sample surface is considered to be hydrophilic if the resulting water contact angle is below 30^{o}. A total of 12 measurements were taken on each sample. The data was reported as an average and standard deviation for each sample.

A streaming potential analyzer (EKA, Anton Paar, Graz, Austria) with an asymmetric clamping cell[42] was used to determine the electrokinetic properties of the sample surfaces. Measurements were taken in KNO_3 over the range of ionic strengths used in the colloid deposition experiments. The instrument was first rinsed with 1 L of DI water followed by 0.5 L of the electrolyte solution used in the measurement. Prior to the streaming potential measurements being taken, the sample surface was equilibrated with the corresponding fresh electrolyte solution for 10 min. The zeta potential of samples was calculated from the obtained streaming potential as described elsewhere[42].

6.2.4 Colloidal particle preparation and characterization.

Fluorescent carboxylate-modified polystyrene latex microspheres (Invitrogen, Eugene, OR) were utilized as model colloids for the deposition experiments. The monodispersed colloids had a mean diameter of 1.1 μm. The electrophoretic mobility of the colloids was determined in KNO_3 electrolyte solutions (1-100 mM) at 25 °C using a ZetaPALS analyzer (Brookhaven Instruments Corporation, Holtsville, NY). The Smoluchowski equation was used to convert the experimentally determined electrophoretic mobility values to zeta potential.[43]

The relative hydrophobicity of the colloids was analyzed using the semi-quantitative microbial adhesion to hydrocarbons (MATH) test[44] which indicates the relative hydrophobicity of the colloids as they partition between n-dodecane and an electrolyte (10 mM KNO_3). Samples were prepared by transferring 4 mL of a colloid suspension (optical density of 0.2-0.25 in 10 mM KNO_3 at 546 nm) to a test tube containing 1 mL of n-dodecane (laboratory grade, Fisher Scientific). Test tubes were then vortexed (AutoTouch Mixer Model 231, Fisher) for 2 min, followed by a 15 min rest period. After this time, allowing for phase separation, the optical density of the colloids in the aqueous phase was measured spectroscopically at 546 nm (BioSpec-mini, Shimadzu Corp). The hydrophobicity of colloids was reported as the percent of total colloids partitioned into the hydrocarbon.

6.2.5 Colloidal deposition experiments.

Colloid deposition experiments were conducted in a rectangular parallel plate flow chamber system described in detail by Chen et al..[38] The bare metal or ZSM-5 coated sample with varying surface roughness was inserted in the center of a cast acrylic flow deck in possession of a groove with dimensions of 9 × 20 mm to achieve a flat surface. The overall dimensions of the flow channel were 6 cm × 1cm × 0.0762 cm. The deposition of fluorescently labeled colloids onto the test surface was imaged by a 40x objective (UPlanFI, Olympus) focused on the center of the sample surface. A fluorescent filter set with an excitation wavelength of 480 nm and emission wavelength of 510 nm was utilized for imaging (Chroma Technology Corp., Brattleboro, VT).

Colloid deposition was recorded with a digital camera (Demo Retiga EXI Monochrome, QImaging) acquiring images every 30 seconds over the course of a 30 minutes injection and analyzed with the supplied software (SimplePCI, Precision Instruments, Inc., Minneapolis, MN). Data acquisition and analysis methods have been previously reported.[38] Briefly, the number of deposited colloids was determined for each time interval by comparing the changes between successive images. Colloid injection concentration was maintained at 2×10^7 particles/mL over the course of the experiments. A flow rate of 2 mL/min was employed, corresponding to an average flow velocity of 0.0044 m/s, a Peclet number of 0.019 (within the diffusion regime[43, 45]), and a shear rate of 34 s^{-146}. Experiments were conducted at

ionic strength conditions of 1, 10 and 100 mM KNO_3 solution at ambient pH (5.6-5.8) and temperature (22–25 ºC).

The kinetics of colloid deposition were measured by calculating the dimensionless Sherwood number (*Sh*).[38] The Sherwood number correlates colloid deposition flux (number of colloids per area per time), *J*; the colloid radius, a_p; the bulk colloidal particle concentration, C_0; and the bulk diffusion coefficient calculated from the Stokes-Einstein equation, D_∞, as follows[43],

$$Sh = \frac{Ja_p}{C_0 D_\infty} \qquad (1)$$

The deposition flux (*J*) was determined by normalizing the initial slope of the number of deposited colloids versus time curve and by the microscope viewing area (205 μm × 153 μm). All experimental conditions were tested a minimum of three times.

6.3 Results and Discussion

6.3.1 Physicochemical properties of test surfaces.

The bare and polished stainless steel (SS), aluminum alloy (Al) and the corresponding ZSM-5 coated surfaces were extensively characterized by X-ray diffraction (XRD), scanning electron microscopy (SEM), energy dispersive analysis of X-ray (EDAX) and surface profilometry. The XRD patterns for ZSM-5 crystals were in agreement with the patterns reported for ZSM-5 (www.iza-online.org) and confirmed the presence of ZSM-5 on all ZSM-5 coated test surfaces (Figure 6.1).

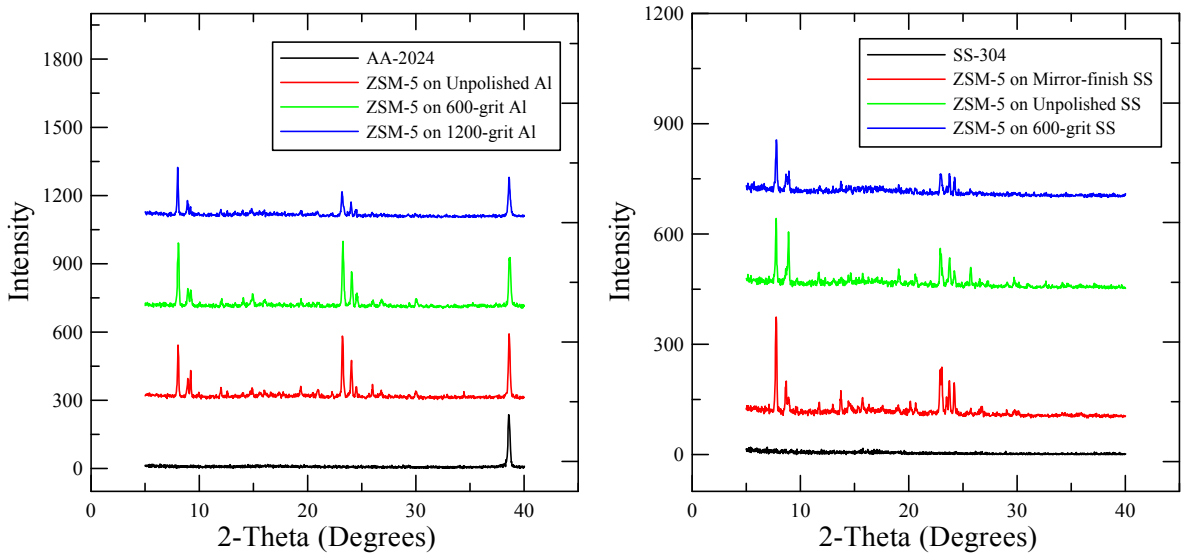

Figure 6.1 X-ray diffraction patterns of (A) bare aluminum alloy AA-2024 (black), ZSM-5 on unpolished Al (red), ZSM-5 on 600-grit polished Al (green), ZSM-5 on 1200-grit polished Al (blue) and (B) bare stainless steel SS-304 (black), ZSM-5 on unpolished SS (red), ZSM-5 on 600-grit polished SS (green) and ZSM-5 on mirror SS (blue).

SEM images of stainless steel, aluminum alloy and ZSM-5 coated samples are shown in Figure 6.2 and 6.3. The SEM images indicate that ZSM-5 coatings have a complete and even coverage over the entire substrate surfaces and the polycrystalline zeolite coatings are fully inter-grown on top of the base metals. On the other hand, it clearly demonstrated that the morphology was visually different between stainless steel and aluminum alloy, the unpolished and polished metal surfaces, and the uncoated and ZSM-5 coated metal surfaces. Semi-quantitative elemental analysis by energy dispersive analysis of X-ray (EDAX) spectroscopy is also presented in Figure 6.2 and 6.3, confirming that the ZSM-5 coatings on stainless steel and aluminum alloy have the same chemical compositions.

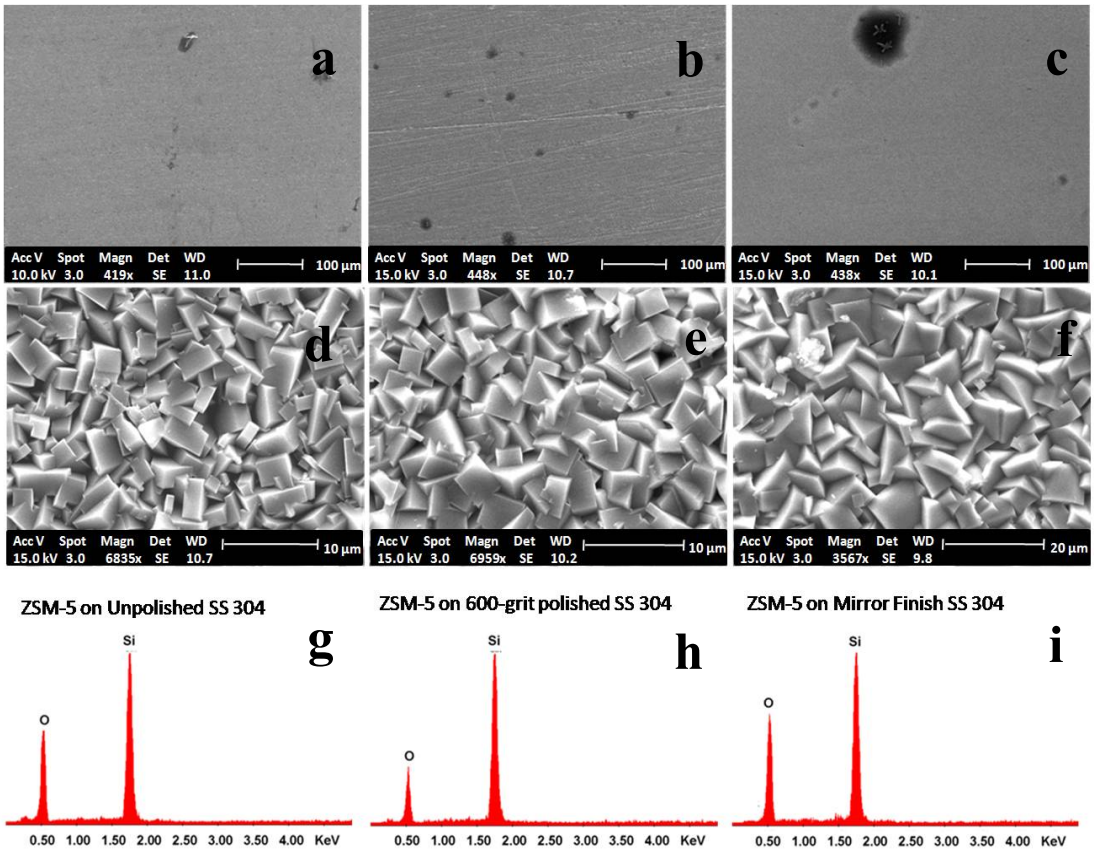

Figure 6.2 SEM images showing (a) unpolished SS, (b) 600-grit polished SS, (c) mirror SS (d) ZSM-5 on unpolished SS, e) ZSM-5 on 600-grit SS and (f) ZSM-5 on mirror SS. EDAX images showing ZSM-5 coating composition on (g) unpolished SS, (h) 600-grit SS and (i) mirror SS.

Table 6.1 presents the surface roughness measurements of the 12 test samples determined by the surface profilometer. In this study, surface roughness is determined as arithmetic average roughness, Ra, which is the most commonly used roughness parameter.[41, 47] Ra is the arithmetical mean of the absolute distances calculated from the middle line of all measured surface peaks and valleys. The lowest Ra value corresponds to the least surface roughness. Ra values obtained for 12 test sample surfaces ranged from 11.2 to 706.0 nm, which suggests the roughness

of test surfaces range from nanoscale to microscale. The surface of stainless steel with mirror finish was the smoothest, with a Ra = 11.2 nm, whereas for unpolished stainless steel and stainless steel polished with 600-grit, Ra increased to 56.3 and 74.5 nm, respectively. The Ra of the unpolished aluminum alloy was 458.8 nm and decreased to 158.4 and 194.1 nm on aluminum alloy surfaces polished by 600-grit and 1200-grit abrasive papers, respectively. Abrading with a larger grit size will not necessarily produce rougher surfaces. This is consistent with the observation by Kerr that the finer the grit size, the rougher the surface finish.[48] Furthermore, the surface roughness data demonstrate that the ZSM-5 coated test surfaces were much rougher than their corresponding bare metal surfaces, as suggested by the SEM images. The surface of ZSM-5 coated on aluminum alloy polished with 1200-grit abrasive papers was the roughest, with a Ra = 706.0 nm.

The zeta potentials of the 12 sample surfaces as a function of ionic strength were determined by streaming potential measurements and are shown in Table 6.1. All test surfaces became less charged with increasing ionic strength as anticipated from electrostatic double layer theory[49]. Stainless steel and aluminum alloy surfaces possessed a positive charge and had similar magnitude of zeta potential over the range of ionic strength conditions tested, while ZSM-5 coatings exhibited a negative charge at 1 mM and a positive charge at 10 mM. There was no statistically significant difference in zeta potentials of like surfaces (same base metal or coating) with varying surface roughness.

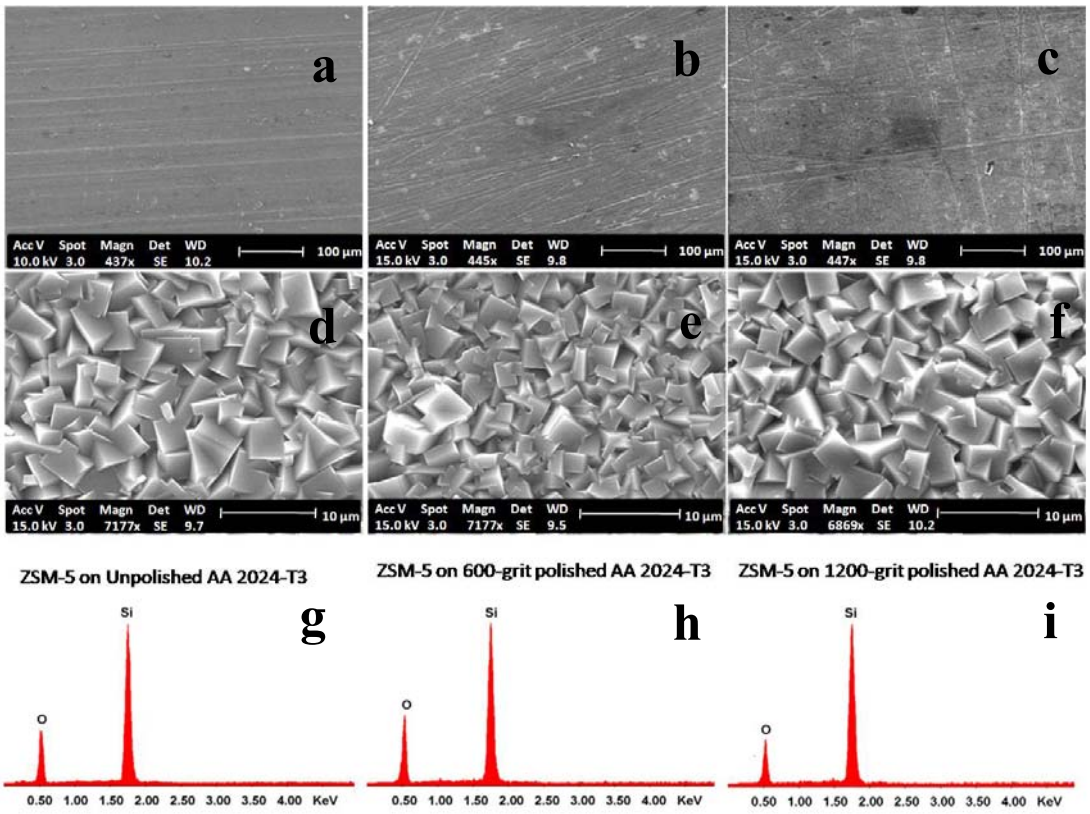

Figure 6.3 SEM images showing (a) unpolished Al, (b) 600-grit Al, (c) 1200-grit Al (d) ZSM-5 on unpolished Al, e) ZSM-5 on 600-grit Al and (f) ZSM-5 on 1200-grit Al. EDAX images showing ZSM-5 coating composition on (g) unpolished Al, (h) 600-grit Al and (i) 1200-grit Al.

The surface hydrophobicity of test samples expressed in terms of water contact angles is presented in Table 6.1. The stainless steel and aluminum alloy surfaces tested were hydrophobic, with contact angles ranging from 75.3° (unpolished stainless steel) to 108.6° (aluminum alloy polished with 1200-grit abrasive papers). The values of the contact angles for ZSM-5 coated stainless steel and aluminum were similar (24.1° - 29.8°) and hydrophilic. In addition, no effect of surface roughness was observed for the contact angle measurements.

Table 6.1 Water contact angle, surface roughness and zeta potential measurements of the test metal and ZSM-5 coated surfaces

Surface Tested	Treated Method	Ra (nm)	Contact Angle (°)	Zeta Potential (mV)	
				1 mM	10 mM
Stainless Steel	mirror	11.2 ± 1.0	87.2 ± 0.8	4.84 ± 0.53	42.72 ± 8.42
	unpolished	56.3 ± 4.1	75.3 ± 2.1	4.59 ± 0.32	50.13 ± 3.18
	600-grit	74.5 ± 6.2	88.5 ± 3.7	4.31 ± 0.22	47.45 ± 7.83
ZSM-5 coated Stainless Steel	mirror	416.9 ± 12.0	27.8 ± 3.3	-10.77 ± 2.31	22.57 ± 7.43
	unpolished	205.3 ± 9.9	29.8 ± 1.4	-12.42 ± 3.11	26.11 ± 4.77
	600-grit	226.7 ± 10.5	26.6 ± 0.4	-11.87 ± 2.46	25.66 ± 3.18
Aluminum	unpolished	458.8 ± 18.1	108.3 ± 2.3	4.59 ± 0.46	45.97 ± 6.39
	600-grit	158.4 ± 4.8	103.6 ± 0.9	3.91 ± 0.63	39.54 ± 3.72
	1200 grit	194.1 ± 7.9	108.6 ± 1.6	4.83 ± 0.59	43.03 ± 5.23
ZSM-5 coated aluminum	unpolished	605.8 ± 26.4	26.3 ± 1.3	-11.39 ± 1.47	24.41 ± 6.38
	600-grit	647.0 ± 25.5	29.0 ± 1.9	-14.12 ± 3.28	27.15 ± 4.56
	1200 grit	706.0 ± 39.6	24.1 ± 1.7	-13.41 ± 2.37	20.72 ± 8.33

6.3.2 Characteristics of colloids.

To determine the extent of electrostatic interactions between model colloids and collector surfaces, zeta potentials of colloids were measured. The colloids exhibited zeta potentials of -85.66 ± 0.49, -91.99 ± 2.65 and -54.10 ± 1.54 mV when suspended in 1, 10 and 100 mM KNO_3, respectively. The results indicated that the carboxylate-modified latex microspheres used in this study were highly negatively charged over the entire range of ionic strength conditions tested. Analysis of the colloid hydrophobicity employing the MATH test established 89.9 ± 0.6% of the colloids in 10 mM KNO_3 solution partitioned into n-dodecane. This suggested the colloids are relatively hydrophobic.

6.3.3 Colloid deposition trends.

The colloid deposition trends were shown in Figure 6.4 for the test metal and zeolite coating surfaces, with values of the Sherwood number plotted as a function of solution ionic strength. It is evident from this figure that ionic strength had a marked effect on the colloid deposition kinetics, as the general trend for all test surfaces was increasing deposition with ionic strength. For instance, there was no measurable colloid deposition at 1 mM KNO_3 solution on the mirror stainless steel and unpolished aluminum surfaces; however, the Sherwood number increased significantly ($P>0.05$) at 10 and 100 mM KNO_3. At 10 and 100 mM, the Sherwood number increased to 0.0206 ± 0.0008 and 0.0301 ± 0.0007 for the mirror stainless steel, and 0.0272 ± 0.0018 and 0.0337 ± 0.0012 for the unpolished aluminum, respectively.

Deposition was dramatically influenced by the surface roughness. As surface roughness of the bare metal increased, the Sherwood number was also generally higher (with one exception). The smoothest stainless steel surface (mirror SS) had a Sherwood number of 0.0206 ± 0.0008 for 10 mM. With increasing roughness (unpolished SS and 600-grit SS), the deposition was enhanced with Sherwood number of 0.0309 ± 0.001 and 0.0340 ± 0.0013 at 10 mM KNO_3, respectively. In the case of the aluminum alloy, Sherwood number was determined to be 0.0398 ± 0.0008 for the smoothest 600-grit surface at the intermediate ionic strength, 10 mM KNO_3. As the measured roughness increased with 1200-grit Al, so did the Sherwood number, to

0.0459 ± 0.0010. The exception to the general trend of enhanced deposition with roughness was unpolished Al, where the roughness was the largest, but did not have the greatest Sherwood number of the bare Al samples.

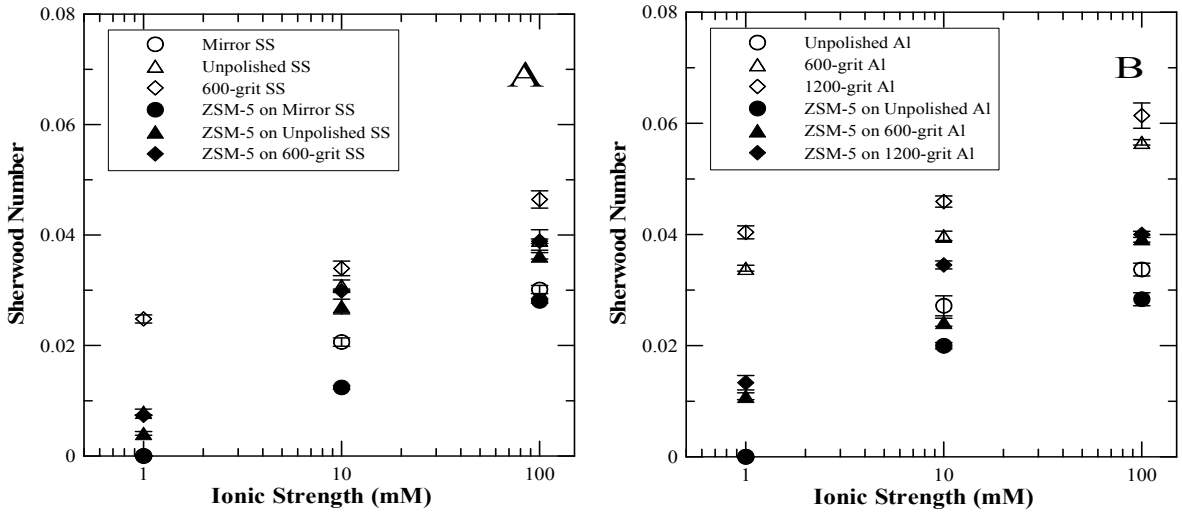

Figure 6.4 Sherwood number of colloids deposited onto metal and ZSM-5 coated surfaces in a parallel plate flow chamber system, determined as a function of ionic strength. Experiments were carried out at ambient pH (5.6-5.8) and temperature (22-25 ºC). Error bars indicate one standard deviation.

Figure 6.4 also displays similar deposition trends on ZSM-5 coatings; in that a generally increasing Sherwood number was observed with greater roughness of the ZSM-5 coated surfaces at all ionic strength conditions tested. Interestingly, the Sherwood number increased in following order of mirror SS, unpolished SS and 600-grit SS for stainless steel, and unpolished Al, 600-grit Al and 1200-grit Al for aluminum alloy, respectively, which is the same Sherwood number increase order for the bare metal surfaces. For Al coated surfaces, this corresponds to increasing Ra.

For two of the three SS coated surfaces, the higher Sherwood number results from the greater Ra. The exception is the mirror coated SS, in which the roughness is the greatest of the three coated SS, but results in the lowest deposition. Additionally, lower values of Sherwood number were observed on ZSM-5 coatings than those on the corresponding bare metal surfaces. The two extremes for Sherwood number onto coatings were 1) no measurable colloid deposition at 1 mM KNO_3 solution on the ZSM-5 coated mirror SS and unpolished Al, and 2) the greatest Sherwood number of 0.0400 ± 0.0005 at 100 mM KNO_3 solution for the coated 1200-grit Al.

The influence of surface roughness on the kinetics of the colloid deposition onto the test metal and ZSM-5 coated surfaces was further evaluated as a function of Ra (Figure 6.5). Generally, these results indicate that surface roughness had a significant impact over the range of ionic strength tested, with the greater surface roughness of surface resulting higher Sherwood numbers. This trend was observed for stainless steel and ZSM-5 coatings on all aluminum alloy substrates. The relationship also held true for the ZSM-5 coated stainless steel with the exception of ZSM-5 coated mirror SS. Additionally, Sherwood number increased with surface roughness on bare aluminum surfaces with the exception of the unpolished Al surface. Both of these exceptional samples were much rougher than the other two sample surfaces in the same category (Table 6.1), and resulted in the least colloid deposition.

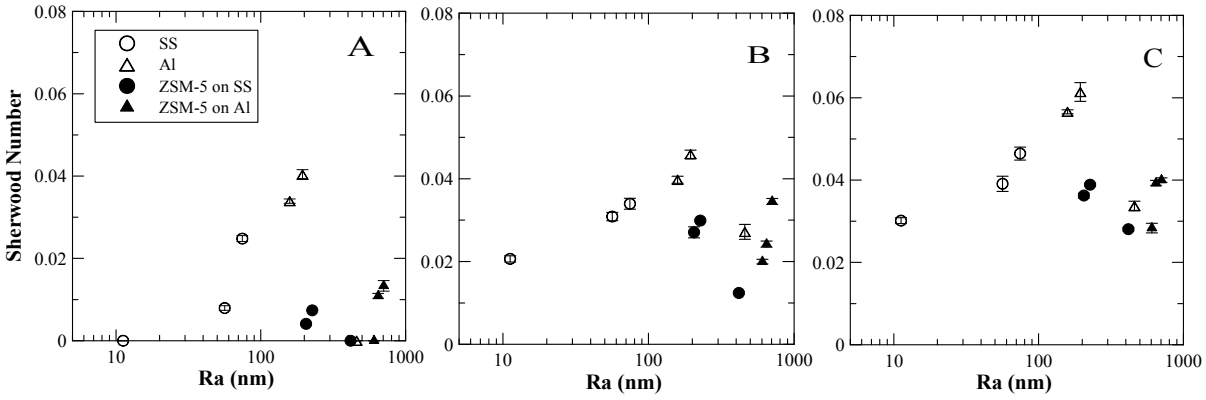

Figure 6.5 Sherwood number of colloids deposited onto metal and ZSM-5 coated surfaces as a function of sample surface roughness, Ra, in a parallel plate flow chamber system at ionic strength of A) 1 mM KNO_3, B) 10 mM KNO_3, C) 100 mM KNO_3.

6.3.4 Physical and chemical factors involved in the kinetics of colloid deposition.

Colloid deposition to a collector surface is governed by two steps: transport to a collector surface and the subsequent interactions between the colloid and surface that occurs upon close approach. The physical properties of the colloid and hydrodynamics of the flow system control the transport of the colloid, meanwhile the deposition is determined by the near surface interactions, including such forces as DLVO-type (electrostatic and van der Waals), hydrophobic, and hydration. The observed sensitivity of colloid deposition to ionic strength (Figure 6.4) indicates that electrostatic forces were involved between the colloids and the coated and bare surfaces. As indicated by measured zeta potentials of the colloids and test surfaces, the colloids were highly negatively charged over the salt concentration tested, ZSM-5

coatings exhibited a negative charge at 1 mM and a positive charge at 10 mM and stainless steel and aluminum alloy surfaces possessed a positive charge, suggesting that repulsive interactions existed between the colloids and ZSM-5 coated surfaces at 1 mM conditions and interactions with collectors became more favorable as ionic strength increased. Therefore, the increase in the ionic strength would result in a decrease of electrostatic repulsive force (or an increase of electrostatic attractive force) and a higher Sherwood number, which was the case in the reported experiments (Figure 6.4).

Zeolite coatings resulted in overall rougher surfaces and lower levels of colloid deposition as compared to bare metal surfaces (Figure 6.4 and 6.5). This effect was most pronounced at the lowest salt concentration tested, at which the electrostatic interactions were repulsive between the colloids and the ZSM-5 coated stainless steel and aluminum alloy and attractive between the colloids and metal surfaces. This further confirms that electrostatic interactions played a role on decreasing colloid deposition on ZSM-5 coatings. These were consistent with previous bacterial tests[38] which also observed less bacterial cell attachment on zeolite coatings than bare stainless steel and aluminum alloy surfaces.

Hydrophobic interaction is another possible mechanism involved. Hydrophobicity can be the major parameter increasing initial bacterial adhesion onto stainless steel[30]. In the current study, the colloid hydrophobicity was determined to be 89.9 ± 0.6%, which suggested the colloids are relatively hydrophobic. It was previously suggested[38, 50] that the addition of a ZSM-5 coating on aluminum alloy and stainless

steel enhances the hydrophilicity, and the trend is confirmed with our contact angle data (see Table 6.1). This increased hydrophilicity of the surface, is contributing to the reduced deposition as the colloids are more likely to deposit on the hydrophobic bare versus hydrophilic coated surfaces. This agrees with our previous work[38], which suggested hydrophobic interactions were contributing to the reducing attachment of the cells onto the test surfaces, as the more hydrophilic the surface was, the less bacterial deposition occurred under identical electrostatic conditions. The greater values of the surface contact angles, this current study measured higher colloid deposition under constant solution chemistry and experimental conditions. However, the hydrophobic interaction was not the dominant factor; otherwise, similar deposition would be observed on surfaces with comparable hydrophobicity (e.g. water contact angle measurement) values (Table 6.1), which was not the case.

6.3.5 Relative importance of surface roughness.

The goal of this study was to evaluate the actual effect of surface roughness, in light of previous bacterial deposition studies reporting and antifouling properties of the zeolite coatings[5, 38]. The results of this study shows that surface roughness had a significant impact on the kinetics of the colloid deposition onto the test metal and ZSM-5 coated surfaces as demonstrated in Figure 6.5. In general, the greater surface roughness of the like samples in each category resulted in higher colloid deposition. The two exceptions were the ZSM-5 coated mirror SS and the unpolished Al surfaces,

which were much rougher than the other two sample surfaces in the same category (Table 6.1), but resulted in the least colloid deposition.

The overall deposition trend was in agreement with several studies that showed a relationship between stainless steel surface finish and bacterial adhesion.[51-54] Arnold et al.[51-53] compared the bacterial attachment between the control stainless steel and electropolished steel and observed significantly less bacterial adhesion as Ra was reduced from 0.14 μm to less than 0.02 μm. However, in many cases, other researchers observed no influence of surface roughness upon bacterial adhesion.[36, 55] This inconsistency in observed trends is attributed to the great variability in research protocols – batch versus flowing systems, solution chemistries, and bacterial strain. In the current study, greater colloid deposition was generally observed on rougher surfaces having the same chemistry with the roughness ranging from nanoscale (stainless steel) to microscale (aluminum alloy and ZSM-5 coatings). Notably, stainless steel samples only possessed nanoscale surface roughness, which was much smaller than the model colloids utilized for the deposition experiments and the rest samples had a Ra ranging from 0.15 – 0.7 μm (Table 6.1).

Even though the impact of surface roughness on the colloid deposition occurred for all test samples over all ionic strength conditions examined, the effect was most pronounced at the lowest ionic strength (Figure 6.5). For instance, there was no measurable colloid deposition on the mirror stainless steel, whereas the Sherwood number became to 0.0079 ± 0.0006 and 0.0248 ± 0.0007 for unpolished and 600-grit

polished stainless steel, respectively, with the surface roughness Ra increasing from 11.2 to 74.5 nm. The observation is in agreement with Hoek and Agarwal's model prediction[56] that nanoscale rougher surfaces are more favorable for colloid deposition. As the surface roughness increased to be microscale, the same trend was observed for the ZSM-5 coatings on all aluminum alloy substrates even though the increase of the surface roughness was minor (Table 6.1). The relationship also held true for the ZSM-5 coatings on stainless steel substrates and the test aluminum alloy surfaces, with exception of the ZSM-5 coated mirror SS and the unpolished Al surfaces, which were much rougher than the other two sample surfaces in the same category, but had the least colloid deposition.

In the case of aluminum alloy samples, SEM images suggested that unpolished Al possessed many fewer scratches and surface irregularities than the 600-grit and 1200-grit Al surfaces even though it had the greatest Ra value in the category. This may be due to the scratches and irregularities on the 600-grit and 1200-grit Al surfaces as shown in Figure 6.3 responsible for the greater Sherwood number than that on the unpolished Al. Arnold and Suzuki[57] showed that stainless steel surfaces with flaws and irregularities were much less resistant to bacterial adhesion. This phenomenon also suggests that surface topography is not sufficiently defined by one roughness parameter. The shape and size of surface irregularities appeared to be more relevant for predicting colloid and bacterial attachment. As to the exception of the ZSM-5 coated mirror SS, it may be due to the process of ZSM-5 synthesis and handling, as the

roughness of the ZSM-5 coated mirror SS was significantly different from the other two sample surfaces in the same category, which resulted in an unexpected colloid deposition behavior as we observed in the deposition experiments.

6.4 CONCLUSION

The deposition kinetics of polystyrene microspheres was examined on the bare and ZSM-5 coated stainless steel and aluminum alloy surfaces. The study was focused on evaluating the relative importance of surface roughness on colloid deposition. Our experimental results demonstrated that surface roughness ranging from nanoscale to microscale had a pronounced impact on the kinetics of the colloid deposition under conditions tested. The greater surface roughness of the like samples resulted in higher colloid deposition, even when surface roughness (Ra) was two orders of magnitude smaller than the colloids. Surface roughness was found to be an important parameter in determining the extent of particle deposition across the range of ionic strength conditions tested. However, it was found that a combination of chemical mechanisms – electrostatic and hydrophobic interactions – as well as physical surface roughness determines the antifouling nature of the zeolite surfaces, and future design of materials and coatings must account for the coupled influence of the chemical and physical parameters.

6.5 REFERENCES

1. Gademann, K. *Chimia* **2007,** 61, (6), 373-377.

2. Gaylarde, C. C.; Morton, L. H. G. *Revista De Microbiologia* **1997,** 28, (4), 221-229.

3. Norde, W. *Zeitschrift Fur Physikalische Chemie* **2007,** 221, (1), 47-63.

4. He, Y. L.; Xu, P.; Li, C. J.; Zhang, B. *Water Res.* **2005,** 39, (17), 4110-4118.

5. McDonnell, A. M. P.; Beving, D.; Wang, A. J.; Chen, W.; Yan, Y. S. *Adv. Funct. Mater.* **2005,** 15, (2), 336-340.

6. Ross, J. *Smithsonian* **1994,** 24, (11), 40-&.

7. Coetser, S. E.; Cloete, T. E. *Crit. Rev. Microbiol.* **2005,** 31, (4), 213-232.
8. Goto, Y. *Water Sci. Technol.* **2002,** 46, (11-12), 45-50.

9. Meesters, K. P. H.; Van Groenestijn, J. W.; Gerritse, J. *Water Res.* **2003,** 37, (3), 525-532.

10. Lu, R. H.; Liu, Q.; Xiao, C. S.; Bai, S.; Chen, H. C.; Wang, F. R. *Acta Microbiologica Sinica* **1984,** 24, (3), 243-249.

11. Dafforn, K. A.; Glasby, T. M.; Johnston, E. L. *Biofouling* **2008,** 24, (1), 23-33.

12. Belfroid, A. C.; Purperhart, M.; Ariese, F. *Mar. Pollut. Bull.* **2000,** 40, (3), 226.

13. Showalter, S.; Savarese, J., Restrictions on the Use of Marine Antifouling Paints Containing Tributyltin and Copper. In California Sea Grant Extension Program: 2004.

14. Walker, S. L. *Colloid. Surface. B* **2005,** 45, 181-188.

15. Walker, S. L.; Hill, J. E.; Redman, J. A.; Elimelech, M. *Appl. Environ. Microb.* **2005,** 71, 3093-3099.

16. van Loosdrecht, M. C. M.; Lyklema, J.; Norde, W.; Schraa, G.; Zehnder, A. J. B. *Appl. Environ. Microb.* **1987,** 53, (8), 1893-1897.

17. Schafer, A.; Harms, H.; Zehnder, A. J. B. *Environ. Sci. Technol.* **1998,** 32, (23), 3704-3712.

18. Gross, M.; Cramton, S. E.; Gotz, F.; Peschel, A. *Infect. Immun.* **2001,** 69, (5), 3423-3426.

19. Kuznar, Z. A.; Elimelech, M. *Langmuir* **2005,** 21, (2), 710-716.

20. Bowen, W. R.; Lovitt, R. W.; Wright, C. J. *J. Mater. Sci.* **2001,** 36, (3), 623-629.

21. Ma, H.; Winslow, C. J.; Logan, B. E. *Colloid. Surface. B* **2008,** 62, (2), 232-237.

22. Zhao, Q.; Liu, Y.; Wang, C.; Wang, S.; Peng, N.; Jeynes, C. *Med. Eng. Phys.* **2008,** 30, (3), 341-349.

23. Shellenberger, K.; Logan, B. E. *Environ. Sci. Technol.* **2002,** 36, (2), 184-189.

24. Mitik-Dineva, N.; Wang, J.; Truong, V. K.; Stoddart, P.; Malherbe, F.; Crawford, R. J.; Ivanova, E. P. *Curr. Microbiol.* **2009,** 58, (3), 268-273.

25. Bhattacharjee, S.; Ko, C. H.; Elimelech, M. *Langmuir* **1998,** 14, (12), 3365-3375.

26. Elimelech, M.; Omelia, C. R. *Langmuir* **1990,** 6, (6), 1153-1163.

27. Johnson, P. R.; Sun, N.; Elimelech, M. *Environ. Sci. Technol.* **1996,** 30, (11), 3284-3293.

28. Song, L. F.; Johnson, P. R.; Elimelech, M. *Environ. Sci. Technol.* **1994,** 28, (6), 1164-1171.

29. Chen, J. Y.; Klemic, J. F.; Elimelech, M. *Nano Lett.* **2002,** 2, (4), 393-396.

30. Vanhaecke, E.; Remon, J. P.; Moors, M.; Raes, F.; Derudder, D.; Vanpeteghem, A. *Appl. Environ. Microbiol.* **1990,** 56, (3), 788-795.

31. Taylor, R. L.; Verran, J.; Lees, G. C.; Ward, A. J. P. *J. Mater. Sci.-Mater. M.* **1998,** 9, (1), 17-22.

32. Tang, H. Y.; Cao, T.; Liang, X. M.; Wang, A. F.; Salley, S. O.; McAllister, J.; Ng, K. Y. S. *J. Biomed. Mater. Res. A* **2009,** 88A, (2), 454-463.

33. DIN 11480, Dairy machines; tanks and apparatus; surfaces. In German National Standard: 1992.

34. Emerson, R. J.; Bergstrom, T. S.; Liu, Y. T.; Soto, E. R.; Brown, C. A.; McGimpsey, W. G.; Camesano, T. A. *Langmuir* **2006,** 22, (26), 11311-11321.

35. Barnes, L. M.; Lo, M. F.; Adams, M. R.; Chamberlain, A. H. L. *Appl. Environ. Microbiol.* **1999,** 65, (10), 4543-4548.

36. Hilbert, L. R.; Bagge-Ravn, D.; Kold, J.; Gram, L. *Int. Biodeter. Biodegr.* **2003,** 52, (3), 175-185.

37. Gubjornsdottir, B.; Einarsson, H.; Thorkelsson, G. *Food Technol. Biotech.* **2005,** 43, (1), 55-61.

38. Chen, G.; Beving, D. E.; Bedi, R. S.; Yan, Y. S.; Walker, S. L. *Langmuir* **2009,** 25, (3), 1620-1626.

39. Luckham, P. F.; Hartley, P. G. *Adv. Colloid Interfac.* **1994,** 49, 341-386.

40. Parrish, W.; Wilson, A. J. C. *Acta Crystallographica* **1954,** 7, (10), 622-622.

41. An, Y. H.; Friedman, R. J. *J. Biomed. Mater. Res.* **1998,** 43, (3), 338-348.

42. Walker, S. L.; Bhattacharjee, S.; Hoek, E. M. V.; Elimelech, M. *Langmuir* **2002,** 18, (6), 2193-2198.

43. Elimelech, M., Gregory, J., Jia, X., Williams, R.A., *Particle Deposition and Aggregation: Measurement, Modeling and Simulation*. Butterworth-Heinemann: 1995; p 441.

44. Pembrey, R. S.; Marshall, K. C.; Schneider, R. P. *Appl. Environ. Microbiol.* **1999,** 65, (7), 2877-2894.

45. Adamczyk, Z.; Vandeven, T. G. M. *J. Colloid Interf. Sci.* **1981,** 80, (2), 340-356.

46. McClaine, J. W.; Ford, R. M. *Biotechnol. Bioeng.* **2002,** 78, (2), 179-189.

47. Whitehead, K. A.; Verran, J. *Food Bioprod. Process.* **2006,** 84, (C4), 253-259.

48. Kerr, A.; Beveridge, C. M.; Cowling, M. J.; Hodgkiess, T.; Parr, A. C. S.; Smith, M. J. *J. Mar. Biol. Assoc. UK* **1999,** 79, (2), 357-359.

49. Poortinga, A. T.; Bos, R.; Norde, W.; Busscher, H. J. *Surf. Sci. Rep.* **2002,** 47, (1), 3-32.

50. McDonnell, A. M. P.; Beving, D.; Wang, A. J.; Chen, W.; Yan, Y. S. *Adv. Funct. Mater.* **2005,** 15, (2), 336-340.

51. Arnold, J. W.; Boothe, D. H.; Suzuki, O.; Bailey, G. W. *J. Microsc.* **2004,** 216, 215-221.

52. Arnold, J. W.; Silvers, S. *Poult. Sci.* **2000,** 79, (8), 1215-1221.

53. Arnold, J. W.; Bailey, G. W. *Poult. Sci.* **2000,** 79, (12), 1839-1845.

54. Medilanski, E.; Kaufmann, K.; Wick, L. Y.; Wanner, O.; Harms, H. *Biofouling* **2002,** 18, (3), 193-203.

55. Verran, J.; Rowe, D. L.; Boyd, R. D. *J. Food Prot.* **2001,** 64, (8), 1183-1187.

56. Hoek, E. M. V.; Agarwal, G. K. *J. Colloid Interf. Sci.* **2006,** 298, (1), 50-58.

57. Arnold, J. W.; Suzuki, O. *T. Asae* **2003,** 46, (6), 1595-1602.

CHAPTER 7

SUMMARY AND CONCLUSIONS

The goal of this doctoral work was to elucidate the extent to which multi-scale physical and chemical heterogeneity contributes to the initial stages of microbial and colloidal deposition. The overall objective was to relate the particle deposition kinetics to the physical and chemical properties of the particle and collector surfaces by systematically adjusting particle type and size, collector surface chemical and/or physical heterogeneity. Two deposition systems were employed: a radial stagnation point flow system and a parallel plate flow chamber system. The transport experiments were complimented by a range of characterization techniques which provided insight into the topography, roughness and hydrophobicity of the collector surface, the size and viability of the cells, the charge characteristics of the particle and collector surfaces, as well as the particle hydrophobicity.

In Chapter 2, experimental deposition data are presented for a groundwater bacterium, *Burkholderia cepacia* G4g and a marine bacterium, *Halomonas pacifica* g on quartz surfaces determined in a radial stagnation point flow cell system. The purpose of the work was to evaluate the role of microbial heterogeneity on bacterial deposition to solid surfaces in water solutions simulating various aquatic environments. Comparable adhesion trends were observed for both bacteria. Specifically, the deposition rates of the two bacteria species in both KCl and $CaCl_2$ solutions increased with ionic strength, a trend consistent with traditional DLVO theory. However, the deposition kinetics of *H. pacifica* g appeared to be much more sensitive to solution chemistry than that of *B. cepacia* G4g. Combined with extensive

cell characterization, it was found that Ca^{2+} ions play a distinct role on bacterial surface charge, hydrophobicity and deposition behaviors. Calcium can bind the surface polymers of bacteria and alter the conformation of these polymers, and it is by this mechanism that Ca^{2+} ions are responsible for the adhesion behavior of the cells. It is further suggested that bacterial adhesion is determined by the combined influence of DLVO interactions, as well as electrosteric interactions associated with solution chemistry and the hydrodynamics of the deposition system.

The effect of "heterogeneity" in particles from the perspective of size is discussed in Chapter 3. Deposition rates of three polystyrene microspheres with sizes of 0.5, 1.1, 1.8 μm and *B. cepacia* G4g were measured on glass under both unfavorable and favorable conditions in a parallel plate flow chamber system. Experimental results demonstrated that particle size had a considerable effect on the deposition of micron-sized colloids and bacteria and confirmed that size contributes to particle transport and interaction with surfaces. It was found that smaller colloids seem to be more sensitive to hydrodynamic interactions compared to larger colloids and bacterial cells. Moreover, comparing the particle deposition kinetics onto the top and bottom surfaces under identical residence times, fluid chemistries and hydrodynamic conditions, results showed that significant deposition differences were observed between the two surfaces, suggesting that gravity was a significant driving force for the initial stages of micron-sized particle deposition, which was also validated by

calculations using the Smoluchowski-Levich approximation and the experimental observations in a $D_2O/H_2O/KCl$ mixture.

In Chapter 4, a new method to create collector surface chemical heterogeneity by varying the zeta potential at microelectrodes with applied electric potentials was introduced. Colloid deposition kinetics was determined in a parallel plate flow chamber system and it was found that remotely controlled zeta potential changes on the microelectrode induced by an external potential gave predictable adhesion trends. Experimental results were adequately described by a patch model consisting of favorable and unfavorable microscopic regions, particularly when a negative potential was applied. Therefore, we proposed colloidal particles respond to local variation in surface potential through electrostatic interactions, altering particle streamlines flowing along the surface, and ultimately the extent of deposition.

The influence of the collector surface physical and chemical heterogeneities on the deposition of marine species, *H. pacifica* g is discussed in Chapter 5. The source of chemical heterogeneity is achieved by using coated bare metal substrata (stainless steel and aluminum alloy) with zeolite to alter surface charge properties. This work presents a critical evaluation of the relative physical and chemical mechanisms controlling bacterial deposition onto bare versus zeolite-coated stainless steel and aluminum alloy in a parallel plate flow chamber system. The attachment behavior of the *H. pacifica* g confirmed that in flowing aquatic environments zeolite coatings reduce the extent of initial bacterial attachment across the range of solution chemistry

and hydrodynamic conditions tested, which could lower the possible level of biofilm formation. Complementary cell and collector surface characterization suggested a combination of two chemical mechanisms - hydrophobic and electrostatic interactions - contribute to the antifouling nature of the zeolite surface.

Finally, to compliment the previously mentioned work, adhesion studies were conducted with polystyrene colloids and discussed in Chapter 6. The metal collector surfaces were systematically polished to alter the surface roughness to investigate the contribution of physical heterogeneity. Experimental results suggested that ZSM-5 coating and surface roughness had a pronounced impact on the kinetics of the colloid deposition. The ZSM-5 coating reduced colloid adhesion compared to the corresponding bare metal surface. In general, the greater surface roughness of like samples resulted in higher colloid deposition. The two exceptions were ZSM-5 coated mirror-polished stainless steel and the unpolished aluminum surfaces, which were rougher than the other two samples of the same metal type, but resulted in the least deposition. These phenomena also suggest that surface topography is not sufficiently defined by one roughness parameter. The shape and size of surface irregularities appear to be more relevant for predicting colloid and bacterial attachment. Based on the extensive characterization of colloid and collector surfaces, it was found that a combination of chemical mechanisms – electrostatic and hydrophobic interactions – as well as physical surface roughness determines the antifouling nature of the zeolite surfaces.

This doctoral research has focused on understanding the physical and chemical heterogeneity contributions to the initial stages of microbial and colloidal deposition in aquatic systems. Over the course of this work, it was found that no single factor dominates the extent of adhesion. Rather, a combination of chemical and physical mechanisms determines the particle deposition behavior as a function of the hydrodynamic and solution conditions presented. The further clarification of the contributions of various heterogeneity property sources to particle deposition, as presented in this dissertation, is an important contribution to this essential knowledge base.

Previous extensive studies on microbial and colloidal deposition have shown discrepancies between experimental observations and theoretical predictions, which has commonly been attributed to the inherent physical and chemical heterogeneities of the particle and solid substrata. Clearly, this research established that the effect of the heterogeneity on particle adhesion was pronounced through altering various interactions between particles and collector surfaces. The heterogeneity factor must be taken into account in future theoretical work. Additionally, this work also quantitatively demonstrated the traditional filtration theory likely underestimates the role of gravity on particle transport. Future work is needed to clarify the specific effect of sedimentation on the transport of particles with varying size in porous media using a heavy water system. Moreover, to develop zeolite antifouling surfaces, the zeolite composition and topography optimization is warranted in future work.